Electrical Characterization and Potential Applications of Graphene-like Nanocarbon and Au Nanoparticle-PDMS Nanocomposite

A thesis submitted in partial fulfillment of the requirements of the degree of

MASTER OF SCIENCE

as a part of Integrated PhD programme (Material Science)

By

Dipanwita Dutta

Chemistry and Physics of Materials Unit

Jawaharlal Nehru Centre for Advanced

Scientific Research (A deemed University)

BANGALORE, INDIA

(April 2014)

Dedicated

To

My Beloved Parents,
to their selfless affection and inspiration...

DECLARATION

I hereby declare that this thesis entitled **"Electrical Characterization and Potential Applications of Graphene-like Nanocarbon and Au Nanoparticle-PDMS Nanocomposite"** is an authentic record of research work carried out by me at the Chemistry and Physics of Materials Unit, Jawaharlal Nehru Centre for Advanced Scientific Research, Bangalore, India under the supervision of Professor G. U. Kulkarni and that it has not been submitted elsewhere for the award of any degree or diploma.

In keeping with the general practice in reporting scientific observations, due acknowledgment has been made whenever the work described is based on the findings of other investigators. Any omission that might have occurred due to oversight or error in judgment is regretted.

Date :

Bangalore, INDIA **Dipanwita Dutta**

CERTIFICATE

Certified that the work described in this thesis titled **"Electrical Characterization and Potential Applications of Graphene-like Nanocarbon and Au Nanoparticle-PDMS Nanocomposite"** has been carried out by Ms. Dipanwita Dutta at the Chemistry and Physics of Materials Unit, Jawaharlal Nehru Centre for Advanced Scientific Research, Bangalore, India under my supervision and that it has not been submitted elsewhere for the award of any degree or diploma.

Date :

Bangalore, INDIA **Prof. G. U. Kulkarni**

(Research Supervisor)

ACKNOWLEDGEMENTS

Firstly, with my deepest gratitude I would like to acknowledge my mentor and research supervisor Professor G. U. Kulkarni. I thank him from the core of my heart for all the guidance he provided me at this early stage of research. His thinking and selfless dedication nourished me in understanding crucial problems in research. I am also grateful to him, for suggesting such riveting projects to work on. His advices on research and career are invaluable. His support was always there not only for my professional life but also for my personal life. I thank you sir for imparting the true value of optimism on me and also for making my research life enjoyable.

I would like to thank Prof. C. N. R. Rao, for giving us the opportunity to do research in such prestigious institute under the guidance of eminent professors. His presence itself is a constant source of inspiration. Apart from being adept, his omnicompetent personality stimulates and motivates people of all age and field. My research supervisor always gave his example which galvanized me to follow his tread to become a successful scientist.

I acknowledge all my professors, Prof. G.U. Kulkarni, Prof. U. Waghmare, Prof. A. Sundaresan, Prof. M. Eswaramoorthy, Prof. K.S. Narayan, Prof. Chandrabhas, Prof. S. Balasubramanian, Prof. S.M. Shivaprasad, Prof. T.K. Maji, Dr. S. Vidhyadhiraja, Prof. S. Narasimhan, Prof. C. Narayanana, Prof. H. Illa, Dr. R. Ganapathy, Prof. R. Datta for their valuable lessons and course works. A special thanks to Prof. U. Waghmare for the valuable discussions, during and after my winter project. I also acknowledge all my professors and teachers for the valuable knowledge they imparted on me during my school and college days.

Constant assistance and a friendly nature of the technical staff helped me doing my experiments smoothly. Here I would like to acknowledge Mr. Srinath and Mr. Srinivas. A special thanks to Dr. S. Basavaraja (AFM), he has been a constant source of help. I am grateful to Mrs. Usha (TEM), Mrs.

Selvi (FESEM), Mr. Anil (XRD), Mr. Vasu (UV, IR, PL, TGA) and Mr. A. Srinivasa Rao for their indispensible support. Ms. Vanitha, Mr. Sunil, Mr. Moorthy, Mr. Gowda, Mr. Dilip and Mr. Peer and all other members of academic and administrative section are acknowledged for their assistance. I am thankful to the computer lab members and the library staffs for their help. I thank DST for the financial assistance.

I am grateful to my lab senior Narendra under whom I completed my summer project. Under his guidance I got the opportunity to learn a lot about research work and many instruments. I would like to show my appreciation to my past and present lab seniors Narendra, Mallik, Ritu, Ganga, Umesh, Kiruthika, Ankush, Sunil, Padmavathy, Swathi, Thripurantaka, Vandana, Dr. Abhay, Dr. Basavaraja, Dr. Radha, Dr. Neena, Dr. Ved Varun, and Dr. Bhuvana. Their discussion on past experience and valuable inputs about research life and experiments helped me immensely.

I thank all my Int. PhD batchmates. My hearty thanks to Sonu and Pranav for all the fun filled moments I spent with them. All my friends here Chandradish, Sonu, Sohini, Syamantak and also my friends outside Dipanwita, Joshita, Zashim, Vandana, Guratinder, Ranajoy thanks to you all for the joyous time we spent and also for supporting me any time I required. Not to forget, my cousins Trina, Nilanjana, Anurag and Barsha, they are acknowledged for the support they provided.

I am grateful to Mrs. Kulkarni for her affection, warmth and care. I also thank Teju and Poorna for all the fun and laughter.

Lastly I would like to acknowledge the most important people of my life, my parents and mama (my uncle). Without their love and encouragement all my efforts would have gone to vain. Their endearing support has been the backbone for what I am today and what I will be in future. The most beautiful thing for me is to see my parents smiling and knowing that I am the reason behind that. My late uncle, who was my first teacher, I acknowledge you for the innumerable fights we had over math problems. I am grateful to you all for whatever you gave me and I dedicate my thesis to you.

PREFACE

This thesis entitled **"Electrical Characterization and Potential Application of Graphene-like Nanocarbon and Au Nanoparticle-PDMS Nanocomposite"** presents the investigation of the nanocarbon material with focus on graphene and turbostratic graphite. Electrical characterization of the Au-PDMS was realized in the last part. The thesis has been allocated into three parts.

Part I introduces nanoscience and nanoparticles and their important properties. Carbon nanomaterials, 2D nanocarbon, graphene and turbostratic graphite have been briefly presented. The novel properties of the turbostratic graphite in realizing devices have been exploited. The last section describes polymer nanocomposites with special stress on metal nanoparticle polymer nanocomposite.

Part II pertains to the electronic and optoelectronic properties of graphene, amorphous carbon and turbostratic graphite. Graphene film have been grown by electrochemical and electrostatic method. The infrared photoresponse behavior of amorphous carbon and graphene has been investigated.

Pencil traces on paper produce turbostratic graphite which shows high mosaicity i.e. rotationally disordered graphene layers. This leads to electronic decoupling between the layers. Passive devices like resistor-capacitor filters could be made by employing this turbostratic graphite as a resistor and ion gel as dielectric. Field effect transistor has been made out of the pencil traces with aid of ion gel having high specific capacitance.

Part III deals with the synthesis of Au-PDMS nanocomposite. Electrical characterization of the capacitor geometry has been done using Au-PDMS as dielectric. Application of pressure on the Au-PDMS leads to improved current values. Other stimuli have been applied as well, like application of electrical stress or passing of nitrogen and toluene vapor through the circuit, and conductivity have been checked. Varying the environment around the circuit steered to improved values of electrical conductivity.

TABLE OF CONTENTS

PART I: OVERVIEW OF NANOPARTICLES AND NANOCOMPOSITES

PART II GRAPHENE AND TURBOSTRATIC GRAPHITE: PROPERTIES AND APPLICATION

II.1 Large area graphene obtained by physical and chemical methods: Infrared Photoconductive Response

II.2 Pencil Drawing on Paper: Field Effect Transistor and R-C Filters

PART III Au-PDMS NANOCOMPOSITE: PROPERTIES AND ELECTRICAL CHARACTERIZATION

LIST OF ACRONYMS

0D	Zero dimensional
1D	One dimensional
2D	Two dimensional
3D	Three dimensional
OP	Optical profiler
PVD	Physical vapor deposition
DOS	Density of States
CNTs	Carbon nanotubes
LED	Light emitting diode
IR	Infrared
PMMA	Polymethyl methacrylate
PDMS	Polydimethylsiloxane
PET	Polyethylene therephthalate
APTMS	(3-Aminopropyl)triethoxysilane
HOPG	Highly oriented pyrolytic graphite
AFM	Atomic force microscopy

PART I

OVERVIEW OF NANOPARTICLES AND NANOCOMPOSITES

I.1. Introduction

The prefix nano came from the Greek word νάνος or the Latin word nannus, both meaning dwarf. At the 11th Conférence Générale des Poids et Mesures (CGPM) in 1960 it was adopted as an official SI prefix, meaning 10^{-9} of an SI base unit.

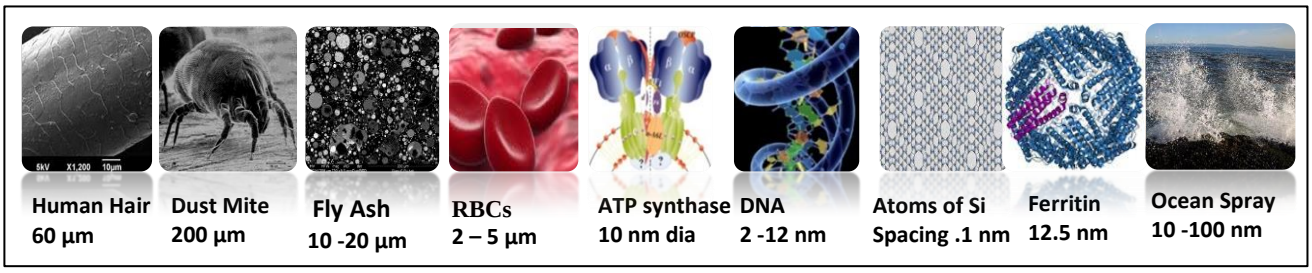

Figure I.1 From micro to nanoscale few natural examples which one comes across daily.

Study on fundamental relationship between physical properties and the material dimensions on the nanometer scale forms the basics of nanoscience.[1] The physical dimension of a material is along the X, Y and Z axes. Nanomaterials are defined as materials with at least one of the above mentioned dimensions in the range of 1-100 nanometers approximately.[1] Nanoparticles are objects with all three external

dimensions at the nanoscale. The properties of the nanomaterial are decided by its dimensions. The behavior of nanomaterials also depends on its surface area more rather than the composition of the particles. Relative-surface area is one of the principal factors that enhance its reactivity, strength and electrical properties.

The properties in macroscopic length scales, like physical, electronic and other properties, can be explained based on classical laws. But at the atomic and molecular length scales, the classical laws fail and quantum mechanics takes over in order to explain the properties and the phenomena. Nanoscale thus bridges the macroscopic and atomic scales.[2]

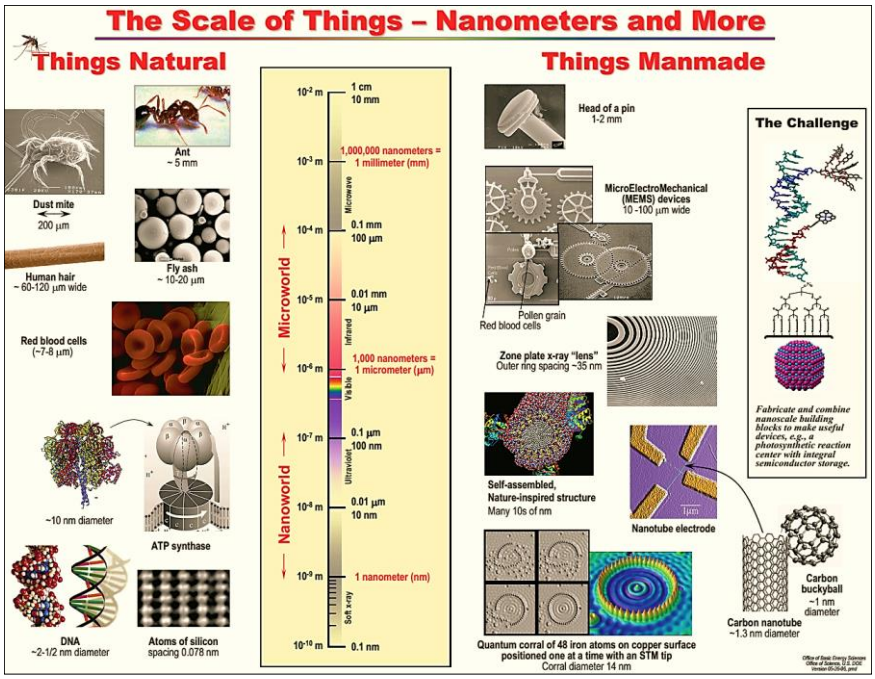

Figure I.2 Comparison between macro, micro and nanoscale with different examples both natural and engineered (reproduced from ref. (2)).

Nanotechnology is the applied stream of nanoscience.[1,3] It deals with the architectural designing at nanoscale. This engineered nanoparticles evolved, are designed with very specific properties related to shape, size, surface properties and chemistry. Engineered nanoparticles are generated via experimental procedures for example CNTs are produced by laser ablation, arc discharge, and chemical vapor

deposition (CVD). Examples of engineered nanomaterials include: carbon buckeyballs or fullerenes; carbon nanotubes; metal or metal oxide nanoparticles (e.g., gold, titanium dioxide);[4] quantum dots,[5] among many others.

Table I.1–Different categories of nanomaterials.[6]

Category of nanomaterials	Examples
0-dimensional nanomaterials	They are also known as nanoparticles and include colloids and quantum dots (tiny particles of semiconductor materials) and their subsets.
1-dimensional nanomaterials	This includes nanowires, nanofibres made from a variety of elements mostly carbon. Examples are nanotubes.
2-dimensional nanomaterials	This includes layers, thin films, platelets and surface coatings. They have been known for quite a long time and it is used mostly in the electronics industry.

Nanoparticles made of metals, semiconductors, or oxides are of particular interest for their mechanical, electrical, magnetic, optical, chemical and other properties. Nanoparticles have been used as quantum dots and as chemical catalysts. They bridge the bulk materials and atomic structures.

I.2 History of Nanomaterials

The first record of nanomaterials goes back to 2600 years ago when Indian sage "Kanada" proposed about the atomistic theory when atom was considered as an indestructible particle of matter. It was since ancient Roman times, 4th century A.D., when the roman colored glasses fabricated from colloidal particles of gold and silver dust, that nanomaterials came to picture. The extraordinary Lycurgus Cup, presently at British Museum still bears the evidence. It displays unique colors, appears green when observed in reflected light (daylight) and becomes red when light is propagated through it. This apparent dichroism is because of the light interaction of the gold particles embedded in the glass matrix of the cup.[7] Damascus steel was used

to produce blades since 500 AD in Damascus.[8] These blades are recognized for their resilience, sharpness, extreme strength and the appeal of their unique surface pattern. Researchers revealed the reason behind these special properties is due to the presence of multi-walled carbon nanotube in the material.[8]

Figure I.3 (a) Damascus blade used in 500A.D. Inset shows the detailing of the steel. (b) The dichroism of Lycurgus cup towards the direction of light illumination. (c) Gold sol prepared by Michael Faraday. Inset shows bulk gold which is yellow in color (reproduced from ref. (8), (9), (10)).[9]

Michael Faraday, the greatest scientist of his time, was the first person to report about the colloidal gold particles in the year 1857. He stated that "the divided state of the metal" was responsible for the various colors of the gold sol.[10] Thus began the investigation on nanostructured materials and it continued for over 70 years until 1940 when precipitated and fumed silica nanoparticles[11] were manufactured in USA and Germany. In the 1960s and 1970s metallic nanopowders for magnetic recording tapes came to picture.[12] In 1976, for the first time, nanocrystals produced by the inert-gas evaporation technique were published by Granqvist and Buhrman.

Probably the most celebrated visionary comment on the advancement of modern nanomaterials was catalyzed by physicist Richard Feynman in 1959 at a meeting of the American Physical Society.[13] Quoting his words "*There's plenty of room at the bottom*", he pioneered the fabrication of nanomaterials for miniaturization of devices. The discovery of fullerenes and carbon nanotubes around 1990s was the starting point of the new era "Nano age" which fast-tracked the quest to improve technological aspects by reducing dimension of every other material in a similar fashion.

I.3 Nanomaterials Unique from bulk

The dimension of the nanomaterial plays a vital role in deciding its properties. The reason is that here the dimension of the object becomes comparable to the mean free path of the electrons in it.[14] Thus the electrons begin to feel as if it is bound resulting in a dramatic change of the properties of the solid. The change depends on the number of atoms and electrons, in contrast to the properties arising from the atoms in bulk state.

I.3.1 Surface to Volume Ratio

Most reactions take place at the surface of a material. Thus the greater the surface area for a given volume, the greater will be the reactivity of the material. In nanotechnology we deal with particles which

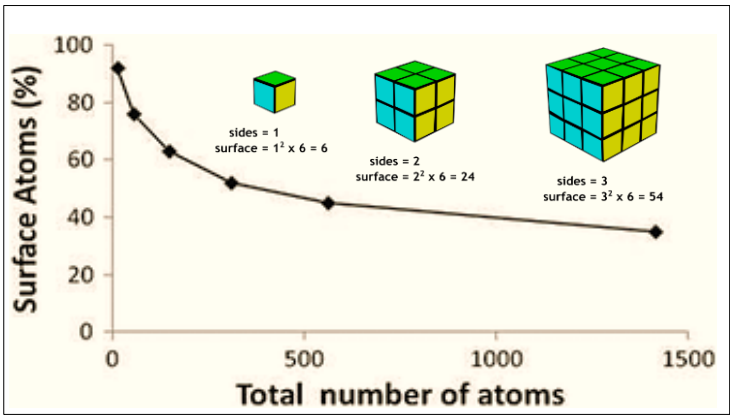

Figure I.4 Plot depicting the dependence of the percentage of the surface atoms on the number of atoms in a particle (reproduced from ref. 15).[15]

have dimension of few nanometers making their surface area to volume ratio dramatically high. This can be illustrated by taking a cube of sugar, which reacts with water and the water dissolves, the outside of the sugar. Now the same cube of sugar when fragmented into many little pieces, each cut makes new outer surfaces for the water to dissolve. Thus the same volume of sugar now has larger surface area.[16] This thus

proved that a particle with a high surface area has a greater number of reaction sites than a particle with low surface area, and thus, results in higher chemical reactivity.[17]

For tis reason at the macroscale, gold behaves as an inert element but at the nanoscale, gold nanoparticles become extremely reactive and can also be used as catalysts.[18] This increased reactivity for surface area to volume ratio can be seen in nature as well, for example in body's digestive system the villi inside the intestine. Within the small intestine, there are millions of folds known as villi that increase the surface area of the inner lining of the digestive tract allowing more nutrients and chemicals to be absorbed at the same time.[19]

I.3.2 Density of States

Density of states (DoS) of a system is the number of states per energy interval, at each energy level, available to be occupied by electrons.[20] High DoS at a specific energy level means that there are many

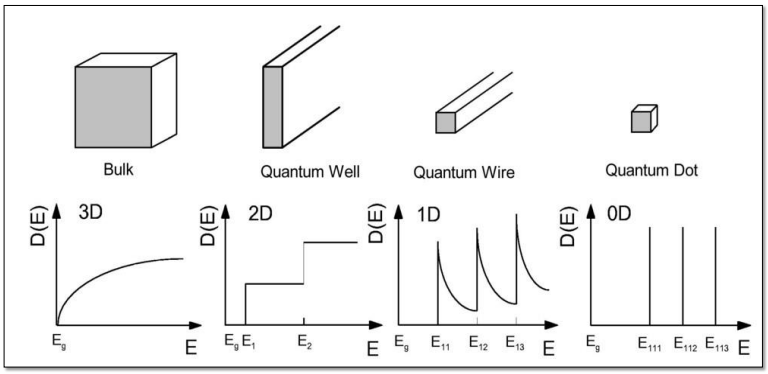

Figure I.5 DoS of the charge carriers for 3D, 2D, 1D and 0D materials (reproduced from ref. 22).

states available for occupation by the electrons. DoS is an average value over the space and time domains occupied by the system.

The DoS of a solid with electrons confined to one, two and three dimensions are named as 2D, 1D and 0D nanomaterials respectively, in comparison with the 3D material.[6,21]

$$DoS = dN/dE = (dN/dk) \times (dk/dE) \quad \text{..... (i)}$$

$$N(k) = \text{k space volume/ vol. per state} = (4/3\ \pi\ k^3) \times V/\ 8\pi^3 \quad \text{.....(ii)}$$

N(k) thus depends on the dimensionality of the system.

The relation between DoS and the energy for 0D, 1D, 2D in comparison with the 3D is given below.

Table I.2-DoS of for materials of different dimensionalities.[22]

Structure	Degree of Confinement	$\frac{dN}{dE}$
Bulk Material	0D	$\sqrt{E}$
Quantum Well	1D	1
Quantum Wire	2D	$1/\sqrt{E}$
Quantum Dot	3D	$\delta(E)$

I.3.3 Quantum Confinement

The quantum confinement effect is observed in particles whose size is too small almost comparable to the wavelength of the electron. As is known that materials in bulk exhibit extended band structures but with the decrement in size, spacing between the levels increases as is described qualitatively by particle in a box model. So as the particle size decreases to nanoscale one or more of its dimension will be confined making the energy levels discrete and this widens up the band gap leading to an increment of the band gap energy.[23]

The spacing between the energy levels is inversely proportional to the dimensions of the material given by the equation

$$\Delta E_n = (2n+1)\, h^2/8mL^2 \ldots\ldots\ldots\ldots\ldots\ldots (iii)$$

where h is Planck's constant, m is the electron mass, L is the dimension of the material and n is the quantum number. As discussed above the band gap and wavelength are inversely related to each other. Increase of bandgap energy means more energy, that is shorter wavelength, will be required for it to be absorbed by the bandgap of the material.[24] The wavelength of the fluorescent light emitted from the nano-sized material, will be higher, because of the quantum confinement so blue shift will occur.[25] Hence tuning of optical absorption or emission by a nano-sized semiconductor over a range of wavelengths is possible.

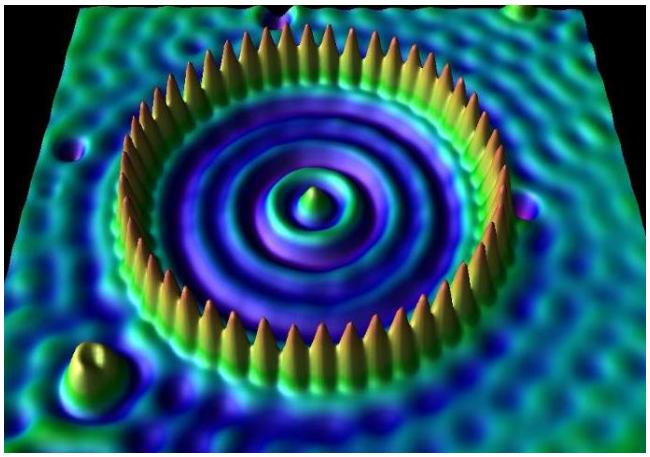

Figure I.6 Experimental evidence of the confined electronic wavefunctions in a quantum corral (reproduced from ref. 26).[26]

A breakthrough result was obtained in 1993 by Eigler et al. when he found quantum corrals, which are nothing but closed structures of single atoms. An ellipitical ring of iron atoms on a copper surface was formed by the tip of a low-temperature scanning tunneling microscope.[27] The ferromagnetic iron atoms reflected the surface electrons of the copper inside the ring into a wave like pattern, as predicted by the

theory of quantum mechanics. Interference effect of the confined electronic wavefunctions thus generated standing wave pattern of electrons, as was known theoretically till then. This was the first experimental mapping of quantum confinement, where the corral formed determines the quantum state of the electron. The invention of scanning probe microscopes to probe out the electronic wavefunctions of the atoms must be appreciated here.[28]

I.4 Synthesis of Nanomaterials

There are two general approaches for the synthesis of nanomaterials and fabrication of nanostructures.[29]

I.4.1 Bottom-Up Approach

Bottom-up methods involve assembly of atoms and molecules leading to the formation of nanospecies. This approach includes mostly chemical routes to assemble the nanoparticles. Self-assembly is one of the key for the assembly of nanomaterials in the bottom-up approach.[30]

The reactions here can be carried out in various phases like gas, liquid as well as solid. The physical forces operating at nanoscale are the ingredients to combine basic units into larger stable structures. The different processes which come under this approach are Pyrolysis, Inert gas condensation, Solvothermal reaction, Sol-gel fabrication etc.

I.4.2 Top-Down Approach

This approach uses larger initial structures, which are then externally-controlled and broken down to nanostructures. Top-down approach is more of a physical technique. Here a bulk material is chipped down to nano species. Physical energy in the form of mechanical, thermal and other high energy sources are used to synthesize the nanomaterials.

Cutting, milling and machining are employed in the mechanical approach.[31] Thermal process mostly exploits pyrolysis and sintering techniques. High energy sources like electric arcs, lasers, solar flux, electron beams etc. are used for the break down the material.[32]

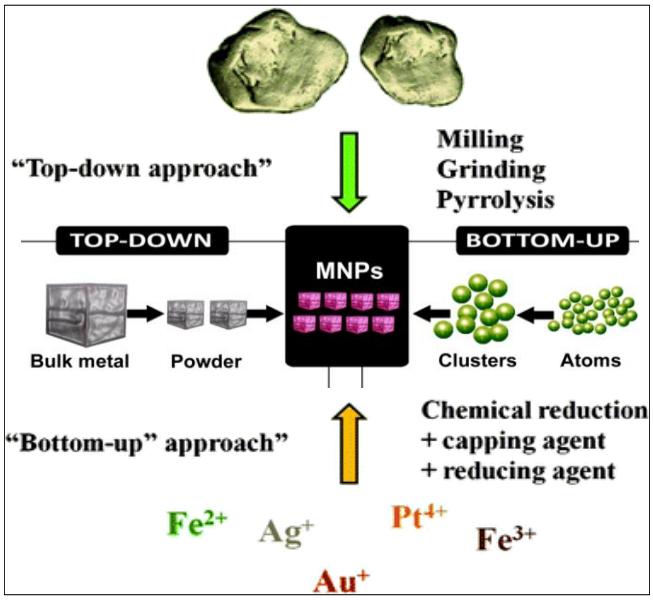

Figure I.7 Schematic representation of the top-down and bottom-up processes for the synthesis of nanomaterials (reproduced from ref. 33).[33]

These approaches use larger (macroscopic) initial structures, which can be externally-controlled in the processing of nanostructures. Other examples include etching through the mask, ball milling etc.

I.5 Properties of Nanomaterials

The nanoparticles exhibit peculiar properties completely different from the bulk. The novel properties which make nanoparticles so unique from its bulk counterpart are its melting point, boiling point, band gap, optical properties, electrical properties, magnetic properties. Among them the electronic, optical and magnetic properties[34] have been discussed below.

I.5.1 Electronic Properties

When electronic property is being dealt, the size of the particle must be kept in mind. As discussed earlier, the energy levels changes from continuum state to quantized and discrete levels as one moves from bulk to nano. The famous phenomenon known as size induced metal-insulator transition plays a role here as a consequence of the reduction in the size.[35] In quantum confinement it has been discussed that the size becomes comparable to de Broglie wavelength of conduction electrons.[36] Because of the reduced dimension there is a lot less electron-phonon scattering giving rise to ballistic transport and mobility value reaches ~10^7 cm^2/s-V in in-plane direction.[37] In nanoscale materials electrons can be steered, deflected and focused very similar to what one does in optics.

When the size is in nano regime, the difference between ionization potential (energy required to remove an electron) and electron affinity (energy gained to add an electron) depends on the diameter of the material.[38] This is known as charging energy given by,

$$C = U/2e \quad \text{..... (iv)}$$

where e is the electronic charge and C is the capacitance.

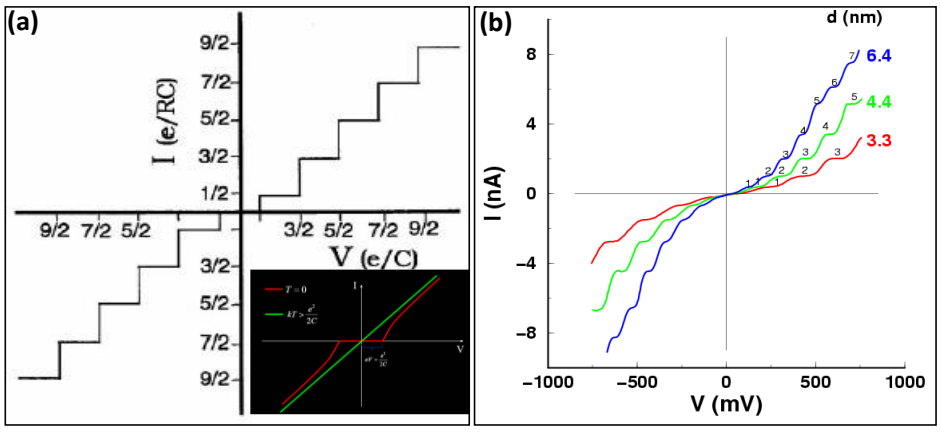

Figure I.8 (a) I-V spectra of nanocrystals (mapping of the charging spectrum) exhibiting Coulomb staircase phenomena. Inset shows the coulomb blockade region and its dependence on temperature. (b) I-V spectra of Pd nanocrystals of different sizes (reproduced from ref. 39).[39]

When electrons tunnel through a potential barrier into the cluster, the capacitance changes and block the entry of the next electron till a threshold potential of the charging field is applied. This phenomenon gives rise to Coulomb gap and Coulomb staircase,[40] which is nothing but low dimensional tunneling effect. Thus charging becomes quantized as can be seen in coulomb staircase, bringing us the discrete regime.[41] The resulting effect is that one can manipulate single electron to realize various functionalities, e.g., single electron transistor (SET) for logical gate or memory cell.[42]

I.5.2 Optical Properties

The optical properties of the nanomaterials were known since 4th century A.D. when Roman artists produced colorful stained glass windows.[43] The optical properties depends on how light interacts with a material which again is dependent on three main factors that is absorption, scattering and emission phenomenon.[44] In case of bulk metals, most of the light falling on the surface gets reflected. But when the size goes to the regime of nanoscale completely different phenomena occurs.[44]

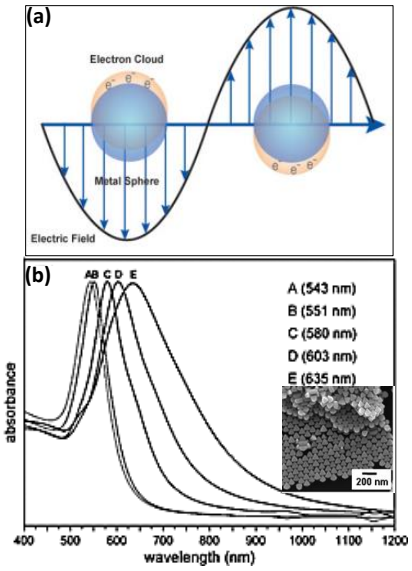

Figure I.9 (a) Schematic showing the oscillation of the conduction electrons in presence of electromagnetic radiation. (b) The SPR absorption spectra corresponding to the different sizes of the AuNPs. Inset shows the SEM image of the octahedral AuNPs (reproduced from 45).[45]

This happens because of what is known as surface plasmon resonance. Light is nothing but electromagnetic radiation, when the electric field component of radiation falls on any material it displaces the free electrons away from the nuclei to form a small dipole. The dipole gets restored to its normal position by the electrostatic interaction between electrons and nuclei, giving rise to an oscillation which gets modulated according to the electric field of the electromagnetic radiation.[46]

Unlike reflection in bulk metal, when both the frequency matches it gives rise to resonance resulting in the absorption. This phenomenon is termed as "surface plasmon resonance (SPR)"absorption. An important aspect for the phenomenon is the increased ratio of surface area to volume present in nanoscale materials. One example is the "quantum size effect" where the optical properties become a function of the particle diameter.[47] This effect is not visible when moving from macro to micro dimensions. It becomes pronounced only when the nanometer size range is reached.[48]

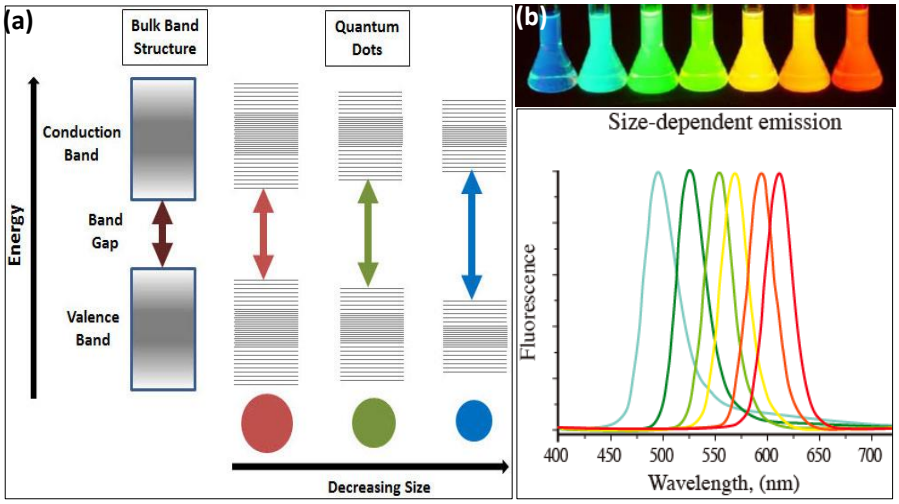

Figure I.10 (a) Band Gap formation with decreasing size of the particle. (b) Photograph showing the beautiful colors emitted by CdSe QDs of different sizes. Emission spectra as a function of size of the CdSe QDs (reproduced from ref. 49).[49]

The optical properties of metal nanoparticles can be tuned by varying the size and shape of the particle.[47] As can be seen from the graph how the SPR band shifts just by changing the diameter of the Au nanoparticle by 100 nm.[50] The shape of the nanoparticle also affects the absorption properties.[51]

Due to quantum confinement, of electrons and holes the band gap in semiconductor material at nanoscale increases.[52] The optical absorption and emission peaks shift towards lower wavelengths because higher energies will be absorbed by the increased band gap. Here also by tuning the size of the quantum dot the emission of the particle can be varied.[52] Thus quantized energy level depends on geometric dimension. This helps in tuning the absorption spectrum. The graph in Figure I.10 illustrates the spectrum for the CdSe quantum dots.[52]

I.5.3 Magnetic Properties

As the particle size is reduced the surface energy increases which leads to spontaneous change in polarization directions. The spontaneous change in such directions below a critical size leads to change in magnetic property.[53] For this reason most nanoparticles show paramagnetic behavior even though the bulk may be ferromagnetic in nature.[54] The paramagnetism thus exhibited is also not a common one. It is quite different from the normal paramagnetism one knows and hence named as superparamagnetism.[55] The coercivity of the nanomaterial strongly depends on its size. A large particle supports multidomain

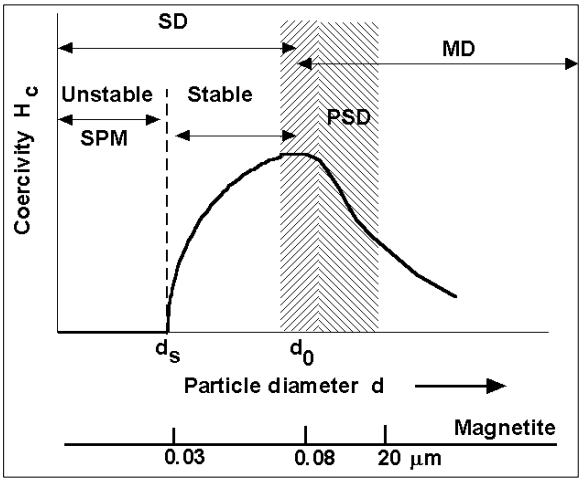

Figure I.11 Particle coercivity (Hc) versus particle diameter (d). The largest coercivity is observed at a particle size d corresponding to the transition from multidomain (MD) to single domain structure (SD) (reproduced from ref. 56).[56]

structure having low coercivity. In contrast, a single-domain particle can change direction of magnetization only by coherent rotation of spins, giving high coercivity value.

When size of the particle is very small, in nano regime, thermal fluctuation leads to low coercivity value giving rise to superparamagnetic nanoparticles. The name is so because its response to an external field is very fast but exhibit negligible coercivity. Superparamagnetic nanoparticles have a wide range of applications.[57]

I.6 Application of Nanomaterials

Nanomaterials because of their fascinating properties can be used in various electronic or optical devices. Their optical and electronic properties can be tuned by their size and shape which again can be changed by the process they are synthesized. Thus they can find application in optoelectronic devices such as organic solar cells, OLEDs etc.[58] These devices work on the principle of electron and energy transfer which is a photo induced process.

It has been reported that nanoparticles has been used as sensors for special purposes, pharmaceutical drugs and quantum dots. The physical properties of the nanomaterials play a very important role in their performance. The novel physical and chemical properties of nanomaterials pave way to design advanced bioelectronic device.[59]

I.7 Carbon Nanomaterial

Carbon (Latin, "Carbo" means coal) sitting in group 14 of the periodic table is the most versatile and unique element.[60] Its atomic number is 6 and exhibits catenation property (an element can form bonds with itself or with other elements) thus giving birth to a generation of organic compounds.[61]

Pure carbon due to its valency can be present in varieties of forms known as the allotropes of carbon.[62] Graphite is the most common among them. Other allotropes include diamond, soot and recently a new avatar has been discovered known as fullerene.[63] Fullerene is nothing but a caged molecule with a formula C_{60}. Carbon-based nanomaterials have attracted particular attention due to their unique structural and physical properties. Carbon nanomaterials are composed of sp^2 bonded graphitic carbon.[64]

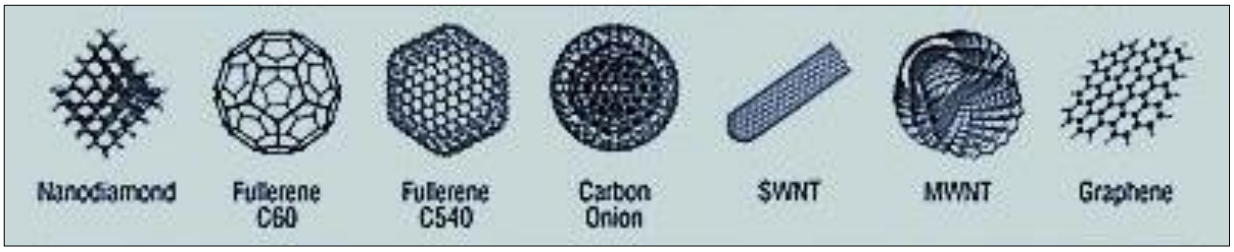

Figure I.12 Allotropes of carbon and carbon nanoparticles showing the varieties of structure it can form.

Among the carbon nanomaterials carbon nanotubes, fullerenes, and mesoporous carbon structures have properties quite different from other forms of carbon such as graphite and diamond. Unlike the conventional graphite phase, carbon nanostructures may be metallic or semiconductor. Due to the exceptional electrical, thermal and mechanical properties they have found application in varieties of field such as composite materials, energy storage,[65] sensors,[66] drug delivery[67] and nanoscale electronic devices. Graphene is perhaps the youngest of the carbon nanomaterials and promises to be a very active field. Already since its 'isolation' in 2004 it has grabbed the attention of the scientific as well as industrial world.[68] The number of publications on graphene rose from ca. 130 in 2005 to ca. 2,800 in 2010. Few of the carbon allotropes have been discussed below.

I.7.1 Graphite

Graphite is a naturally found product on earth in the form of minerals such as marble and gneiss. It comes from the Greek word “graphein” which means to draw or write. Graphite is formed of stacked, loosely

bound layers composed of interconnected hexagonal honeycomb rings of carbon atoms making it one of the softest materials known. It is a layered material with planar structure, with shorter in-plane bond length having a C-C bond distance of 0.142 nm. These layers are stacked together via weak van der Waals forces with a distance of 0.335 nm between the layers along the c-axis. Graphite has the distinction of being the only non-metallic substance which is an efficient conductor of electricity.[69] Its high thermal and electrical conductivity, soft and greasy texture and structural strength are amongst the most appealing physical properties.[70,71]

The two known forms of graphite, with hexagonal (ABABAB.. stacking) and rhombohedral (ABCABC.. stacking) stacking, have similar physical properties. Graphite being an anisotropic material, its properties are different in in-plane and out of plane.

I.7.2 Carbon Nanotubes

Carbon nanotubes are nothing but 1D carbon nanomaterials. They are single sheets of graphite rolled up into cylinders. The diameter of the tubes is in the nanometer regime. Typically a single walled nanotube has diameter of 1nm. The aspect ratio that is the ratio of length and diameter is high thus endorsing very unusual electrical property to it. Rolling up of few layers of graphite result in forming multi walled carbon nanotubes, which exhibit metallic behavior.[72]

I.7.3 Fullerenes

In 1996 Harold W. Kroto won the Nobel Prize for Chemistry for the discovery of a new allotrope of carbon. The new form was named Buckminsterfullerene. They are caged molecules having formula C_{60}. They possess good mechanical strength and electrical conductivity. Fullerenes are obtained by passing high current between two very close graphite electrodes in an inert atmosphere. Till date varieties of fullerenes have been produced like C70, C72, C76, C84 and even C100.[73]

I.7.4 Graphene

Graphene, an extraordinary, strong, 2D and single atom thick sp^2 carbon lattice, has caused waves of excitement in our scientific world. Graphene is world's strongest, thinnest (one atom thin), harder than diamond, transparent and bendable carbon nanomaterial.

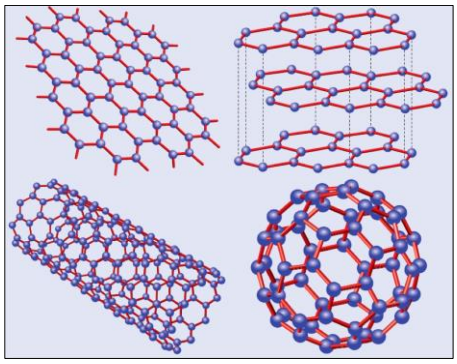

Figure I.13 Graphene, mother of all graphitic forms. Graphene is a 2D building material for carbon materials of all other dimensionalities. It can be stacked into 3D graphite, rolled into 1D nanotubes or wrapped up into 0D buckyballs (reproduced from ref. 74).[74]

It exhibits extraordinary fecundity thus inspiring the birth of new two-dimensional materials. It even garnered researchers a Nobel Prize in physics in 2010.[75-77] Graphene is a zero band gap material and the E–k relation is linear for low energies near the six corners of the hexagonal Brillouin zone. The charge

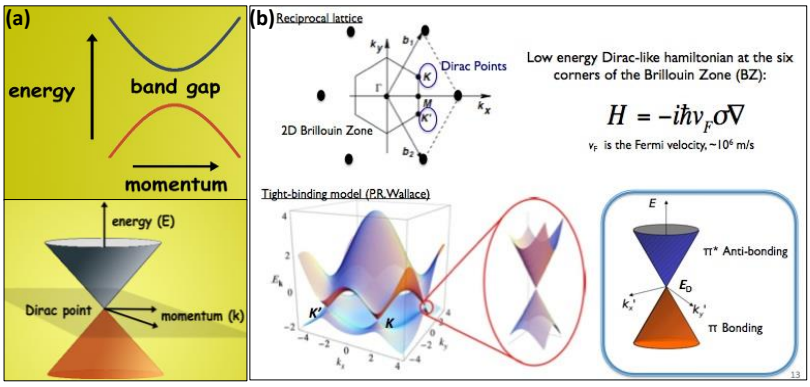

Figure I.14 (a) The band structure of graphene in the honeycomb lattice. (b) The enlarged picture shows the conical band structure close to one of the Dirac points (reproduced from ref. 78).[78]

carrier behaves as massless Fermi particles (zero effective mass). It behaves like relativistic particles which can be described by the Dirac equation for Fermions. Hence, charge carriers here are called Dirac Fermions which obey the Dirac equation.[79] The Fermi velocity $v_F \sim 10^6$ m/s. The six corners of the Brillouin zone are called the Dirac points. Graphene exhibits ambipolar electric field effect because of the presence of both electrons and holes as charge carriers. It is 97% transparent and absorbs only 2.3% of the incident visible light. Graphene, also exhibits the quantum Hall effect.[80] Thus, due to its intriguing electronic and optoelectronic properties, graphene has become a hot topic of research during the last decade.[81,82]

I.7.5 Turbostratic Graphite

Highly oriented pyrolytic graphite (HOPG) is synthetic graphite, produced by vacuum annealing process under high pressure or stress. Due to the annealing process most of the times the end product, that is graphene, will have some defects. One among them includes the defect of registry between the graphitic planes. The manner in which the stacking happens can be classified into two categories. Bernally stacked graphite, (ABABAB stacking), which has the registry of the carbon atoms between any two graphene layers.

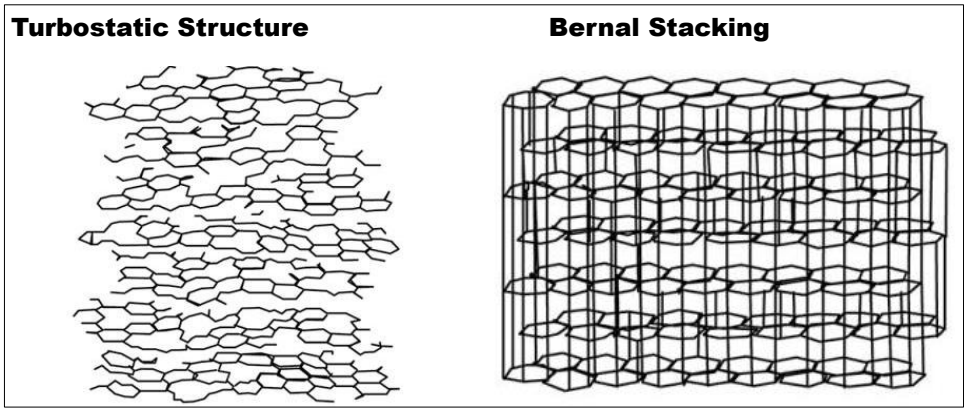

Figure I.15 A schematic representation of hexagonal turbostratic graphite as compared to a three dimensional Bernal-stacked graphite lattice (reproduced from ref. 83).[83]

The second type is the turbostratic graphite. Here each layer is rotated by a certain angle with respect to its neighbouring layer, thus there is lack of registry between two layers. This rotational disorder leads to the electronic decoupling among the graphene layers. The turbostratic graphite is also known as 2D graphite.[83] Mosaicity gives a measure of the angular mis-orientation between two graphene layers.

Raman gives information about the type of stacking of the layers along the c-axis. The shape of the 2D band indicates the stacking order of the graphite layers along the c-axis. For turbostratic graphite, 2D band is seen as single peak where as for Bernally stacked graphite, it is seen as a peak with a shoulder at lower wave number.

I.7.6 Nanocarbon- Raman Sensitive

Raman spectroscopy is used for studying low frequency modes like vibrational and rotational modes. Raman is a scattering phenomenon. It depends on inelastic scattering of photons by phonons and thus polarization changes. So Raman always needs a source for polarizing the molecule. Again this polarisability is a function of interatomic distance making Raman spectrum sensitive to small changes in the local bond lengths, bond angles to provide unique information about molecular morphology.[84]

- **D band**

It is known as the defective band. The breathing motion of six atom rings gives rise to this band. A defect is required for its activation. Thus perfect graphite with no defect won't give rise to D bands. This involves phonons of the k (k is the wave vector for the electronic transition) zone boundary of the brillouin zone. The phonon mode which satisfies the condition k=q/2 (q is the phonon wave vector) is the origin of the D peak with A_{1g} symmetry.

Its position is at 1350 cm^{-1} and changes with excitation energy. D band reveals the disorders in the electronic structure such as defects, grain boundaries, and functional groups in the sp^2 carbon lattice. The

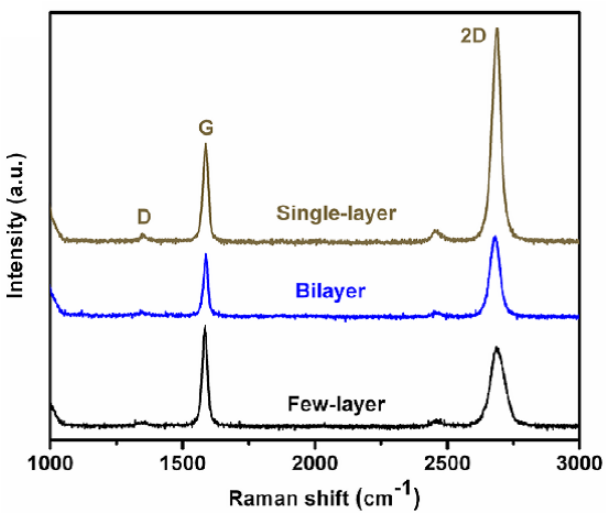

Figure I.16 Raman spectra from different types of sp^2 nanocarbons (reproduced from ref. 85).[85]

more intense the peak and greater the FWHM of the D band the more is the defect and lower is the electronic quality of the graphitic lattice.[86,87]

- **G band**

It is named as the graphitic band. The in-plane bond stretching of sp^2 carbon atoms gives rise to such band. G band occurs at all sp^2 sites and it does not require a defect to initiate it, unlike the D band. G band position is at 1580 cm^{-1}. Here the zone center phonons instead of zone boundary phonons, with E_{2g} symmetry are required for its origin. Dispersion is proportional to the degree of disorder. So G band also disperses more when the degree of defect or disorder is high.[88]

- **2D band**

If D band is taken as the fundamental, 2D band is nothing but its overtone. But it is only because of the position. As such D and 2D bands are completely different giving different information, complementary to each other. 2D band gives periodicity and how the graphene layers are stacked along the c-axis. Its position is at 2700 cm^{-1}.[86] The non-center zone boundary phonons are responsible for its origin. Double resonance Raman phenomenon is used to explain its genesis. For a single layer of graphene 2D band is

single and sharp with FWHM 20-30 cm^{-1}. But as the number of layers increase FWHM of 2D band increases. Thus more number of peaks are required to be fitted. The 2D band for single layer graphene and turbostratic graphite is similar, that is it shows a single peak. But in the case of turbostratic stacking, the FWHM of 2D band is 20-30 cm^{-1} higher as compared to the Bernal stacked one.[89,90]

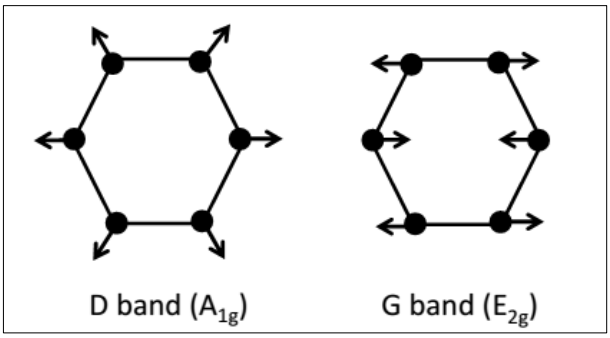

Figure I.17 Schematic representation of D and G bands.

The latter is thus known as 2D graphite also. As the disorder increases, D band will become more prominent compared to 2D band.[91,92]

I_D/I_G ratio: In Raman spectroscopy the I_D/I_G ratio gives the in-plane crystallite size (La)

$$\mathbf{La(nm) = 560/E^4_{laser}(I_D/I_G)^{-1}}$$ (E_{laser} is the laser excitation energy in eV.)

It thus shows the abundance of six-fold aromatic rings and gives information of the sp^2 carbon cluster area.

I_G/I_{2D} ratio: This ratio bestow upon the number of graphene layers. The ratio is 0.2-0.4 for a single layer. But as the number of layers increase the ratio changes. It becomes 0.5-4 for a few layer graphene.[91]

I.8 Nanocomposites

Nanocomposites are materials where nanosized particles are incorporated into a matrix of another material. The reinforced material must have one of the dimensions in the nanometer range among them the most popular ones are nanoparticles, nanofibers and nanoclays. They are having smaller filer size so the surface to volume ratio increases drastically. The result of embedding the nanoparticles in a matrix shows drastic improvement in properties such as mechanical strength, toughness and electrical or thermal conductivity. The property thus obtained can be a mixture of that possessed by the materials or maybe a completely new property unknown to the parental material.[93]

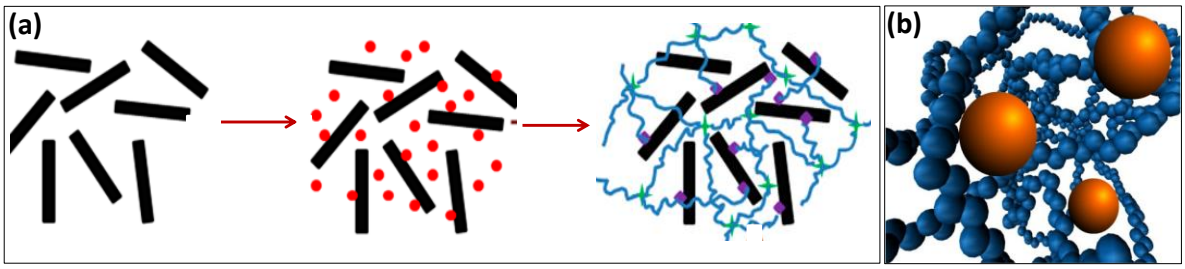

Figure I.18 (a) Steps showing how a nanocomposite is formed. (b) The nanoparticle lying inside matrix of the nanocomposite (reproduced from ref. 94).

The properties of nano-composite materials thus depend on the properties of their individual parents and also on the morphology, size and shape of the nanoparticles used and also on the interfacial characteristics.[94] Nanocomposites are well known in the research field. Effort is being made to control the nanoscale structures via innovative synthetic approaches so that varieties of novel properties of the nanocomposite can be achieved.

Experimentally it has been shown that all types of nanocomposite materials lead to new or else improved properties rather than their macrocomposite counterparts. Hence it paves way to new applications in fields such as mechanics, non-linear optics, battery cathodes, nano-wires, sensors and other systems.[95]

1.8.1 Polymer Nanocomposite

This consists of a polymer having nanoparticles dispersed in the polymer matrix.[96] Polymer nanoscience is the study about polymer-nanoparticle matrices, where nanoparticles must have least one of the dimension in the nanometer regime.

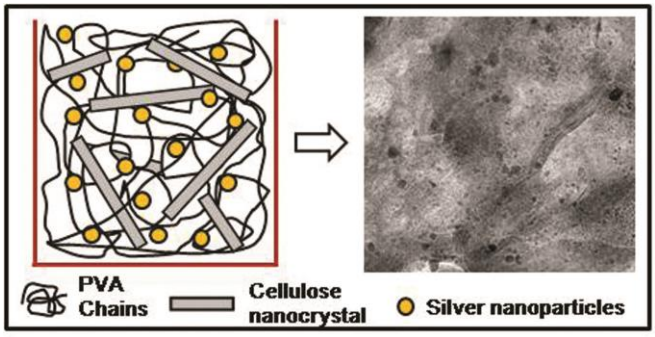

Figure I.19 Hybrid nanocomposite of cellulose nanocrystals and silver nanoparticles as reinforcing fillers for the polymer PVA (reproduced from ref. 97).[97]

As discussed earlier, with decrement in particle size there is increase in surface area-to-volume ratio, which leads to dominant behavior of atoms on the surface area of the particle inside the matrix. This affects the interaction of the particles within the composite. The interaction of the nanoparticle with other particles within the mixture increases. Hence improvements of the properties like strength, heat resistance, etc. are visible.

Polymer nanocomposites will soon generate smart membranes, new catalysts and sensors and new generation of smart microelectronic, photonic components and systems, imaging, therapy and controlled release properties.[98] The real potential however will remain untapped, until the nanoscale mechanisms responsible for such properties are unveiled and are exploited.

- Metal nanoparticle polymer nanonomposites

Here metal nanoparticles are incorporated inside polymer matrix to improve the mechanical and electrical property of the nanocomposite.[99] As is known metal nanoparticles exhibit quite unique optical and electronic properties than their bulk form. When reinforced inside a polymer it changes the behavior of the conventional polymer as such because of the increased inter particle interaction.[100] The most common polymers used are PAN, PP, PMMA, PVC etc. Metal naocomposite shows very interesting functional application because the properties of the nanosized metals stays unmodified mostly even after it is embedded in the polymer sea. This nanocomposite will surely represent an adequate solution to the present and future technological demands because of their novel properties.[101]

References

1 G. L. Hornyak, J. J. M., H. F. Tibbals and J. Dutta. *Fundamentals of Nanotechnology*. (CRC Press, 2008).

2 *U.S. Department of Energy*,<http://science.energy.gov/bes/news-and-resources/scale-of-things-chart/>(2006) (last accessed: 1st April,2014).

3 al., T. P. e. *A text book of Nanoscience and Nanotechnology*. (Tata McGraw Hill Education pvt Ltd, 2013).

4 Niederberger, M. & Garnweitner, G. Organic Reaction Pathways in the Nonaqueous Synthesis of Metal Oxide Nanoparticles. *Chemistry – A European Journal* 12, 7282-7302, (2006).

5 Alivisatos, A. P. Semiconductor Clusters, Nanocrystals, and Quantum Dots. *Science* 271, 933-937, (1996).

6 Siegel, R. W. *Nanophasematerials, In Encyclopedia of Applied Physics*. Vol. 11 1-27 (ed.Weinheim:VCH, 1994).

7 Tait, H. *Five thousand years of glass*. (The British Museum Press, 1991).

8 Verhoeven, J. & Pendray, A. The mystery of the Damascus sword. *Muse* 2, 35-43, (1998).

9 Freestone, I., Meeks, N., Sax, M. & Higgitt, C. The Lycurgus cup—a roman nanotechnology. *Gold Bulletin* 40, 270-277, (2007).

10 Faraday, M. *Philosophical Transactions of the Royal Society of London* 147, (1857).

11 Rao, K. S., El-Hami, K., Kodaki, T., Matsushige, K. & Makino, K. A novel method for synthesis of silica nanoparticles. *Journal of Colloid and Interface Science* 289, 125-131, (2005).

12 Omoto, H., Pyun, D. C. H. & Yoo Yoshida T. (Google Patents, 2011).

13 Feynman, R. P. *Caltech Eng. Sci* 23, (1960).

14 Huang, C., Feng, Y., Zhang, X., Li, J. & Wang, G. Electron mean free path model for rectangular nanowire, nanofilm and nanoparticle. *Physica B: Condensed Matter* 438, 17-21, (2014).

15 Primo, A., Corma, A. & García, H. Titania supported gold nanoparticles as photocatalyst. *Physical Chemistry Chemical Physics* 13, 886-910, (2011).

16 Edelstein, A. S. & Cammaratra, R. *Nanomaterials: synthesis, properties and applications*. (CRC Press, 1998).

17 Bond, G. C. Heterogeneous catalysis. (1987).

18 Haruta, M. Catalysis: gold rush. *Nature* 437, 1098-1099, (2005).

19 Wilson, J. P. Surface area of the small intestine in man. *Gut* 8, 618-621, (1967).

20 Harrison, W. A. Electronic Structure and the Properties of Solids. (1989).

21 García-Calzón, J. A. & Díaz-García, M. E. Synthesis and analytical potential of silica nanotubes. *TrAC Trends in Analytical Chemistry* 35, 27-38, (2012).

22 Kittel, C. & McEuen, P. *Introduction to solid state physics*. Vol. 8 (Wiley New York, 1986).

23 Vladimir V. Mitin, D. I. S., Nizami Z. Vagidov. *Quantum Mechanics for Nanostructures*. (Cambridge University Press, 20-May-2010).

24 Wang, J.-J., Hu, J.-S., Guo, Y.-G. & Wan, L.-J. Eco-friendly visible-wavelength photodetectors based on bandgap engineerable nanomaterials. *Journal of Materials Chemistry* 21, 17582-17589, (2011).

25 Raza, S., Yan, W., Stenger, N., Wubs, M. & Mortensen, N. A. Blueshift of the surface plasmon resonance in silver nanoparticles: substrate effects. *Opt. Express* 21, 27344-27355, (2013).

26 Ma, J. Visitors' Interpretations of Images of the Nanoscale. *Nanoscale Informal Science Education Network, July*, (2008).

27 Crommie, M. F., Lutz, C. P. & Eigler, D. M. Confinement of Electrons to Quantum Corrals on a Metal Surface. *Science* 262, 218-220, (1993).

28 Wiesendanger, R. *Scanning probe microscopy and spectroscopy: methods and applications*. (Cambridge University Press, 1994).

29 Wang, X., Zhuang, J., Peng, Q. & Li, Y. A general strategy for nanocrystal synthesis. *Nature* 437, 121-124, (2005).

30 Minelli, C. *Bottom-up approaches for organizing nanoparticles with polymers*, Section De Chimie Et Genie Chimique Pour L'obtention Du Grade De Docteur ÈS Sciences Par laurea in fisica, Università degli Studi di Firenze, (2004).

31 Rao, C. N. R., Kulkarni, G. U., Thomas, P. J. & Edwards, P. P. Metal nanoparticles and their assemblies. *Chemical Society Reviews* 29, 27-35, (2000).

32 Kelsall, R. W., Hamley, I. W., Geoghegan, M. & Wiley, J. *Nanoscale science and technology*. (Wiley Online Library, 2005).

33 Teow, Y., Asharani, P., Hande, M. P. & Valiyaveettil, S. Health impact and safety of engineered nanomaterials. *Chemical Communications* 47, 7025-7038, (2011).

34 Ghorai, S. *Chemical, phsical and mechanical properties of nanomaterials and its applications*, Universit of Iowa, (2013).

35 Edwards, P., Johnston, R., Rao, C., Tunstall, D. & Hensel, F. The metal–insulator transition: a perspective. *Philosophical Transactions of the Royal Society of London. Series A: Mathematical, Physical and Engineering Sciences* 356, 5-22, (1998).

36 Bhushan, B. *Handbook of Nanotechnology*. (Springer, 2004).

37 Berger, C., Song, Z., Li, T., Li, X., Ogbazghi, A. Y., Feng, R., Dai, Z., Marchenkov, A. N., Conrad, E. H., First, P. N. & de Heer, W. A. Ultrathin Epitaxial Graphite: 2D Electron Gas Properties and a Route toward Graphene-based Nanoelectronics. *The Journal of Physical Chemistry B* 108, 19912-19916, (2004).

38 An analytic relationship between size and ionization potential of transition-metal clusters. *Chemical Physics Letters* 254, 21, (1996).

39 Rao, C., Kulkarni, G., Thomas, P. J. & Edwards, P. P. Size-dependent chemistry: Properties of nanocrystals. *Chemistry-a European Journal* 8, 28-35, (2002).

40 Song, B., Ryndyk, D. A. & Cuniberti, G. Molecular junctions in the Coulomb blockade regime: Rectification and nesting. *Physical Review B* 76, 045408, (2007).

41 P. J. Thomas, G. U. K. a. C. N. R. R. *Chem. Phys. Lett.* 321, (2000).

42 Wei, W., Jie, H. & Lombardi, F. in *Nanoscale Architectures (NANOARCH), IEEE/ACM International Symposium*, 16-23, (2011)

43 http://www.metmuseum.org/toah/hd/glas/hd_glas.htm (last accessed 1st April, 2014).

44 Puzder, A., Williamson, A. J., Reboredo, F. A. & Galli, G. Structural Stability and Optical Properties of Nanomaterials with Reconstructed Surfaces. *Physical Review Letters* 91, 157405, (2003).

45 Sajanlal, P. R., Sreeprasad, T. S., Samal, A. K. & Pradeep, T. Anisotropic nanomaterials: structure, growth, assembly, and functions. *Nano Reviews* 2, 5883_5881-5883_5862, (2011).

46 K. L. Kelly, E. C., L. L. Zhao and G. C. Schatz. *J. Phys. Chem. B* 107, (2002).

47 Jain, P. K., Lee, K. S., El-Sayed, I. H. & El-Sayed, M. A. Calculated absorption and scattering properties of gold nanoparticles of different size, shape, and composition: applications in biological imaging and biomedicine. *The Journal of Physical Chemistry B* 110, 7238-7248, (2006).

48 Mock, J. J., Barbic, M., Smith, D. R., Schultz, D. A. & Schultz, S. Shape effects in plasmon resonance of individual colloidal silver nanoparticles. *The Journal of Chemical Physics* 116, 6755-6759, (2002).

49 Torchynska, T. & Vorobiev, Y. *Semiconductor II-VI Quantum Dots with Interface States and Their Biomedical Applications*. (2011).

50 N. N. Long, L. V. V., C. D. Kiem, S. C. Doanh, C. T. Nguyet, P. T. Hang, N. D.Thien and L. M. Quynh. *J. Phys.: Conference Series*. Vol. 187 012026 (2009).

51 Eustis, S. & El-Sayed, M. A. Why gold nanoparticles are more precious than pretty gold: Noble metal surface plasmon resonance and its enhancement of the radiative and nonradiative properties of nanocrystals of different shapes. *Chemical Society Reviews* 35, 209-217, (2006).

52 http://nanocluster.mit.edu/research.php (last accessed: 1st April,2014).

53 Peddis, D., Cannas, C., Musinu, A. & Piccaluga, G. Magnetism in Nanoparticles: Beyond the Effect of Particle Size. *Chemistry – A European Journal* 15, 7822-7829, (2009).

54 Leslie-Pelecky, D. L. & Rieke, R. D. Magnetic Properties of Nanostructured Materials. *Chemistry of Materials* 8, 1770-1783, (1996).

55 Gupta, N. B. a. A. *J. Mater. Res.* 26, (2011).

56 Schmid, G. in *Nanoparticles* 1-3 (Wiley-VCH Verlag GmbH & Co. KGaA, 2005).

57 Neuberger, T., Schöpf, B., Hofmann, H., Hofmann, M. & von Rechenberg, B. Superparamagnetic nanoparticles for biomedical applications: Possibilities and limitations of a new drug delivery system. *Journal of Magnetism and Magnetic Materials* 293, 483-496, (2005).

58 Stateikina, I. *Optoelectronic Semiconductor Devices-Principals and Characteristics*, Concordia University, (2002).

59 ongjun Li, Y. G. a. H. L. *Smart Nanomaterials for Sensor Application*. 3-41 (Bentham Science).

60 Particle Data, G., Wohl, C. G., Cahn, R. N., Rittenberg, A., Trippe, T. G., Yost, G. P., Porter, F. C., Hernandez, J. J., Montanet, L., Hendrick, R. E., Crawford, R. L., Roos, M., Törnqvist, N. A., Höhler, G., Aguilar-Benitez, M., Shimada, T., Losty, M. J., Gopal, G. P., Walck, C., Shrock, R. E., Frosch, R., Roper, L. D., Trower, W. P. & Armstrong, B. Review of particle properties. *Reviews of Modern Physics* 56, S1-S299, (1984).

61 Pauling, L. *The Nature of the Chemical Bond*. (Cornell University Press, 1960).

62 Rao, C. N. R., Sood, A. K., Subrahmanyam, K. S. & Govindaraj, A. Graphene: The New Two-Dimensional Nanomaterial. *Angewandte Chemie International Edition* 48, 7752-7777, (2009).

63 http://nanogloss.com/nanotubes/the-history-of-carbon-nanotubes-who-invented-the-nanotube/axzz2wsdIWfwp (last accessed: 1st April, 2014).

64 Hirsch, A. The era of carbon allotropes. *Nat Mater* 9, 868-871, (2010).

65 Zhang, H., Cao, G., Wang, Z., Yang, Y., Shi, Z. & Gu, Z. Growth of Manganese Oxide Nanoflowers on Vertically-Aligned Carbon Nanotube Arrays for High-Rate Electrochemical Capacitive Energy Storage. *Nano Letters* 8, 2664-2668, (2008).

66 Llobet, E. Gas sensors using carbon nanomaterials: A review. *Sensors and Actuators B: Chemical* 179, 32-45, (2013).

67 Bianco, A., Kostarelos, K. & Prato, M. Applications of carbon nanotubes in drug delivery. *Current Opinion in Chemical Biology* 9, 674-679, (2005).

68 Gilje, S., Han, S., Wang, M., Wang, K. L. & Kaner, R. B. A Chemical Route to Graphene for Device Applications. *Nano Letters* 7, 3394-3398, (2007).

69 Sengupta, R., Bhattacharya, M., Bandyopadhyay, S. & Bhowmick, A. K. A review on the mechanical and electrical properties of graphite and modified graphite reinforced polymer composites. *Progress in Polymer Science* 36, 638-670, (2011).

70 Brodie, B. C. On the Atomic Weight of Graphite. *Philosophical Transactions of the Royal Society of London* 149, 249-259, (1859).

71 Robertson, J. Hard amorphous (diamond-like) carbons. *Progress in Solid State Chemistry* 21, 199-333, (1991).

72 R. Saito, G. D., and M. S. Dresselhaus. *Physical Properties of Carbon Nanotubes*. (Imperial College Press, 1998).

73 Dresselhaus, M. S. D., G.; Eklund, P. C. *Science of Fullerenes and Carbon Nanotubes*. (Academic Press, 1996).

74 Neto, A. C., Guinea, F. & Peres, N. M. Drawing conclusions from graphene. *Physics World* 19, 33, (2006).

75 Novoselov, A. K. G. a. K. S. *Nat. Mat.* 6, (2007).

76 Novoselov, K. S., Geim, A. K., Morozov, S. V., Jiang, D., Zhang, Y., Dubonos, S. V., Grigorieva, I. V. & Firsov, A. A. Electric Field Effect in Atomically Thin Carbon Films. *Science* 306, 666-669, (2004).

77 Gusynin, V. P. & Sharapov, S. G. Unconventional Integer Quantum Hall Effect in Graphene. *Physical Review Letters* 95, 146801, (2005).

78 Castro Neto, A. H., Guinea, F., Peres, N. M. R., Novoselov, K. S. & Geim, A. K. The electronic properties of graphene. *Reviews of Modern Physics* 81, 109-162, (2009).

79 Wallace, P. R. The Band Theory of Graphite. *Physical Review* 71, 622-634, (1947).

80 Jiang, Z., Zhang, Y., Tan, Y. W., Stormer, H. L. & Kim, P. Quantum Hall effect in graphene. *Solid State Communications* 143, 14-19, (2007).

81 Ezawa, M. Peculiar width dependence of the electronic properties of carbon nanoribbons. *Physical Review B* 73, 045432, (2006).

82 Li, L., Wu, G., Yang, G., Peng, J., Zhao, J. & Zhu, J.-J. Focusing on luminescent graphene quantum dots: current status and future perspectives. *Nanoscale* 5, 4015-4039, (2013).

83 Miremadi, B. K. & Colbow, K. A hydrogen selective gas sensor from highly oriented films of carbon, obtained by fracturing charcoal. *Sensors and Actuators B: Chemical* 46, 30-34, (1998).

84 Pimenta, M. A., Dresselhaus, G., Dresselhaus, M. S., Cancado, L. G., Jorio, A. & Saito, R. Studying disorder in graphite-based systems by Raman spectroscopy. *Physical Chemistry Chemical Physics* 9, 1276-1290, (2007).

85 Wu, W., Yu, Q., Peng, P., Liu, Z., Bao, J. & Pei, S.-S. Control of thickness uniformity and grain size in graphene films for transparent conductive electrodes. *Nanotechnology* 23, 035603, (2012).

86 Dresselhaus, M. S. J., Ado Hofmann, Mario Dresselhaus, Gene Saito, Riichiro. Perspectives on carbon nanotubes and graphene Raman spectroscopy. *Nano letters* 10, 751-758, (2010).

87 Matthews, M. J., Pimenta, M. A., Dresselhaus, G., Dresselhaus, M. S. & Endo, M. Origin of dispersive effects of the Raman band in carbon materials. *Physical Review B* 59, R6585-R6588, (1999).

88 Ferrari, A. C. Raman spectroscopy of graphene and graphite: disorder, electron–phonon coupling, doping and nonadiabatic effects. *Solid State Communications* 143, 47-57, (2007).

89 Everhart, C. L. AFM-Assisted Etching and Electrical Characterization of Graphene.

90 Mak, K. F., Shan, J. & Heinz, T. F. Electronic Structure of Few-Layer Graphene: Experimental Demonstration of Strong Dependence on Stacking Sequence. *Physical Review Letters* 104, 176404, (2010).

91 Ferrari, A. C. R., J. Interpretation of Raman spectra of disordered and amorphous carbon. *Physical Review B* 61, 14095-14107, (2000).

92 Ferrari, A. C., Meyer, J. C., Scardaci, V., Casiraghi, C., Lazzeri, M., Mauri, F., Piscanec, S., Jiang, D., Novoselov, K. S., Roth, S. & Geim, A. K. Raman Spectrum of Graphene and Graphene Layers. *Physical Review Letters* 97, 187401, (2006).

93 Chen, L., Rende, D., Schadler, L. S. & Ozisik, R. Polymer nanocomposite foams. *Journal of Materials Chemistry A* 1, 3837-3850, (2013).

94 Ray, S. S. & Bousmina, M. *Polymer nanocomposites and their applications*. (American Scientific Stevenson Ranch, CA, 2006).

95 Lalwani, G., Henslee, A. M., Farshid, B., Lin, L., Kasper, F. K., Qin, Y.-X., Mikos, A. G. & Sitharaman, B. Two-Dimensional Nanostructure-Reinforced Biodegradable Polymeric Nanocomposites for Bone Tissue Engineering. *Biomacromolecules* 14, 900-909, (2013).

96 Lu, X., Zhang, W., Wang, C., Wen, T.-C. & Wei, Y. One-dimensional conducting polymer nanocomposites: Synthesis, properties and applications. *Progress in Polymer Science* 36, 671-712, (2011).

97 Kumar, A. P., Depan, D., Singh Tomer, N. & Singh, R. P. Nanoscale particles for polymer degradation and stabilization—trends and future perspectives. *Progress in Polymer Science* 34, 479-515, (2009).

98 Chung, J. H.-Y., Simmons, A. & Poole-Warren, L. A. Non-degradable polymer nanocomposites for drug delivery. *Expert Opinion on Drug Delivery* 8, 765-778, (2011).

99 Shirakawa, H., Louis, E. J., MacDiarmid, A. G., Chiang, C. K. & Heeger, A. J. Synthesis of electrically conducting organic polymers: halogen derivatives of polyacetylene, (CH). *Journal of the Chemical Society, Chemical Communications*, 578-580, (1977).

100 Reddy, K. R., Lee, K.-P., Lee, Y. & Gopalan, A. I. Facile synthesis of conducting polymer–metal hybrid nanocomposite by in situ chemical oxidative polymerization with negatively charged metal nanoparticles. *Materials Letters* 62, 1815-1818, (2008).

101 Pillalamarri, S. K., Blum, F. D., Tokuhiro, A. T. & Bertino, M. F. One-Pot Synthesis of Polyaniline−Metal Nanocomposites. *Chemistry of Materials* 17, 5941-5944, (2005).

PART II

GRAPHENE AND TURBOSTRATIC GRAPHITE: PROPERTIES AND APPLICATION

Summary

Graphene is known for its versatility and its usage in various functional electronic and optoelectronic devices. Graphene with its extraordinary properties made itself the pivot and the most intricate fragment of this project. This project examines on how to obtain few layers of graphene and its characterization. Amorphous carbon obtained in such attempts was used to check the IR photoconductive response. Finally RC filter and transistor action have been checked for pencil trace on paper.

Four methods were employed to obtain graphene. Two of them were electrochemical and the other two, physical methods. Raman being sensitive to carbon materials it was used for characterization of the graphene obtained by the above mentioned techniques. The electrochemical methods include: (i) Electrochemical delamination method and (ii) Thermal annealing of Ni electroplated carbon materials. The electrochemical delamination method was used to obtain large area graphene on soft substrates like, PMMA.

**Experiments were done in collaboration with Dr. Narendra Kurra..*

The electrolyte used was NaOH and graphite rod and Ni/graphene was used as anode and cathode respectively. The obtained few layers of graphene on PMMA were placed on a SiO_2/Si substrate and graphene was transferred on the Si substrate by dissolving the PMMA using acetone. For the electroplating method pencil, carbon-fiber and polymethylmethacrylate (PMMA) was used as carbon sources. Graphene layers were directly grown on the insulating substrates via thermal annealing (700 °C) of the carbon sources in presence of Ni catalyst. However in such attempts amorphous carbon films (as observed by Raman) were obtained. All these methods involved chemicals and wet synthesis in chemical laboratories. The objective was thus to develop a solvent free, room temperature, simple and direct method for obtaining graphene on any substrate. The physical methods includes: (i) Scotch tape technique (ii) Electrostatic delamination (iii) Pencil trace on paper. First the well-known scotch tape technique was used and few layers of graphene were obtained on SiO_2/Si substrate. For the electrostatic method high voltage was applied between two electrodes which were kept at close proximity. HOPG was attached to one electrode and substrate was kept on the other electrode. Due to application of electric field graphene layers should get delaminated and settle on the substrate. The obtained result was amorphous carbon and not few layer graphene as confirmed by Raman spectroscopy.

A study of the infrared (IR) photoconductive responses of graphitic films was investigated for amorphous carbon obtained on Si substrate by thermal annealing of Ni electroplated carbon materials. Literature survey on the photoconductive nature of the graphene films reports that it is due to the generation of photoexcited charge carriers, whereas the photoresponse of the bulk graphitic films is bolometric in nature where the resistance changes are due to thermal effects. The IR photoresponse from these graphitic films were correlated with the Raman peak intensities which were very sensitive to the nature of the graphene deposited.

Pencil drawing on paper is nothing but graphite of turbostratic nature, confirmed by Raman studies. The turbostratic graphite is essentially a 2D system. Due to electronic decoupling of the graphene layers, it was predicted that they may have some electronic properties similar to those of graphene. Pencil drawings

have been employed as resistor and an ion gel, 1-butyl-3-methyl-imidazolium octylsulfate mixed with PDMS as dielectric for the fabrication of paper based RC filters. The filter produced showed a cut-off frequency of ~ 9 kHz. Ambipolar electric field effect was observed for the pencil-traces on paper at low operating voltages with the aid of an ion gel as gate dielectric. The carrier mobilities were found to be ~ 106 and 59 cm^2/Vs for holes and electrons respectively. Mobility value showed only 15% variation among the few devices tested, truly remarkable given the simplicity of the fabrication process.

II.1. LARGE AREA GRAPHENE OBTAINED BY PHYSICAL AND CHEMICAL METHODS: INFRARED PHOTOCONDUCTIVE RESPONSE

II.1.1 Introduction

Graphene, an extraordinary, strong, 2D and single atom thick, sp^2 carbon lattice fascinating material,[1] has caused waves of excitement in our scientific world.[2] The charge carriers in graphene behave like massless Dirac Fermions[3] and also exhibit unique properties[4,5] such as ambipolar electric field effect and quantum Hall effect.[6,7] Its application in electronics,[8] optics,[9] quantum theory[7] and mechanics[10] have attained the epic in today's research.[11]

The charge carriers in graphene shows ballistic transport with very high mobility 15,000 cm^2/Vs.[12] This remains unaffected even when lateral dimensions is changed to micrometer range.[13] The electronic properties of graphene[14] shows semi-metallic behavior[15] and it can be tuned to semiconducting state by changing the lateral dimensions.[16] The reduction in mobility values of the charge carriers due to edge effects may limit the usage of graphene in electronic applications.[17] There have been attempts like chemical exfoliation, liquid-phase exfoliation[18] and chemical vapor deposition[19] to obtain large area graphene.[20,21] These methods produce randomly distributed graphene sheets on a given substrate. Thus locating them for device fabrication becomes difficult. In order to exercise a control over the site specific placement of graphene,[22] methods such as electrostatic exfoliation[23] and site specific stamping of graphite have been developed.

A large amount of intraband and interband transitions in the valence and conduction bands is observed in graphene.[24] Due to this graphene absorbs over a wide range of electromagnetic radiation. Because of its

high mobility value 15000 cm^2/Vs, graphene has been exploited to fabricate ultrafast photodetectors.[25] The photoresponse from graphene based on p-n junction, fast hot carrier in graphene and the generation of photocurrents have been investigated.[26,27] For hot-electron bolometer, demonstrated using graphene,[28] the resistance changes because of thermal effects and not photoexcited charge carriers. The thermal or the photoexited responses depends on the absorption coefficient and thermal conductivity of the material.[29] Graphene for such purposes is usually obtained via mechanical exfoliation, epitaxial film growth, chemical vapour deposition or chemical exfoliation of graphene films.

II.1.2. Scope of Present Investigation

In literature varieties of methods are reported to produce graphene. Systematic studies discussing about the influence of number of graphene layers[30] and defects in relation to the bulk graphite[30] and amorphous carbon on the IR photoresponse are not there in literature. Here, in this study different methods, both physical and chemical were employed (already reported) to grow FLG films directly on insulating substrates (quartz, SiO_2). Among the physical methods used, electrostatic exfoliation holds a promise for efficient graphene growth and future application. This is because it solely depends on electric field energy and does not involve any chemicals, making the growth of graphene site specific, clean and solvent free. By tuning the amount of electric field and the time for which it is applied the number of graphene layers can be controlled. Among the chemical methods, Ni coated carbon materials when annealed at a temperature of 700 °C can produce graphene. This method used is also site specific and the annealing temperature is lower than the reported values. The IR photoconductive response of amorphous carbon, obtained in such attempts to get graphene was studied. The obtained amorphous carbon films showed a maximum photoresponse of 58.8%. The IR response of the bulk graphitic films is known to be bolometric in nature where the change in resistance is due to thermal effects. Controlling the thickness and crystallite size of the graphene layers, one can tune the IR photoresponse from photoconductive to bolometric

regime.[31] Similarly the photoresponse behaviour of the amorphous carbon can be improved further depending on the growth mechanism.

II.1.3. Experimental Section

Materials required

HOPG purchased from NT-MDT, ZYB, SiO_2/Si substrate 300 nm single sided polished (Vin karola), Carbon nanofiber (1cm X 9μm) purchased from Sigma Aldrich, Ni/Graphene purchased from Graphene supermarket (10mm X 10nm). Chemicals used were anisole (99%), amyl acetate (95%), isopropanol (98%), double distilled water, nitrogen gas, sodium chloride (99.9%), nickel chloride (98%) and acetone (99%).

Methods to get Large Area Graphene

The famous scotch tape method for obtaining few layer graphene was first attempted. Graphene layers were mechanically exfoliated from the HOPG surface by scotch tape and characterized using Raman spectroscopy.[32,33] HOPG was used as the source for graphene.[28]

For Electrostatic delamination of graphene,[23] SiO_2/Si was taken as the substrate and patterned highly oriented pyroltic graphite (HOPG) was taken for exfoliating graphene from it. A lab built screw gauge setup was used to rotate and bring the HOPG substrate to close proximity with the insulating substrate.[34] A 50 V power supply was used. HOPG and the substrate were stuck to the electrodes using copper tapes.

There are many reports in literature regarding electrochemical exfoliation of graphene.[35,36] For obtaining large area graphene on a soft surface[37] like PMMA, PMMA was first dissolved in 2 wt% anisole. It was then spin coated at a speed of 1000 rpm for 60 secs, using Polaron Sputter Coater SC502, uniformly on

Ni/Graphene.[38] For the electrochemical cell, NaCl (1 M) was taken as electrolyte and graphite rod and Ni/Graphene plate was used as anode and cathode respectively.

The electroplating method was carried out using carbon fiber, pencil lead and PMMA as carbon source. Pencil rod and carbon fiber were electroplated with nickel. For the electroplating process graphite rod was used as anode and carbon fiber or pencil rod, to be electroplated, was used as cathode. $NiCl_2$, 6 H_2O in 0.12 M HCl was taken as the electroplating solution. Ni mesh covered with PMMA was taken as well to produce patterned graphene. The electroplated carbon sources were vacuum annealed at 700 °C inside a PVD chamber. Ni mesh coated with PMMA was vacuum annealed at same condition. PMMA here was used as a carbon source.[39] For every experiment involving SiO_2 (300 nm)/Si wafers, the wafers were cleaned by sonicating it in acetone and isopropanol and finally dried by blowing dry nitrogen.

The graphene and amorphous carbon thus obtained by the above methods were further characterized using Raman[40] in backscattering geometry. A 532 nm excitation from a Nd:YAG solid state laser (model GDLM -5015L, Photop Swutech, China) and a custom-built Raman spectrometer equipped with a SPEX TRIAX 550 monochromator and a CCD detector (Spectrum One with CCD3000 controller, ISA Jobin Yvon) was used for Rama measurements. Optical images were taken using optical microscope (LabEN instruments).[41,42] Because of the novel interaction of graphene with light and electric field the number of graphene layers can be predicted by the optical images.[8] Height measurements were done using atomic force microscope (AFM),[43,44] using Veeco Dimension 3100 SPM. Tapping and contact mode imaging was carried out using standard etched Si or Si_3N_4 cantilevers respectively. Electrical characterization was done using Keithley 236. The resistance before and after IR laser (1064 nm) illumination, was monitored using a digital multimeter (TestLink, India) with computer control. A constant bias voltage of 10 mV was applied. During the measurements similar device configuration was maintained.

II.1.4. Results and Discussion

Scotch tape method

For the scotch tape method, scotch tape was stuck on HOPG surface and then it was peeled off. Few layers of graphene were mechanically exfoliated by the adhesive and it got stuck to the scotch tape. It was then placed on SiO_2 (300nm)/Si substrate and pressed firmly, finally the scotch tape was removed. Figure II.1 shows the steps employed for the scotch tape technique.

Figure II.1 Schematic showing the steps followed in the scotch tape technique to get few layers of graphene.

The optical microscope image revealed clean layers of graphene.[8] Due to the presence of adhesive of the scotch tape on the substrate the height could not be calculated properly by the AFM image (Figure II.2). Vacuum annealing of the substrate SiO_2/Si removed the adhesive completely.

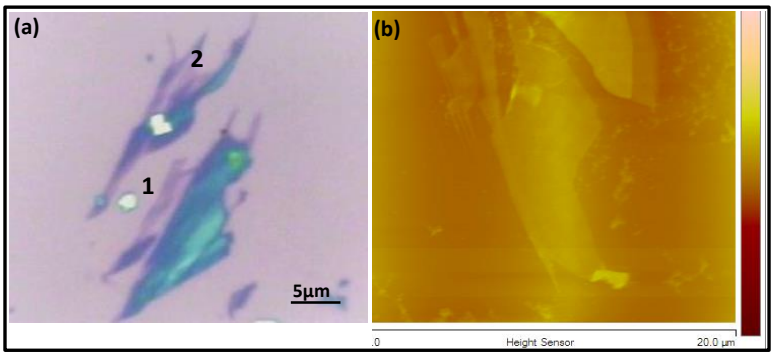

Figure II.2 (a) Optical micrograph showing few layer of graphene on SiO_2 substrate by scotch tape method. (b) AFM topography of the graphene stripes obtained.

Raman being very sensitive to carbon materials it was used to check the quality of graphene thus obtained.[40] Raman measurements were done at two different positions of the obtained graphene layers. The negligible D band along with sharp and intense G band at 1557 cm^{-1} proved that few layers of graphene of high quality were obtained. The I_G/I_{2D} ratio was calculated to be around 2 which proved that 4 to 5 layers of graphene were obtained (Figure II.3).

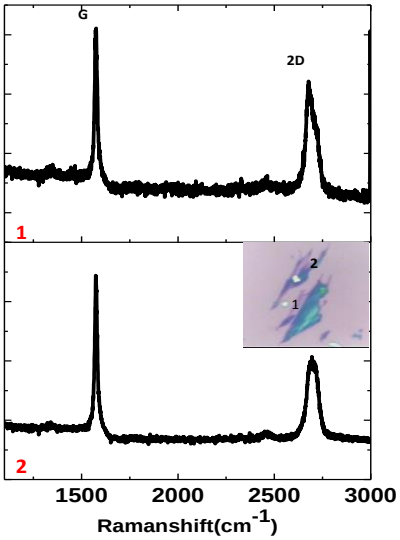

Figure II.3 Raman spectra recorded at region 1 and 2 as shown in the inset. I_G/I_{2D} ratio is 2.

Electrostatic exfoliation

The electrostatic exfoliation depends on the electrostatic pressure given by the equation

$$P = \varepsilon_0 \varepsilon_r V^2 / (2x\ d^2) \ldots\ldots\ldots\ldots\ldots\ldots\ldots\ldots \text{(i)}$$

where d = 300 nm maintained all the time, ε0 permittivity of vacuum and εr is the relative permittivity of the dielectric and V is the applied voltage. The value of this pressure gives the amount of force required to exfoliate one layer of graphene ribbon using electrostatic interaction. The dielectric breakdown of SiO_2 of 300 nm width is around 10 MV/cm, putting an upper limit to the pressure that can be applied.[45]

The power applied was 50 V so the electric field generated was calculated by the equation

$$E = V/d = 50\ V\ /300\ nm = 1\ MV/cm \quad \text{..... (ii)}$$

(where d is the thickness of the substrate) was much below the dielectric breakdown of SiO_2. Figure II.4 shows the digital image and the schematic of the experimental setup.

HOPG was patterned directly by laser ablative method using a compact CD grating.[46] The patterned HOPG was then stuck to one electrode and the SiO_2/Si substrate was attached to the other electrode with the help of copper tapes (Figure II.4).

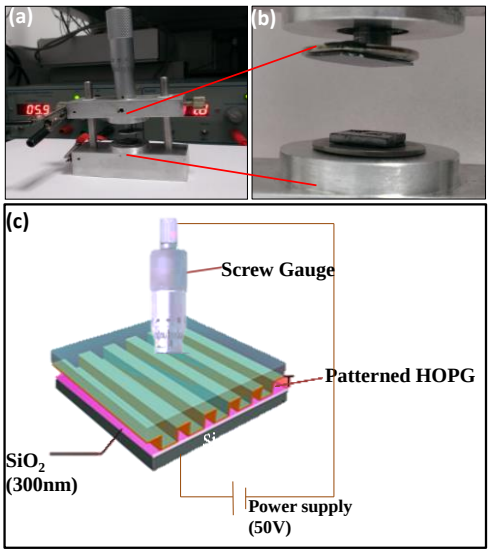

Figure II.4 (a) Image showing the setup for the electrostatic transfer of graphene. (b) The magnified image showing stubs carrying HOPG and SiO_2/Si substrate. (c) Schematic depicting the overall electrostatic transfer procedure.

The screw gauge was rotated to bring the substrate and HOPG to close proximity (Figure II.4a). 50 V was applied for 5 minutes across the electrodes. The electrostatic pressure applied on HOPG to peel of graphene layers from it was calculated by using equation (i). The value came out to be 12.36 kPa on an area of 1 cm x 1 cm, which is quite high, considering the weak Van der Waals force, to peel off the graphitic layers. Silicon substrate was then taken out and observed under optical microscope. The optical

image (Figure II.5) shows the transferred graphene ribbons of width 1μm approximately but the yellow tinged patches indicates that many layers of graphene were transferred rather than single layer. Raman peaks[47] (Figure II.5) revealed the amorphous nature of the carbon obtained. From the intense D-band at 1350 cm^{-1} and the low and broad 2-D band, it was concluded that the obtained carbon was amorphous in nature and not few layers of graphene.[48]

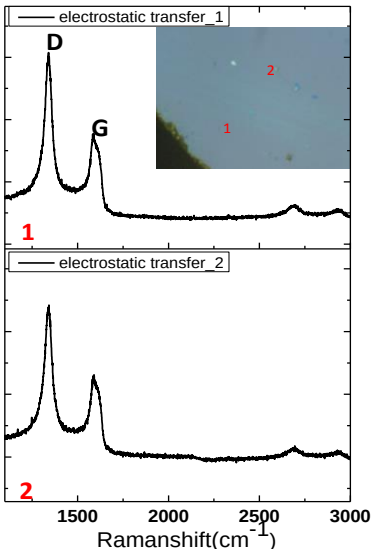

Figure II.5 Raman spectra recorded at two different regions as shown in the inset. Inset shows optical micrograph of the graphene ribbons transferred on a SiO_2/Si substrate by electrostatic method.

Electrochemical Delamination

Electrochemical methods, involving varieties of material as cathode and anode, for obtaining graphene are reported in literature.[49,41] In the present method, for the cathode PMMA was spin coated uniformly on the nickel (Ni) plate containing the graphene sheet and then heated for 10 minutes at 180 °C. PMMA was dissolved across the border using acetone to simplify the peel off process. NaCl (1 M) was taken as the electrolyte and graphite rod as the anode (Figure II.6). For the electrochemical reaction a constant source of 5 V was applied across the electrodes. PMMA got peeled off from the nickel surface along with graphene. This PMMA containing graphene was placed on a silicon substrate firmly and acetone was poured on it to dissolve away the PMMA and leave the bare graphene on the silicon substrate.

In the electrochemical cell, the H^+ produced penetrates through the PMMA edges and loosens the PMMA off the Ni surface. The PMMA along with graphene comes off leaving behind bare nickel at the cathode as shown in the schematic (Figure II.6). If nickel came out along with PMMA/graphene, it was dipped in nitric acid before pouring acetone, so that nickel gets dissolved in the nitric acid.

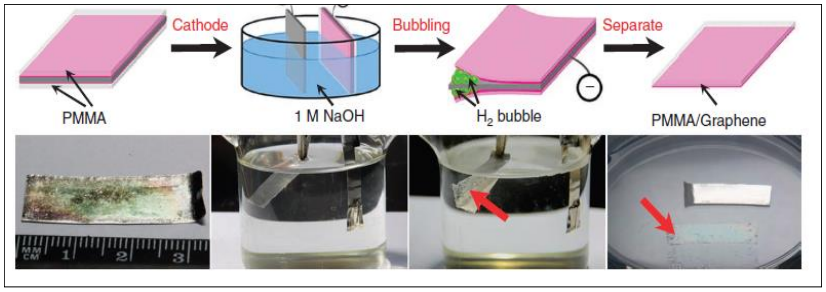

Figure II.6 Schematic showing the electrochemical process where graphite rod was used as anode and 1M NaOH as electrolyte. PMMA coated (thickness 500 nm) on Ni/ graphene was used as cathode (reproduced from ref. 50).[50]

The graphene obtained on PMMA and silicon substrate was observed under optical microscope. The image shows large area transfer of graphene a stretch of almost 9 μm (Figure II.7a). Raman was checked at two different positions (Figure II.7b). A sharp G band was observed at 1573 cm^{-1} with very less intense D band. The I_G/I_{2D} ratio was calculated to be 2.22 which correspond to 4 to 5 layers of graphene.

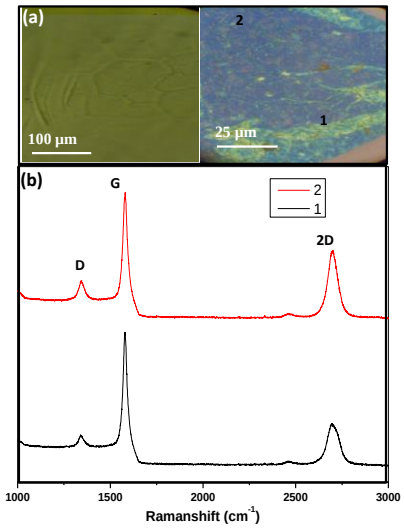

Figure II.7 (a) Optical image of domains of graphene on PMMA and on SiO_2/Si substrate obtained by electrochemical method. (b) Raman spectra recorded from region 1 and 2. I_G/I_{2D} ratio calculated to be 2.2.

Annealing method with aid of nickel electroplating

Thermal annealing of carbon sources using a metal catalyst[52] for large area graphene deposition is well reported in literature.[51,53] For the present method, nickel was electroplated on the carbon sources. $NiCl_2$ solution was used as electroplating solution. The electrolyte was obtained by dissolcing 1 g of $NiCl_2$, 6 H_2O in 150 ml of 0.12 M HCl. Carbon fiber attached to the glass plate using silver paste was used as cathode (Figure II.8) and graphite rod as anode. C-fiber being hydrophobic in nature, 2 ml of IPA was added to every 50 ml of the electroplating solution to make the fiber hydrophilic. A constant source of 30 V was supplied for 10 minutes during the electroplating process.

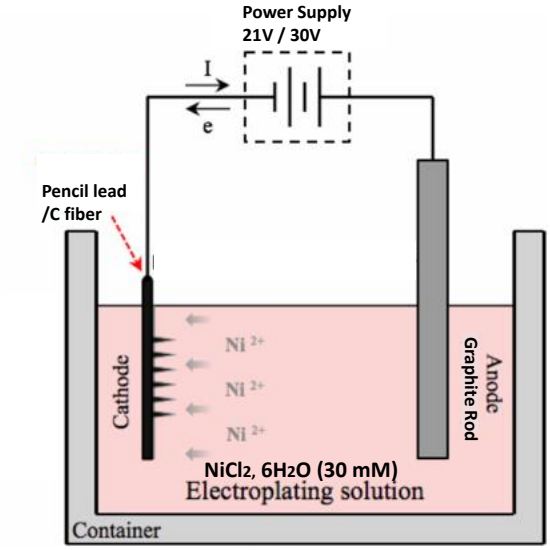

Figure II.8 Schematic showing the process of electroplating of pencil lead/ C-fiber with Ni using $NiCl_2$, 6 H_2O (30 mM) as the electroplating solution and graphite as anode. When C-fiber was electroplated IPA was added to the solution to make the fiber hydrophilic.

Next pencil lead was used as the carbon source and was coated with nickel using the same electroplating solution. For the electrochemical reaction a constant voltage of 21 V was applied for 10 minutes. Energy dispersive spectroscopic (EDS) mapping was performed using EDAX Genesis V4.52 (USA). The EDS mapping was performed at 10 kV with a beam current of 1.1 nA, the dwell time per pixel being 25 µs. EDAX mapping shows the distribution of the constituent elements (Figure II.9).

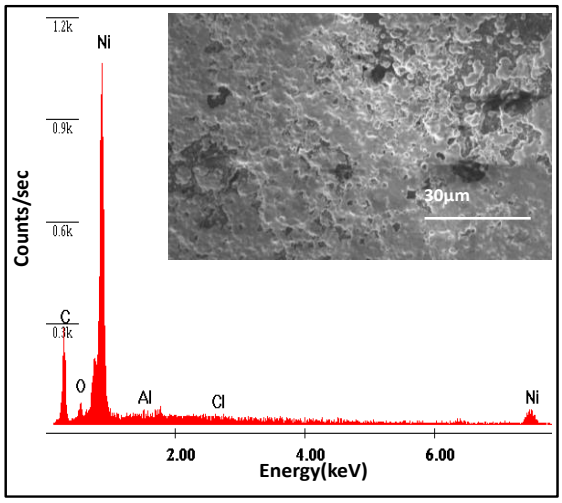

Figure II.9. EDAX of pencil lead covered with Ni. Inset presents the SEM data (the white portions are the ones covered with Ni and black region is that of only lead).

The data reveals the proficient coating of Ni on the lead of pencil. EDAX also promulgated the SEM image, which shows the uniform coating of Ni on pencil lead.

Finally Ni mesh coated with PMMA was used to obtain large area patterned graphene. The electroplated carbon materials were vacuum annealed at temperature 600 – 700 °C.

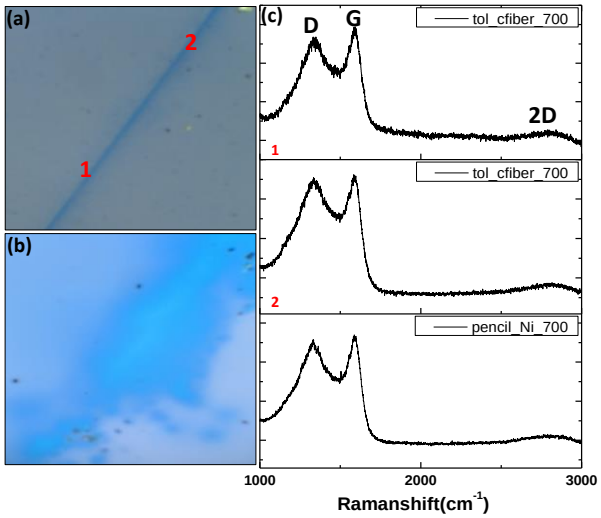

Figure II.10 (a) Optical image of the imprint of graphitic material deposited by annealing C-fiber kept on SiO_2/Si substrate. (b) Optical image of the imprint of graphitic material produced by annealing Ni-coated pencil placed on SiO_2/Si substrate. (c) Raman data for region 1 and 2 of the optical image (a) and for (b).

At high temperature annealing, carbon seeps through Ni and few layers of graphene imprint must form on the substrate. The optical image (Figure II.10) divulges the imprint of graphene formed after the annealing was complete. But the Raman peaks (Figure II.10) exhibited characteristics of amorphous carbon rather than few layers of graphene.[17] The intensity of the D band is high at 1348 cm^{-1} revealing that the disruption of c axis periodicity and broad (almost non-existent) 2D band disclosed that the carbon deposited is amorphous in nature. The reason for the deposition to be amorphous in nature is maybe due to the low temperature annealing (600 to 700 °C).[51] The temperature reported for graphene deposition using Ni catalyst are still higher around 800 to 1000 °C.[54] For thermal annealing, the carbon fiber or the pencil coated with nickel was tightly wound against the substrate to facilitate the deposition of graphene across the line of contact between nickel and the substrate.

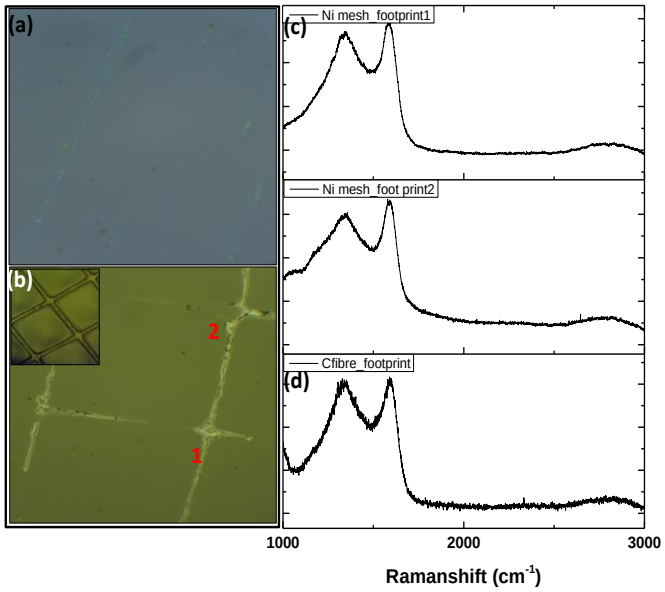

Figure II.11 (a) Optical image of the footprint of the annealed C-fiber on SiO_2/Si substrate (using electroplating technique). (b) Optical micrograph of the imprint of patterned carbon produced by annealing Ni-mesh coated with PMMA. Inset shows optical image of Ni-mesh coated with PMMA. (c) Raman spectra recorded for region 1 and 2 of the Ni mesh footprint (d) Raman spectra for C-fibers footprint electroplated with Ni.

The pressure applied on the carbon source (C-fiber and pencil lead) to keep it attached to the substrate also played a role, for the deposition to be amorphous in nature. The Ni mesh footprint also exhibited

similar results (Figure II.11b). Thus control study, by changing the pressure applied and the temperature for annealing is required.

The amorphous carbon obtained by the Ni mesh was a patterned one (Figure II.11b). It was further electrically characterised. Quartz was used as substrate and silver paste was drawn at the two edges of the amorphous carbon mesh to make contacts (Figure II.12). As the optical image shows, 3 lines of the mesh were connected across the silver paste.

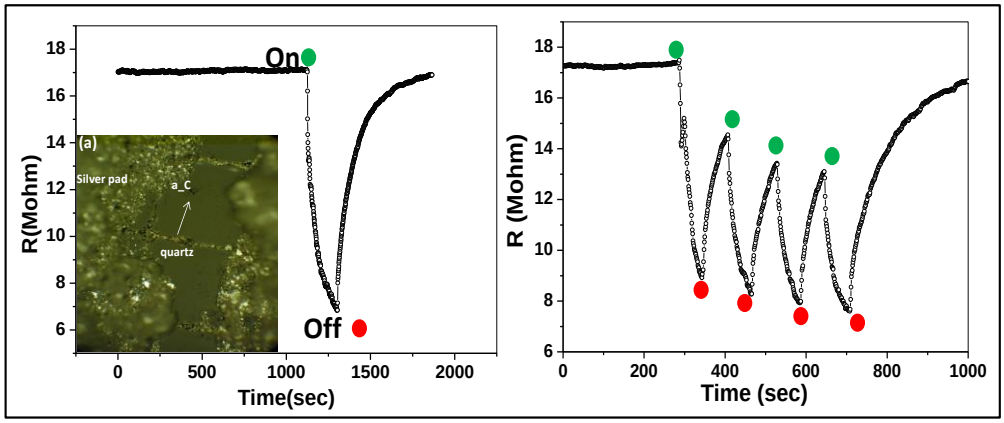

Figure II.12 (a) IR temporal behavior for one cycle. The inset shows the optical image having 3 lines of amorphous carbon mesh connected by silver paste applied on both sides. (b) IR temporal behavior for 4 cycles. The IR photoresponse was calculated to be 58.8%.

IR photoresponse was studied. IR radiation (source: incandescent bulb, 60 W, 1064nm) at a distance of 15 cm from the substrate was used. The temperature near the circuit was around 40-50 °C. The resistance changed from 17 to 7 MΩ corresponding to a photoresponse of 58% (Figure II.13). The increase in the photocurrent with illumination can be attributed to the generation of photoexcited charge carriers. It was observed that the final resistance was not attaining the original base resistance after the IR beam was turned off. This may be due to the non-equilibrium of photoexcited charge carriers.[55]

To understand the photoconductive effects in a given system one must understand the interplay between trapping and recombination. Defect acts as trapping sites which helps the excitation of electrons. Defects

can also act as holes where the electron recombination can happen easily and the hole is thus released to valence band. Trapping of charge carriers increases photoresponse whereas recombination decreases it. Defect can also act as a scattering site which essentially increases the electrical resistance. Amorphous carbon is endowed with more number of defects than graphene so the current is less and resistance value is in mega ohms. At the junction of the metal contact and carbon photoexcitation causes electron-hole pair generation. When sufficient time is given they gets separated and give rise to photocurrent.[56] A temperature dependent study of the photocurrent would enlighten upon the influence of traps and recombination centres on charge carriers.

II.1.5. Conclusion

Four different methods have been exploited to produce graphene. Among which two were wet processes, electrochemical and electroplating one and the other two were the dry solvent free processes scotch tape and electrostatic one. The scotch tape technique and the electrochemical delamination results produced graphene, similar to the ones already produced in literature. The electrostatic exfoliation method revealed amorphous nature rather than the typical graphene features. More focus is to be given to this method in order to improve it, since theoretically delamination of the graphene sheet by applying electrostatic force is possible because of the weak Van der Waals interaction between the graphene layers. Further the electroplating procedure need to be ameliorated, to obtain graphene, by changing the parameters like temperature and pressure. Circuits were made out of the amorphous carbons produced, which showed mega ohms resistance. The photoresponse was found to be around 58%. Thus an IR detector can be made out of it. Future work may include electrostatic method and improved electroplating method using pencil lead (at low temperature) for large area production of site specific graphene. The electrostatic method does not require solvents or any wet bench. It will be a dry, clean method for producing large area graphene by tuning the electrostatic force.

II.2. PENCIL DRAWING ON PAPER: FIELD EFFECT TRANSISTOR AND R-C FILTERS

II.2.1. Introduction

Pencil, derived from the French word “pincel”, writing on a paper is a day-to-day practice since 16th century. Pencils create marks via physical abrasion and leaves behind a trail of solid core material that remains adhered to a sheet of paper. Most pencil cores are made of graphite[57,58] mixed with kaolin based clay binder. The left grey or black marks on paper can be easily erased making it so special.[59-61] This humble deposit contains some interesting graphitic species, if not seriously single or few layer graphene! The multi layers of graphene present makes it conducting. Pencil writing on paper has various applications[62] such as supercapacitors,[63] piezoresistive sensors,[64] air electrode of a Li-air battery[65] and also as electrode material for UV sensors.[66,67]

Paper is believed to have been invented by Ts'ai Lun in105 A.D. in China, where it reached an advanced stage of development. The word "paper" is etymologically derived from *papyrus*, an ancient Greek term for the *Cyperus papyrus* plant. In recent years paper has become popular in electronic applications because of its ubiquity.[68-71] Paper has already been employed in energy storage devices,[72,73] but for devices such as field effect transistors (FETs) which requires smooth dielectric layers[68-71] it was long believed that paper is not a well suited material. Dielectric, with high capacitance, deposition has to be done at ambient conditions, and not at high temperature.[74,75] This conditions are necessary otherwise it might affect the paper substrate. Certain ionic liquids (e.g. 1-ethyl-3-methylimidazolium bis(trifluoromethylsulfonyl)imide), form electrochemical double layers (EDLs). They also possess high

thermal stability and high ion conductivity (~0.02 S/cm) at room temperature, and therefore can be used as a dielectric medium for low voltage operation of flexible FETs.[76-80]

II.2.2. Scope of Present Investigation

The electric field effect, IR photoresponse and active, passive filters from turbostratic graphite i.e. pencil trace on paper has not been much investigated in literature. Here, in this study IR photoresponse, field effect transistor and filter effect were realized from pencil marks on paper using iongel as dielectric. The devices showed ambipolar electric field effect. Carrier mobilities were calculated to be around hundred cm^2/Vs under low operating voltages (< 3 V). IR photoresponse have been fabricated by using pencil trace as a resistor and RC filter effect were realized using pencil mark and ion gel as a capacitor dielectric.

II.2.3. Experimental Section

Normal A4 papers of thickness 100 μm for making pencil marks were used. Pencil used in this study was APSARA, HB grade having graphite content of ~70%. The morphology of the pencil markings were investigated using field emission SEM (Nova Nano SEM 600, FEI Company). Raman spectra of EBICD samples were recorded. AFM imaging was done on a diInnova SPM (Veeco, USA) using Si probes (model, RTESPA, spring constant 40 N/m) in tapping mode. Transmission electron microscopy (TEM) has been recorded on the pencil powder dispersed in the chloroform solvent.

Top gate dielectric used in this study is ion gel based, composed of polydimethylsiloxane and ionic liquid (1-butyl-3-methyl-imidazoliumoctyl sulfate) in the ratio 1:0.2, with typical capacitances of $0.3\mu F/cm^2$. Paper substrates with the pencil marks along with the Ag contacts and top gate dielectric were baked at 150 ºC for 10-15 minutes.

II.2.4. Results and Discussion

The morphology of the pencil rod and its trace on paper surface has been examined. The surface of the pencil rod appears to be corrugated with petal-like morphology of graphitic layers. The random alignment of the cellulose fibers of the paper was imaged using optical profiler. AFM topography and optical profilometric images of the pencil -trace on paper, revealing its domain structure.

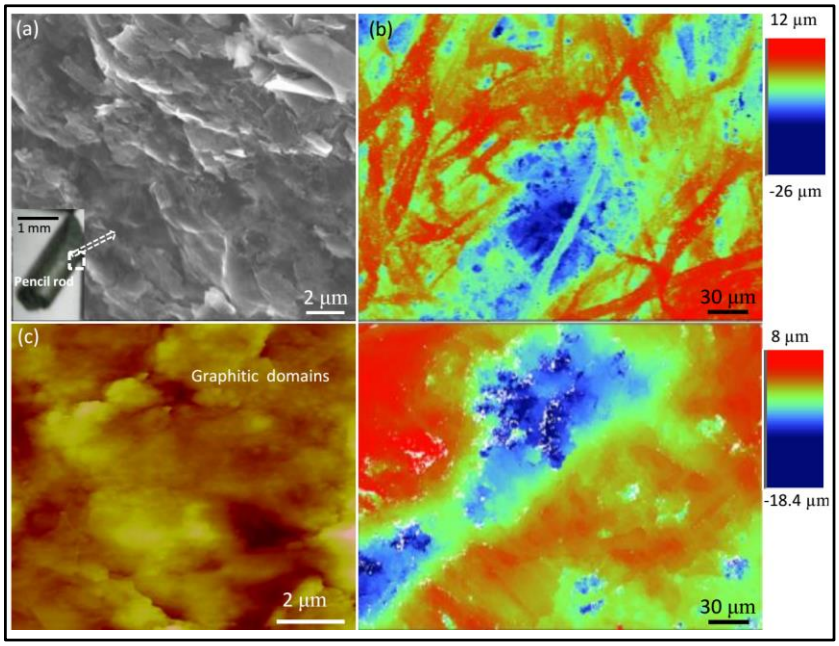

Figure II.13 (a) SEM image showing the surface morphology of the pencil rod, inset shows the optical micrograph of the pencil rod. (b) Optical profilometric image showing the cellulose fibers of the plane paper surface (c) AFM topography and (d) optical profiolometric images of the pencil trace on the paper.

The layer nature of the domains is apparent as shown in the inset of Figure II.13. The EDS spectrum is shown in Figure II.13, showing the signals for C, Fe, Ca and Mg. Energy dispersive spectroscopy (EDS) maps in Figure II.13 shows the distribution of the constituent elements, Fe, Ca and Mg, present in the graphitic matrix of the pencil-trace. TEM micrograph showing the nanocomposite constitution of the pencil powder where clay particles were seen among the graphitic layers (Figure II.14). The crystalline nature of the graphitic domains is evident from the electron diffraction pattern with hexagonal symmetry

of the spots[81] (see inset of Figure II.14). Raman spectrum recorded from the pencil-trace made on a stainless steel substrate (Figure II.14, red curve) comprises of three prominent peaks at 1348, 1574 cm^{-1} and 2701 cm^{-1} which correspond to the D, G and 2D bands respectively. The G band arises from stretching of sp^2 bonded carbon lattice and D band originates from the presence of defects in the form of edges and grain boundaries. Using the estimated I_D/I_G ratio (~0.2), the average crystallite size of the graphitic domains[82] was calculated to be ~100 nm. The position, width and shape of 2D band provide the information about number of layers, type of stacking along the c-axis of graphitic samples.

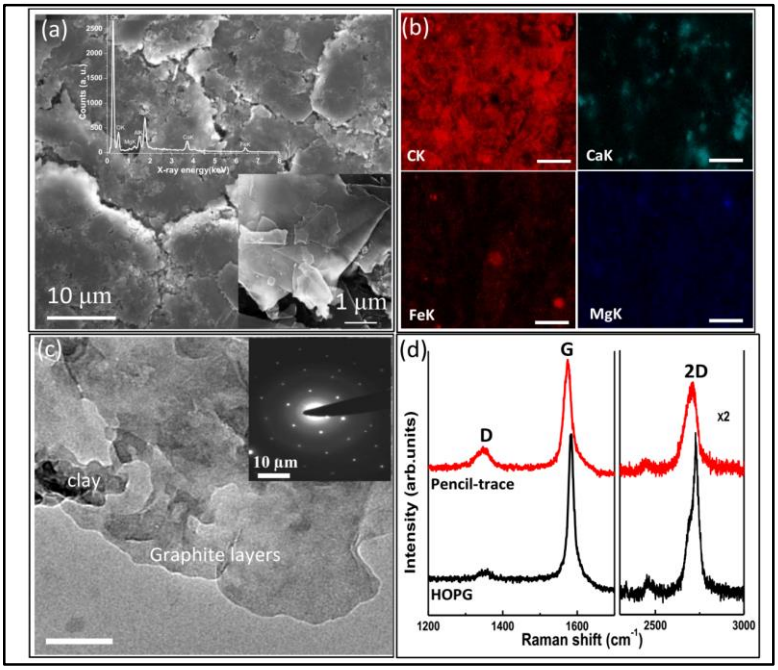

Figure II.14 (a) FESEM images showing morphology of graphitic layers in pencil trace on paper along with the EDS spectrum. Inset shows a magnified view. The corresponding EDS maps of graphitic carbon (CK) along with the metallic elements present in the clay (FeK, CaK and MgK), scale bar 10 µm (b). (c) TEM micrograph of the graphitic layers, with the electron diffraction pattern in the inset, the sample for TEM was prepared by crushing a pencil rod into fine powder and dispersing it in chloroform followed by depositing on to a holey carbon grid. (d) Raman spectrum of the pencil trace (red curve) compared with HOPG (black curve). The 2D band intensities have been multiplied by two.

In the case of pencil trace, the 2D band appears as a single symmetric peak at 2701 cm^{-1} with a width of 85 cm^{-1} (red curve, Figure II.14) which is quite different compared to asymmetric peak of HOPG (black curve, Figure II.14). The former is typical of turbostratic graphite, a close cousin of graphene.[83] Due to

mis-orientation of graphene layers along the c-axis, there is substantial electronic decoupling of the layers leading essentially to a 2D system.

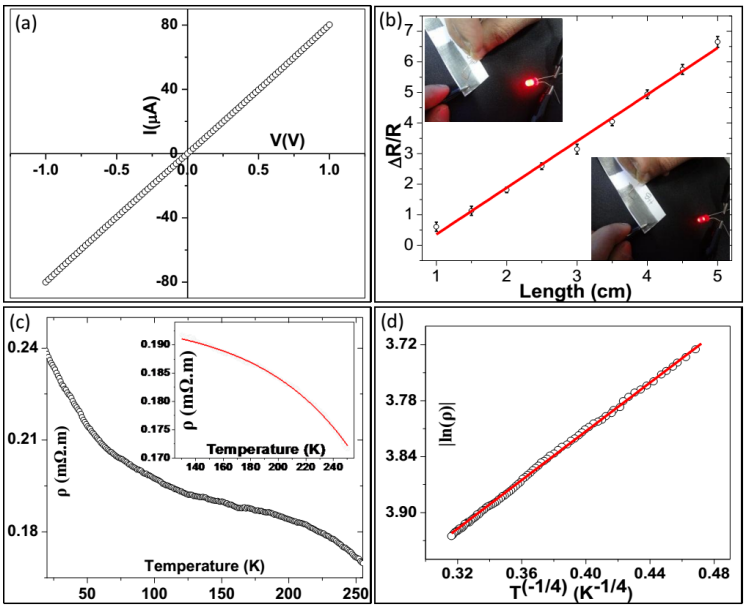

Figure II.15 (a) Two probe current-voltage characteristics of a pencil-trace on paper substrate. (b) Normalized resistance of the pencil-trace on paper (width, 3 mm; thickness, 50 μm) over different lengths. Insets show photographs of varying brightness of a LED based on the resistance of the pencil-trace, (c) Four-probe resistivity of the pencil measured between 20 and 250 K. The distance between contacts was 1 mm with a width and thickness of the trace, ~ 3 mm and 50 μm respectively. Inset plot showing the resistivity of the pencil-trace varying as $\rho \sim \exp((-T0/T))$ above 100 K, where T_o is constant, T is the temperature. (d) $|\ln(\rho)|$ vs $T^{-1/4}$ plot, which is linear, characteristic of VRH model of electrical transport at low temperatures (20-100 K).

In order to investigate the electrical properties of the pencil trace on paper, its I-V characteristics were measured. A given trace with ~ 5 mm width was found to have a resistance of 12.5 kΩ. The resistance was found to vary linearly with length of the trace, confirming uniformity of the deposit. Temperature dependent resistivity measurement was performed using a physical properties measurement system. The resistivity of the pencil trace decreases from 0.24 to 0.17mΩ.m with increasing temperature, indicating the semiconducting behaviour. Resistivity of the pencil-trace is ~ 3 orders magnitude higher compared to that of bulk graphite (ρ_{bulk}~ 0.4 μΩ.m). This can be attributed to the scattering of the charge carriers by the intercalated clay particles, edges and boundaries of the interconnected graphitic domains.

As the graphite crystallites are interconnected with each other, the electrical transport at low temperatures (20-100 K) can be explained using the variable range hopping (VRH) model.[84] As shown in Figure II.15, $|\ln(\rho)|$ is seen varying linearly with $T^{-1/4}$ (in the 20-100 K range), characteristic of Mott type VRH[84,85] implying that the Coulomb interactions are negligible in the conduction mechanism. At higher temperatures (above 100 K), resistivity decreases exponentially, characteristic of an activated transport behaviour.

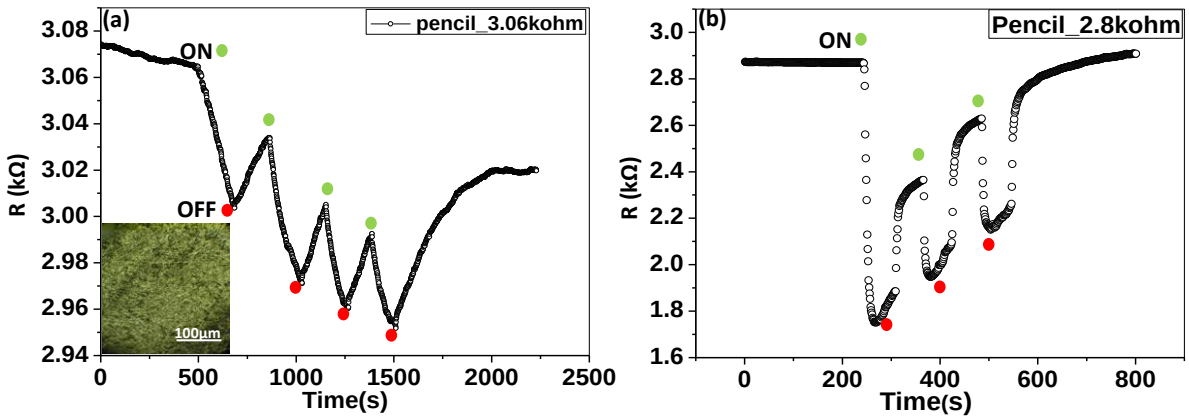

Figure II.16 (a) IR temporal behavior using incandescent bulb on pencil mark of 3.06 kohm. Inset shows optical image of pencil drawn on sheet (b) IR temporal behavior for pencil 2 kohm with IR (1064nm) power of 30 $mWcm^{-2}$.

The IR photoresponse properties of pencil trace on paper have been illustrated in Figure II.16. A decrease in resistance from 3.07 to 3 kΩ, corresponding to a photoresponse of 2.05%, was observed for pencil trace illuminated with incandescent bulb (Figure II.16a). The resistance decreased from 2.9 to 1.5 kΩ with photoresponse of 38.93% for pencil trace illuminated with IR radiation, with a power of 30 mW/cm^2 (Figure II.16b).

The increase in the photocurrent with IR illumination is due to the generation of photoexcited charge carriers. The excitation of charge carriers happens near the metal pencil interface at the contacts. The final resistance value was not attaining the original base resistance immediately after turning off the IR source.

The reason for this may be attributed to the non-equilibrium photoexcited charge carriers or the defects present in the pencil trace.

Ion gel used as the dielectric was prepared by mixing PDMS with ionic liquid (1-butyl-3-methyl-imidazolium octylsulfate) in the ratio 5:1, which showed a typical dc specific capacitance of 0.3 μF cm^{-2}. The higher gate capacitance of the ion gel is due to the formation of electrochemical double layer.[77]

Simple first-order passive filters were made by employing pencil-trace on paper as a resistor and ion gel (made of PDMS and ionic liquid) as dielectric between two Ag contacts as capacitor. The input signal (V_{in}) was applied using a function generator at voltage amplitude of 1 V, to the series combination (both the resistor and capacitor together) and the output signal (Vout) was measured using an oscilloscope across the capacitor (see Figure II.17).

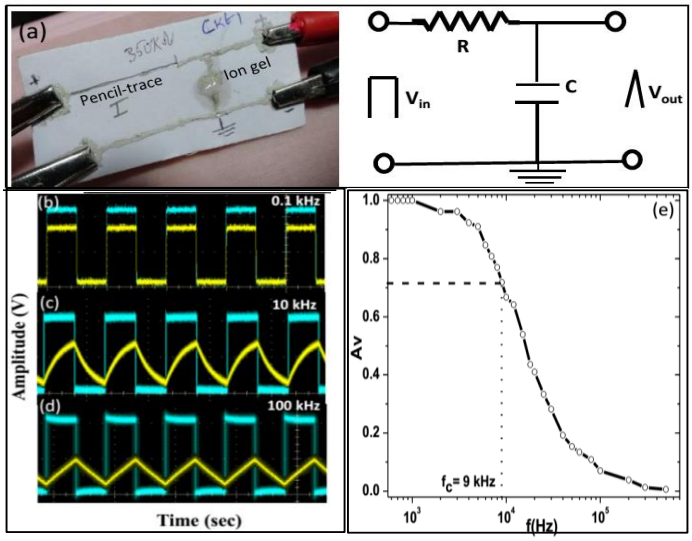

Figure II.17 (a) Photograph showing a resistor-capacitor (RC) low pass filter on paper and its circuit diagram. The transient response from the filter at (b) 0.1 kHz, (c) 10 kHz and (d) 100 kHz. Input and output wave forms are shown with sky blue and yellow, respectively. (e) Normalized output voltage response with frequency of the RC low pass filter. The cut-off frequency corresponding to 0.707 of the maximum response is 9 kHz.

The resistance of the pencil-trace is found to be 350 kΩ. The input signal is a square wave-shaped signal (blue curves in Figure II.17) with almost vertical step input and the response of this integrator changed dramatically with increasing frequency. At low frequencies (100 Hz), the input and output wave forms are of similar shape except that the amplitude of the output is lower compared to the input due to charging of the capacitor. At higher frequencies (~10 kHz), the output voltage response converted to a triangular shaped waveform which can be attributed to the frequency dependent reactance of the capacitor (see Figures II.17). At higher frequencies (~100 kHz), the output became a well-shaped triangular wave (see Figure II.17). The performance of the circuit is as expected of a RC filter; the higher the input frequency, the lower will be the output amplitude due to decreasing capacitive reactance ($Xc = 1/2\pi fC$ where f is the frequency and C is the capacitnace). The normalized output voltage with frequency of the RC low pass filter is shown in Figure II.17.

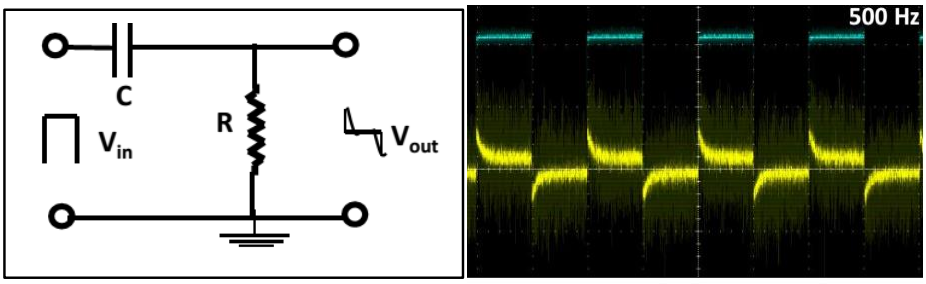

Figure II.18 RC differentiator circuit and the voltage response at 500 Hz. Sky blue curve is the input signal and yellow curve is for the output signal.

The frequency corresponds to 0.707 level of the normalized output voltage which is the cut-off voltage (f_c) which is found to be 9kHz.[86] The time constant (τ) can be equated to the cut-off frequency (fc) of the RC low pass filter by the following equation

$$fc = 1/2\pi\tau = 1/2\pi RC$$

The phase shift angle (ϕ) is given by the following equation

$$\phi = -\arctan(2\pi fcRC)$$

At fc, the phase angle is found to be -45^{o}, out of phase with respect to the input signal. As the input voltage changes charging up of the output voltage (the voltage across the capacitor) happens, which lags behind the input signal.

The higher the input frequency applied to the filter the more the capacitor lags and thus, the circuit goes "out of phase". The above study shows the possibility of making such circuit elements. Besides this integrator, a RC based differentiator circuit was also built simply by interchanging the positions of the resistor and capacitor of the integrator circuit.

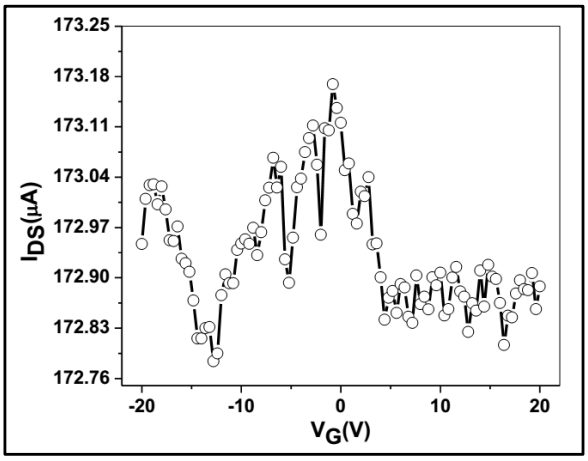

Figure II.19 Transfer curve of the pencil-trace with the paper as gate dielectric, no field effect was observed.

Pencil trace on paper was then exploited as active element in field effect transistors. Ag paint was laid out with a paint brush forming source, drain electrodes on paper contacting the pencil trace. Initially, paper was used as gate dielectric in the in-plane geometry with Ag as gate electrode. Transistor characteristics recorded using a Keithley-4200 semiconductor characterization system produced no measurable field effect (Figure II.19).

A drop of the ion gel was placed on top of the pencil trace and baked for 15 minutes. While being hot, Ag paint was applied which dried instantly forming the gate electrode (inset of Figure II.20).

Figure II.20 shows the output characteristics obtained, where the I_{DS} (source-drain current) varies linearly with V_{DS} (source-drain voltage) with a base resistance of ~11 kΩ for zero gate voltage (V_G= 0) indicating ohmic contact between the pencil-trace/Ag interface. The output characteristics showed increase in the current with varying gate voltages from 1.5 to -1.5 V (Figure II.20).

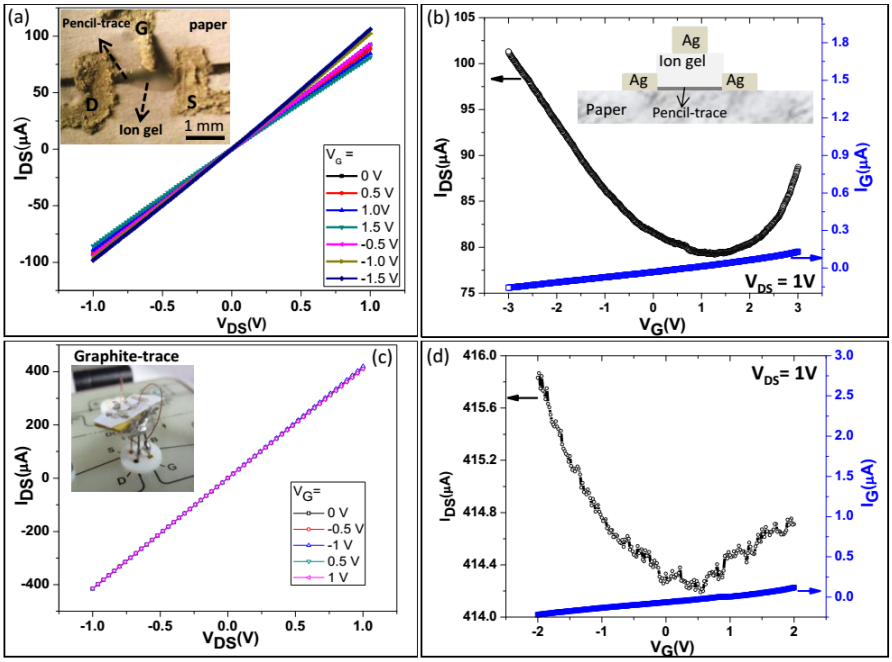

Figure II.20. (a) Output and (b) transfer characteristics of the pencil trace on paper with PDMS-IL ion gel as top gate dielectric. Inset shows the optical micrograph of the pencil trace on a paper with the source, drain and gate as Ag paint and ion gel as top gate dielectric. The gate leakage current (blue curve) is also shown. Inset shows the geometry of the pencil-trace FET with ion gel as dielectric. (c) Output and (d) transfer characteristics of a HOPG trace on paper with ion-gel as gate dielectric, similar to the device shown above. Inset shows a photograph of a mounted paper FET device. The devices were baked at 150 ºC for 15 minutes. All measurements were carried out in ambient conditions.

Transfer characteristics (Figure II.20) reflected the ambipolar nature where the positive and negative regions of gate voltage represent electron and hole transport respectively.[75] The asymmetry in the transfer curve indicates that the hole and electron mobilities are not equal. This may be attributed to the unintentional doping of pencil marks by the water molecules through capillaries of the paper which may suppress the electron mobility. The broad Dirac point minimum in the transfer curve can be attributed to

the deriving of electric field effect from multilayers of graphene in the pencil trace.[87] The gate leakage current (see Figure II.20) is at least 2-3 orders of magnitude lower compared to the channel current.

It is clear that the ion gel due to its high gate capacitance is effective in deriving the electric field effect from the pencil trace at such low operating voltages. The carrier (holes and electrons) mobilities (μ) were estimated from the channel transconductance (gm ~7 and 3.9 μA/V for holes and electrons respectively) of the FET, $g_m = (dI_{DS}/dV_G) = (W/L)\mu C_o V_{DS}$ in the linear regime of the I_{DS}-V_G curve, where W/L is the width-to-length ratio of the channel and C_o is the gate capacitance per unit area. Taking W/L as 0.2 and Co as 0.3 μF/cm^2, the hole and electron mobilities were estimated to be $\mu_h \sim 106$ cm^2/Vs and $\mu_e \sim 59$ cm^2/Vs. In contrast to the turbostratic nature of the pencil trace, a HOPG trace (which is completely graphitic) was made on paper by rubbing and the FET characteristics were examined while using the same ion gel as dielectric. The output characteristics showed only a little dependence on the gate voltage.

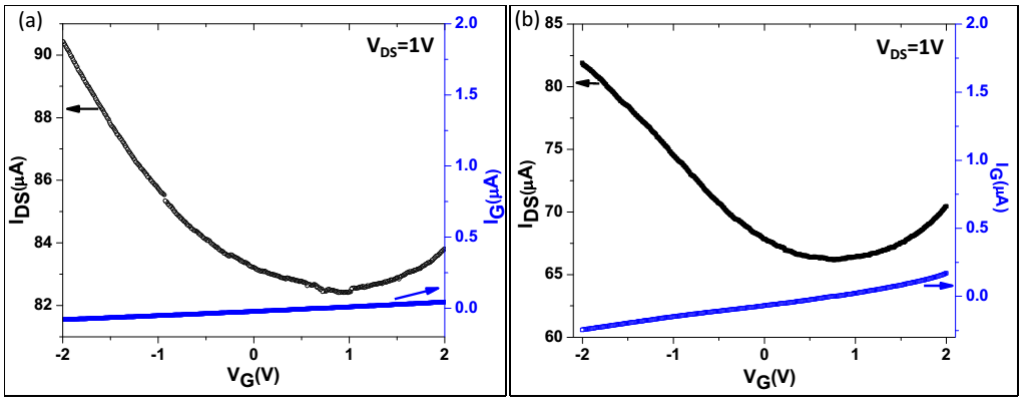

Figure II.21 (a) and (b) Transfer curves of the pencil traces on the paper with ion gel as top gate dielectric. (Hole and electron mobilities are found to be $\mu_h \sim$ 81, 112 and $\mu_e \sim$ 63, 69 cm^2/Vs for (a) and (b) respectively).

The transfer curve (Figure II.21) showed the ambipolar behavior with change in the I_{DS} of 1.5 μA and 0.5 μA for the hole and electron branches according to the applied gate voltages respectively. This indicates that electric field effect is less in the case of HOPG trace, which may be due to higher screening effects.[75] The pencil trace being turbostratic in nature with the intercalated clay particles, behaves like a 2D

graphite system which is revealed through the observation of significant electric field effect induced by the gate. Transfer characteristics of two more devices exhibited high mobility values but with some variation (~15%) (Figure II.21). Given that the substrate (paper) is rough and non-uniformity of pencil traces may cause the variation in the mobility values. The mobility values are less compared to the literature values obtained with graphite crystallites on SiO_2 surface[75] but are much higher compared to the reduced graphene oxide based devices.[88]

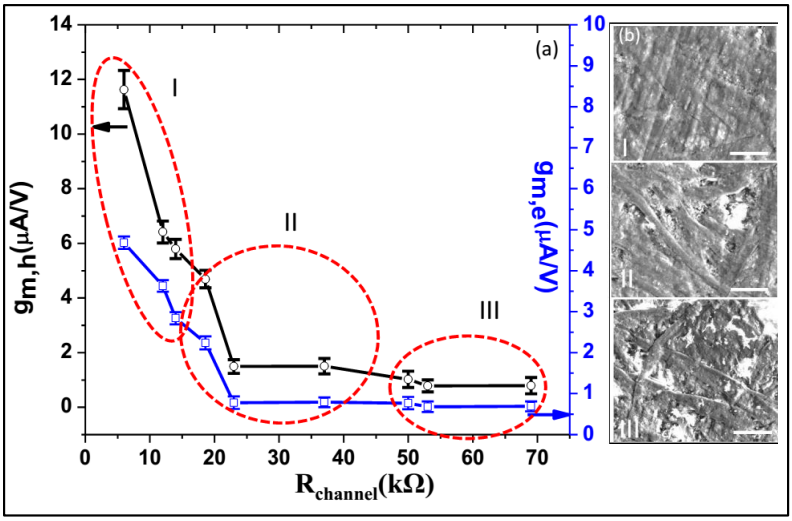

Figure II.22 (a) Transconductance with respect to the varying resistance of the pencil-traces on paper. (b) The corresponding SEM morphology of the pencil-traces. Scale bar, 50 μm.

The electric field effect on the pencil-traces with varying resistances has also been investigated. It is observed that thicker pencil-traces with resistances up to 10 kΩ, showed a significant transconductance of 12-5 μS for holes and 4-2 μS for electrons. As the resistance of pencil trace on paper increases transconductance gradually decreases (see region II, Figure II.22) and becomes negligible at higher channel resistance above 50 kΩ (region III, see Figure II.22).

The corresponding SEM morphology of the pencil-traces in Figure II.22 show that the low resistance thick trace is smooth and therefore the electrical transport is facile while the thinner pencil-traces may depend on percolative paths for electrical transport as the bottom cellulose fibers seem to intercept and

disturbs the connectivity of the graphite domains of the pencil trace. Such scattering leads to lesser transverse electric field effect from the gate electrode (see Figure II.22)

The changes in the resistance of the channel and gate were studied with respect to the bending angle. It is observed that the resistance of the pencil mark changes significantly up to 160% at a maximum bending angle of 90º. The gate resistance, however, changes only up to 15% at a bending angle of 90º. Thus it is seen that the ion gel dielectric is stable against substrate bending.

It is noteworthy to mention the turbostratic nature of the graphite in pencil trace. The study exploits the pencil mark in making an active element of a field effect transistor. As substrate, common paper has been used for varous purposes, attractive by all means. The dielectric properties of paper were supplemented by a PDMS based ion gel which formed conformal contact with the mating surface. Pencil traces with varied thicknesses can be obtained by applying different predefined pressures or by using pencils of different grades. This offers interesting variations in device properties. The Ag electrodes may be inkjet printed for the large area fabrication of pencil based FETs on paper. The passive circuits such as filters of higher orders can be built on a paper substrates in a cost effective manner.

II.2.5. Conclusion

In conclusion, IR photorsponse, RC filter as well as FET action based on pencil trace on paper was observed. An ion-gel was used as a capacitor and gate dielectric for building the paper based filters and transistor. Graphite crystallites were found to be turbostratic in nature. It exhibited ambipolar electric field effect at low operating voltages. The carrier mobilities were calculated to be ~ 106 and 59 cm^2/Vs for holes and electrons respectively. The RC filter exhibited a cut-off frequency of 9 kHz for a square wave input in the range of 100 Hz – 100 kHz, the output being a triangular wave. The method of fabricating filters and transistors on paper substrate are not only simple and cost effective but also solvent free. Since it is biocompatible, pencil traces on paper based devices, can be used for use-and-throw applications.

Being a direct-write method, it holds a great promise for graphite based electronic devices on paper. Future work includes usage of pencil plotters where constant forces can be applied on pencil for fabrication of large area pencil-trace based devices. This paves a new path to produce futuristic devices for green electronics.

References

1 Weiss, N. O., Zhou, H., Liao, L., Liu, Y., Jiang, S., Huang, Y. & Duan, X. Graphene: An Emerging Electronic Material (Adv. Mater. 43/2012). *Advanced Materials* 24, 5776-5776, (2012).

2 Geim, A. K. & Novoselov, K. S. The rise of graphene. *Nat Mater* 6, 183-191, (2007).

3 Novoselov, K. S., Geim, A. K., Morozov, S. V., Jiang, D., Katsnelson, M. I., Grigorieva, I. V., Dubonos, S. V. & Firsov, A. A. Two-dimensional gas of massless Dirac fermions in graphene. *Nature* 438, 197-200, (2005).

4 Novoselov, K. S., Jiang, Z., Zhang, Y., Morozov, S. V., Stormer, H. L., Zeitler, U., Maan, J. C., Boebinger, G. S., Kim, P. & Geim, A. K. Room-Temperature Quantum Hall Effect in Graphene. *Science* 315, 1379, (2007).

5 Gusynin, V. P. & Sharapov, S. G. Unconventional Integer Quantum Hall Effect in Graphene. *Physical Review Letters* 95, 146801, (2005).

6 Jiang, Z., Zhang, Y., Tan, Y. W., Stormer, H. L. & Kim, P. Quantum Hall effect in graphene. *Solid State Communications* 143, 14-19, (2007).

7 Zhang, Y., Tan, Y.-W., Stormer, H. L. & Kim, P. Experimental observation of the quantum Hall effect and Berry's phase in graphene. *Nature* 438, 201-204, (2005).

8 Novoselov, K. S., Geim, A. K., Morozov, S. V., Jiang, D., Zhang, Y., Dubonos, S. V., Grigorieva, I. V. & Firsov, A. A. Electric field effect in atomically thin carbon films. *Science* 306, 666-669, (2004).

9 Quhe, R., Ma, J., Zeng, Z., Tang, K., Zheng, J., Wang, Y., Ni, Z., Wang, L., Gao, Z., Shi, J. & Lu, J. Tunable band gap in few-layer graphene by surface adsorption. *Sci. Rep.* 3, (2013).

10 Lee, C., Wei, X., Kysar, J. W. & Hone, J. Measurement of the elastic properties and intrinsic strength of monolayer graphene. *Science* 321, 385-388, (2008).

11 Dhiman, P., Yavari, F., Mi, X., Gullapalli, H., Shi, Y., Ajayan, P. M. & Koratkar, N. Harvesting Energy from Water Flow over Graphene. *Nano letters* 11, 3123-3127, (2011).

12 Dorgan, V. E. Mobility and saturation velocity in graphene on silicon dioxide, University of Illinois, (2010).

13 Khomyakov, P. A., Giovannetti, G., Rusu, P. C., Brocks, G., van den Brink, J. & Kelly, P. J. First-principles study of the interaction and charge transfer between graphene and metals. *Physical Review B* 79, 195425, (2009).

14 Castro Neto, A. H., Guinea, F., Peres, N. M. R., Novoselov, K. S. & Geim, A. K. The electronic properties of graphene. *Reviews of Modern Physics* 81, 109-162, (2009).

15 Henriksen, E. A., Nandi, D. & Eisenstein, J. P. Quantum Hall Effect and Semimetallic Behavior of Dual-Gated ABA-Stacked Trilayer Graphene. *Physical Review X* 2, 011004, (2012).

16 Lizzit, S., Larciprete, R., Lacovig, P., Kostov, K. L. & Menzel, D. Ultrafast Charge Transfer at Monolayer Graphene Surfaces with Varied Substrate Coupling. *ACS Nano* 7, 4359-4366, (2013).

17 Sagar, A., Lee, E. J. H., Balasubramanian, K., Burghard, M. & Kern, K. Effect of Stacking Order on the Electric-Field induced carrier modulation in graphene bilayers. *Nano letters* 9, 3124-3128, (2009).

18 Cooper, A. J., Wilson, N. R., Kinloch, I. A. & Dryfe, R. A. W. Single stage electrochemical exfoliation method for the production of few-layer graphene via intercalation of tetraalkylammonium cations. *Carbon* 66, 340-350, (2014).

19 Chae, S. J., Güneş, F., Kim, K. K., Kim, E. S., Han, G. H., Kim, S. M., Shin, H.-J., Yoon, S.-M., Choi, J.-Y., Park, M. H., Yang, C. W., Pribat, D. & Lee, Y. H. Synthesis of Large-Area Graphene Layers on Poly-Nickel Substrate by Chemical Vapor Deposition: Wrinkle Formation. *Advanced Materials* 21, 2328-2333, (2009).

20 Eletskii A V, I. I. M., Knizhnik A A, Krasikov D N Graphene: fabrication methods and thermophysical properties. *Phys. Usp.* 54, 227–258, (2011).

21 Unarunotai, S., Koepke, J. C., Tsai, C.-L., Du, F., Chialvo, C. E., Murata, Y., Haasch, R., Petrov, I., Mason, N., Shim, M., Lyding, J. & Rogers, J. A. Layer-by-Layer Transfer of Multiple, Large Area Sheets of Graphene Grown in Multilayer Stacks on a Single SiC Wafer. *ACS Nano* 4, 5591-5598, (2010).

22 Park, J. B., Yoo, J.-H. & Grigoropoulos, C. P. Multi-scale graphene patterns on arbitrary substrates via laser-assisted transfer-printing process. *Applied Physics Letters* 101, (2012).

23 Liang, X., Chang, A. S. P., Zhang, Y., Harteneck, B. D., Choo, H., Olynick, D. L. & Cabrini, S. Electrostatic Force Assisted Exfoliation of Prepatterned Few-Layer Graphenes into Device Sites. *Nano letters* 9, 467-472, (2008).

24 Dawlaty, J. M., Shivaraman, S., Strait, J., George, P., Chandrashekhar, M., Rana, F., Spencer, M. G., Veksler, D. & Chen, Y. Measurement of the optical absorption spectra of epitaxial graphene from terahertz to visible. *Applied Physics Letters* 93, (2008).

25 Xia, F., Mueller, T., Lin, Y.-m., Valdes-Garcia, A. & Avouris, P. Ultrafast graphene photodetector. *Nat Nano* 4, 839-843, (2009).

26 Patil, V., Capone, A., Strauf, S. & Yang, E.-H. Improved photoresponse with enhanced photoelectric contribution in fully suspended graphene photodetectors. *Sci. Rep.* 3, (2013).

27 Gabor, N. M., Song, J. C. W., Ma, Q., Nair, N. L., Taychatanapat, T., Watanabe, K., Taniguchi, T., Levitov, L. S. & Jarillo-Herrero, P. Hot Carrier–Assisted Intrinsic Photoresponse in Graphene. *Science* 334, 648-652, (2011).

28 Yan, J., Kim, M. H., Elle, J. A., Sushkov, A. B., Jenkins, G. S., Milchberg, H. M., Fuhrer, M. S. & Drew, H. D. Dual-gated bilayer graphene hot-electron bolometer. *Nat Nano* 7, 472-478, (2012).

29 Ebbesen, T. W. & Hiura, H. Graphene in 3-dimensions: Towards graphite origami. *Advanced Materials* 7, 582-586, (1995).

30 Partoens, B. & Peeters, F. M. From graphene to graphite: Electronic structure *Physical Review B* 74, 075404, (2006).

31 Ick Son, D., Yeon Yang, H., Whan Kim, T. & Il Park, W. Photoresponse mechanisms of ultraviolet photodetectors based on colloidal ZnO quantum dot-graphene nanocomposites. *Applied Physics Letters* 102, (2013).

32 Allen, M. J., Tung, V. C. & Kaner, R. B. Honeycomb Carbon: A Review of Graphene. *Chemical Reviews* 110, 132-145, (2009).

33 Dresselhaus, M., Jorio, A. & Saito, R. Characterizing graphene, graphite, and carbon nanotubes by Raman spectroscopy. *Annu. Rev. Condens. Matter Phys.* 1, 89-108, (2010).

34 Do, J. W. Electrostatic transfer of graphene grown on copper foil and nanosoldering of carbon nanotube junctions. (2012).

35 Su, C.-Y., Lu, A.-Y., Xu, Y., Chen, F.-R., Khlobystov, A. N. & Li, L.-J. High-Quality Thin Graphene Films from Fast Electrochemical Exfoliation. *ACS Nano* 5, 2332-2339, (2011).

36 Zhou, M., Tang, J., Cheng, Q., Xu, G., Cui, P. & Qin, L.-C. Few-layer graphene obtained by electrochemical exfoliation of graphite cathode. *Chemical Physics Letters* 572, 61-65, (2013).

37 Song, J., Kam, F.-Y., Png, R.-Q., Seah, W.-L., Zhuo, J.-M., Lim, G.-K., Ho, P. K. H. & Chua, L.-L. A general method for transferring graphene onto soft surfaces. *Nat Nano* 8, 356-362, (2013).

38 Hu, Q.-h., Wang, X.-t., Chen, H. & Wang, Z.-f. Synthesis of Ni/graphene sheets by an electroless Ni-plating method. *New Carbon Materials* 27, 35-41, (2012).

39 Sun, Z., Yan, Z., Yao, J., Beitler, E., Zhu, Y. & Tour, J. M. Growth of graphene from solid carbon sources. *Nature* 468, 549-552, (2010).

40 Malard, L. M., Pimenta, M. A., Dresselhaus, G. & Dresselhaus, M. S. Raman spectroscopy in graphene. *Physics Reports* 473, 51-87, (2009).

41 de la Rosa, C. J. L., Sun, J., Lindvall, N., Cole, M. T., Nam, Y., Löffler, M., Olsson, E., Teo, K. B. K. & Yurgens, A. Frame assisted H2O electrolysis induced H2 bubbling transfer of large area graphene grown by chemical vapor deposition on Cu. *Applied Physics Letters* 102, (2013).

42 Sutter, P. & Sutter, E. Microscopy of Graphene Growth, Processing, and Properties. *Advanced Functional Materials* 23, 2617-2634, (2013).

43 Ishigami, M., Chen, J. H., Cullen, W. G., Fuhrer, M. S. & Williams, E. D. Atomic Structure of Graphene on SiO2. *Nano letters* 7, 1643-1648, (2007).

44 Gordillo, M. C. & Martí, J. Structure of water adsorbed on a single graphene sheet. *Physical Review B* 78, 075432, (2008).

45 McPherson, J. W., Khamankar, R. B. & Shanware, A. Complementary model for intrinsic time-dependent dielectric breakdown in SiO2 dielectrics. *Journal of Applied Physics* 88, 5351-5359, (2000).

46 Kurra, N., Sagade, A. A. & Kulkarni, G. U. Ultrafast Direct Ablative Patterning of HOPG by Single Laser Pulses to Produce Graphene Ribbons. *Advanced Functional Materials* 21, 3836-3842, (2011).

47 Popov, V. N. & Lambin, P. Theoretical Raman intensity of the G and 2D bands of strained graphene. *Carbon* 54, 86-93, (2013).

48 Hiura, H., Ebbesen, T. W., Fujita, J., Tanigaki, K. & Takada, T. Role of sp3 defect structures in graphite and carbon nanotubes. *Nature* 367, 148-151, (1994).

49 Yu, Q., Lian, J., Siriponglert, S., Li, H., Chen, Y. P. & Pei, S.-S. Graphene segregated on Ni surfaces and transferred to insulators. *Applied Physics Letters* 93, (2008).

50 Gao, L., Ren, W., Xu, H., Jin, L., Wang, Z., Ma, T., Ma, L.-P., Zhang, Z., Fu, Q., Peng, L.-M., Bao, X. & Cheng, H.-M. Repeated growth and bubbling transfer of graphene with millimetre-size single-crystal grains using platinum. *Nat Commun* 3, 699, (2012).

51 Gan, L., Rudi, S., Cui, C. & Strasser, P. Ni-Catalyzed Growth of Graphene Layers during Thermal Annealing: Implications for the Synthesis of Carbon-Supported Pt□Ni Fuel-Cell Catalysts. *ChemCatChem* 5, 2691-2694, (2013).

52 Pak, Y., Jeong, H., Lee, K.-H., Song, H., Kwon, T., Park, J., Park, W., Jeong, M.-S., Lee, T., Seo, S. & Jung, G.-Y. Large-Area Fabrication of Periodic Sub-15 nm-Width Single-Layer Graphene Nanorings. *Advanced Materials* 25, 199-204, (2013).

53 Zheng, M., Takei, K., Hsia, B., Fang, H., Zhang, X., Ferralis, N., Ko, H., Chueh, Y.-L., Zhang, Y., Maboudian, R. & Javey, A. Metal-catalyzed crystallization of amorphous carbon to graphene. *Applied Physics Letters* 96, (2010).

54 Chu, J. H., Kwak, J., Kwon, T.-Y., Park, S.-D., Go, H., Kim, S. Y., Park, K., Kang, S. & Kwon, S.-Y. Facile Synthesis of Few-Layer Graphene with a Controllable Thickness Using Rapid Thermal Annealing. *ACS Applied Materials & Interfaces* 4, 1777-1782, (2012).

55 Gilgueng Hwang, J. C. A., Emir Vela, Sinan Haliyo, Stéphane Régnier, "Graphene as Thin Film Infrared Optoelectronic Sensor", International Symposium on Optomechatronic Technologies (ISOT), Istanbul, Turkey,9, 21-23, (2009).

56 Vasko, F. T. & Ryzhii, V. Photoconductivity of intrinsic graphene. *Physical Review B* 77, 195433, (2008).

57 Dresselhaus, M. S. & Dresselhaus, G. Intercalation compounds of graphite. *Advances in Physics* 51, 1-186, (2002).

58 Bhowmik, R. N. Ferromagnetism in lead graphite-pencils and magnetic composite with CoFe2O4 particles. *Composites Part B: Engineering* 43, 503-509, (2012).

59 S. Cain, A. A. C., R. Brunnelle and A. Lyter. *J. Forensic Sci.* 23, (1978).

60 Totty, J. A. Z. a. R. N. *J. Forensic Sci.* 25, (1980).

61 Denman, J. A., Kempson, I. M., Skinner, W. M. & Kirkbride, K. P. Discrimination of pencil markings on paper using elemental analysis: an initial investigation. *Forensic Science International* 175, 123-129, (2008).

62 Mandal, P., Dey, R. & Chakraborty, S. Electrokinetics with "paper-and-pencil" devices. *Lab on a Chip* 12, 4026-4028, (2012).

63 Zheng, G., Hu, L., Wu, H., Xie, X. & Cui, Y. Paper supercapacitors by a solvent-free drawing method. *Energy & Environmental Science* 4, 3368-3373, (2011).

64 Ren, T.-L., Tian, H., Xie, D. & Yang, Y. Flexible Graphite-on-Paper Piezoresistive Sensors. *Sensors* 12, 6685-6694, (2012).

65 Wang, Y. & Zhou, H. To draw an air electrode of a Li-air battery by pencil. *Energy & Environmental Science* 4, 1704-1707, (2011).

66 Gimenez, A. J., Yanez-Limon, J. & Seminario, J. M. Paper-based photoconductive infrared sensor. *The Journal of Physical Chemistry C* 115, 18829-18834, (2011).

67 ul Hasan, K., Nur, O. & Willander, M. Screen printed ZnO ultraviolet photoconductive sensor on pencil drawn circuitry over paper. *Applied Physics Letters* 100, (2012).

68 Kim, D.-H., Kim, Y.-S., Wu, J., Liu, Z., Song, J., Kim, H.-S., Huang, Y. Y., Hwang, K.-C. & Rogers, J. A. Ultrathin silicon circuits with strain-isolation layers and mesh layouts for high-performance electronics on fabric, vinyl, leather, and paper. *Advanced Materials* 21, 3703-3707, (2009).

69 Nie, Z., Nijhuis, C. A., Gong, J., Chen, X., Kumachev, A., Martinez, A. W., Narovlyansky, M. & Whitesides, G. M. Electrochemical sensing in paper-based microfluidic devices. *Lab Chip* 10, 477-483, (2010).

70 Russo, A., Ahn, B. Y., Adams, J. J., Duoss, E. B., Bernhard, J. T. & Lewis, J. A. Pen-on-Paper Flexible Electronics. *Advanced Materials* 23, 3426-3430, (2011).

71 Tobjörk, D. & Österbacka, R. Paper Electronics. *Advanced Materials* 23, 1935-1961, (2011).
72 Hu, L., Choi, J. W., Yang, Y., Jeong, S., La Mantia, F., Cui, L. F. & Cui, Y. Highly conductive paper for energy-storage devices. *Proc Natl Acad Sci U S A* 106, 21490-21494, (2009).
73 Kordás, K., Mustonen, T., Tóth, G., Jantunen, H., Lajunen, M., Soldano, C., Talapatra, S., Kar, S., Vajtai, R. & Ajayan, P. M. Inkjet printing of electrically conductive patterns of carbon nanotubes. *Small* 2, 1021-1025, (2006).
74 Lin, Y.-M., Dimitrakopoulos, C., Jenkins, K. A., Farmer, D. B., Chiu, H.-Y., Grill, A. & Avouris, P. 100-GHz transistors from wafer-scale epitaxial graphene. *Science* 327, 662-662, (2010).
75 Sagar, A., Balasubramanian, K., Burghard, M. & Kern, K. Electric field effect in graphite crystallites. *Applied Physics Letters* 100, (2012).
76 Misra, R., McCarthy, M. & Hebard, A. F. Electric field gating with ionic liquids. *Applied Physics Letters* 90, 052905, (2007).
77 Cho, J. H., Lee, J., He, Y., Kim, B. S., Lodge, T. P. & Frisbie, C. D. High-Capacitance Ion Gel Gate Dielectrics with Faster Polarization Response Times for Organic Thin Film Transistors. *Advanced Materials* 20, 686-690, (2008).
78 Cho, J. H., Lee, J., Xia, Y., Kim, B., He, Y., Renn, M. J., Lodge, T. P. & Frisbie, C. D. Printable ion-gel gate dielectrics for low-voltage polymer thin-film transistors on plastic. *Nature materials* 7, 900-906, (2008).
79 Yuan, H., Shimotani, H., Tsukazaki, A., Ohtomo, A., Kawasaki, M. & Iwasa, Y. High-Density Carrier Accumulation in ZnO Field-Effect Transistors Gated by Electric Double Layers of Ionic Liquids. *Advanced Functional Materials* 19, 1046-1053, (2009).
80 Kim, B. J., Jang, H., Lee, S.-K., Hong, B. H., Ahn, J.-H. & Cho, J. H. High-performance flexible graphene field effect transistors with ion gel gate dielectrics. *Nano letters* 10, 3464-3466, (2010).
81 Hernandez, Y., Nicolosi, V., Lotya, M., Blighe, F. M., Sun, Z., De, S., McGovern, I. T., Holland, B., Byrne, M., Gun'Ko, Y. K., Boland, J. J., Niraj, P., Duesberg, G., Krishnamurthy, S., Goodhue, R., Hutchison, J., Scardaci, V., Ferrari, A. C. & Coleman, J. N. High-yield production of graphene by liquid-phase exfoliation of graphite. *Nat Nanotechnol* 3, 563-568, (2008).
82 M. A. Pimenta, G. D., M. S. Dresselhaus, L. G. Cancado, A. Jorio and R. Saito *Phys. Chem. Chem. Phys.* 9, (2007).
83 L. M. Malard, M. A. P., G. Dresselhaus and M. S. Dresselhaus. *Phys. Rep.* 473, (2009).
84 Yu, D., Wang, C., Wehrenberg, B. L. & Guyot-Sionnest, P. Variable range hopping conduction in semiconductor nanocrystal solids. *Phys Rev Lett* 92, 25, (2004).
85 S. S. N. Bharadwaja, C. V., N. Fieldhouse, S. Ashok, M. W. Horn and T. N. Jackson. *Appl. Phys. Lett.* 94, (2009).
86 Chen, B., Cui, T., Liu, Y. & Varahramyan, K. All-polymer RC filter circuits fabricated with inkjet printing technology. *Solid-State Electronics* 47, 841-847, (2003).
87 K. Nagashio, T. N., K. Kita and A. Toriumi *Appl. Phys. Express* 2, (2009).
88 Kim, B. J., Kang, M. S., Pham, V. H., Cuong, T. V., Kim, E. J., Chung, J. S., Hur, S. H. & Cho, J. H. Low-voltage solution-processed graphene transistors based on chemically and solvothermally reduced graphene oxide. *Journal of Materials Chemistry* 21, 13068-13073, (2011).

PART III

Au-PDMS NANOCOMPOSITE: PROPERTIES AND ELECTRICAL CHARACTERIZATION

Summary

In recent years polymer circuits and devices have received growing interest because of their low cost fabrication procedure. Conductive polymers are well known in literature because they can conduct electricity and store charge throughout their volume. Few examples are polyaniline, polypyrrole etc. They have sp^2 hybridized carbon. The p_z orbitals present in them overlap with each other and form what is known as delocalized orbitals. The electrons present in these p_z orbitals have high mobility. But for insulating polymers such is not the case. To achieve improved conductivity, irradiation or doping (by oxidation) of the polymer is done.

Au nanoparticles-poly (dimethylsiloxane) (AuNPsPDMS) nanocomposites is quite well known in the scientific community. This nanocomposite is prepared by the standard in-situ method which is entirely a green process. $KAuCl_4$ and PDMS were used as Au-precursor and reducing agent respectively. Because of the Au nanoparticles the nanocomposites prepared exhibit novel properties, completely unknown to the

** Marked experiments were done in collaboration with Dr. Ritu Gupta.*

PDMS matrix as such. Study was carried out to understand the role of different ambience on the nanocomposite.

The importance and effects of capacitor geometry on the electrical property of Au-PDMS was examined. The mobility of charge carriers in the devices were determined by the Mott Gurney law. The conduction value of the nanocomposite was quite low. So different methods were tried to increase and improve the conduction value of the polymer composite. Effects of substrates on the devices were analyzed by changing the top electrode to glass and PET. The top electrode made from PET substrates showed more stability than the ones made with glass. Current versus voltage measurements were carried out using the Source Measurement Unit Keithley 236 and the Semiconductor Characterisation System Keithley 4200. As is known in literature, current through the nanocomposite decreases when toluene is added to it. Contrary to this an increment in current was observed when toluene vapor was passed through the samples having capacitor geometry. Performance of the device under the application of pressure was also studied. Apart from this electrical stress was created inside Au-PDMS by applying a shock of 100V for 10 seconds. The behavior of the circuit was investigated in an inert atmosphere of nitrogen and in toluene vapor. Significant changes in current were observed each time. Inspection of both capacitor and in-plane geometry using nanocomposite as the dielectric was carried out to check the influence of toluene vapor. In order to prevent the shorting of the electrodes a surface activator was used and the performance characteristics were measured. Finally metallization of the Au-PDMS composite was done and conductivity values of the devices built from it were compared to check how conducting and stable the gold film was. The development of accurate models for charge carrier conduction and mobility is a crucial step to design any device. Two probe temperature dependent studies were carried out to enlighten upon the type of charge carriers in the Au-PDMS composite.

PDMS being non-toxic and the procedure followed to produce it was a green process so the end product was environment and human friendly. PDMS has already found its uses in a wide variety of applications because of its rheological property. By increasing the conductivity as discussed earlier it can be

incorporated in various other applications. The devices made have the potential to be used as touch sensors, stress and strain gauges etc.

III.1 Introduction

The field of nanoscience is one of the most prevalent and popular areas of current research. Polymer science and technology takes a conspicuous part in it.[1] The properties of the polymer like mechanical,[2,3] optical,[4] electrical and also the dielectric properties have been studied for few decades.

Dielectric constant is given by the ratio of the permittivity of the dielectric to the permittivity of vacuum. Permittivity expresses the ability of a material to polarize in response to an applied field.[5] The search for a dielectric which can be made into thin films having low sheet resistance, flexibility and also biocompatibility has dragged a lot of attention.[6,7,8] Inorganic substrates like mica have been traditionally used as a dielectric medium. However polymers like coronene, PMMA are gaining wider use in this field.[9]

Polymers are formed when a large number of molecules called monomers are joined sequentially, forming a chain.[10] Polymers can be either polar or non-polar, determined by the chain geometry[11] which further affects the dielectric properties of the polymer.[8] Few examples of polar polymers are PMMA, PVC etc. while non-polar polymers include PTFE,[12] PS etc. The electronic polarization is instantaneous at any frequency for both types of polymer. However, polar polymers require greater time to align the dipoles when electric field is applied. Polymers have gained its application as a dielectric over the inorganic counterpart because of their simple processability involving spin coating, whereas inorganic materials which are generally used as dielectric have high thermal properties and require extreme processing temperatures. Other properties which make polymers an attractive dielectric are their immersion in organic substrate and their flexibility.[13,14]

In general polymers are highly insulating. However, few semiconducting polymers have been developed so far.[15] The most important among them being the conjugated conducting polymers.[16,17,18] To become electrically conductive, a polymer has to imitate the behavior of a metal, that is, its electrons has to be free

to move around and not bound to the atoms. Conjugated polymer consists of alternate single and double bonds, called conjugated double bonds. The conjugated structure becomes conducting through a continuous overlapping of d-orbitals along the polymer backbone.[17,18] Since most organic polymers do not have intrinsic charge carriers, the required charge carriers can be provided by partial oxidation (p-doping) of the polymer chain or by partial reduction (n-doping) with electron donors. Through such doping process, charged defects are introduced, which could then be available as the charge carriers. Doping is mainly done by adding inorganic particles to the polymer matrix to form a composite. For polymers where there is limited π-bonding overlapping, conduction of charge carriers happens due to quantum mechanical tunnelling.[19,20] This tunnelling nature of the charge transport is also referred to as hopping.[21] Hopping of charge carriers depends upon the energy gap between HOMO and LUMO levels. Carrier mobility depends on the abundance of levels for the electrons or holes with similar energy to move to. The greater the abundance more will be the hopping.[10,22]

Polymer nanocomposites[23,24] are materials having particles of nanoscopic size dispersed in the polymer medium.[25] Addition of nanoparticles changes the polymer properties drastically, sometimes completely renovating the properties of the pristine.[26] This includes amending properties like strength, barrier properties, conductivity and even heat resistance.[27,28] A range of different metal nanoparticles and their combination with varieties of conjugated polymers have been studied recently.[29] The synthesis of the metal nanocomposite is an ongoing research in the scientific field.[30,31] They are mostly prepared by low cost fabrication processes like spin coating and other simple chemical processes.[32,33] Thus the polymer industries have received growing interest in the scientific world as a completely new avatar the nanocomposite.[10]

Electrical properties of the metal nanoparticles[34] have invigorated much interest in the scientific community because of its peculiar behavior, which is completely different from its bulk counterpart.[21,35] It is well known in literature how electron transfer takes place by quantum tunneling in metal nanoparticles. They also give rise to the fascinating property of single electron tunneling.[36,37] When metal nanoparticles

are embedded in polymer matrix the conductivity of the matrix gets enhanced.[38,39] When non-conjugated linkers connect these nanoparticles, electron tunneling is the predominant mechanism for electrical conduction. The conductivity does not follow the ohmic behavior always.[40] As a result a different theory other than the Ohms law is required to find the mobility of the charge carrier in the polymer matrix.

A significant amount of theoretical work has been done to understand the space charge limited flow for any electrode system[41,42] with a gap in nanometer regime.[43] However, experiments to verify such predictions are limited, because of the difficulties involved in fabrication and measurement. There are two main laws governing the space charge limited current namely the Childs law or the Child-Langmuir law and the Mott-Gurney law.[44,45]

Childs law states that the space charge limited current in a plane parallel diode varies directly as the three halves power of the anode voltage V_a and inversely as the square of the distance 'd' separating the anode and the cathode, given by the equation

$$I_a = J \times S = \frac{4}{9}\epsilon\sqrt{2e/m_e}\, S V_a^{3/2}/d^2 \quad \ldots\ldots\ldots\ldots\ldots\ldots \text{(i)}$$

Where, I_a is the anode current, J is the current density and S is the anode inner surface area, e is the electronic charge, m_e is the mass of the electron ε is the absolute permittivity of the medium and V_a is the applied voltage.

For a current density J and an applied voltage V, experimentally observed Mott Gurney law gives $J \alpha V^2$. This is applicable for a steady state, trap free space charge limited conduction inside a plane parallel dielectric capacitor.[44] It depends on the assumptions of: (i) the presence of only one type of carrier i.e. either electrons or holes as charge carriers in the dielectric (ii) the absence of intrinsic (ohmic) conductivity and (iii) the existence of constant permittivity.[45]

III.2 Scope of Present Investigation

Polydimethysiloxane also known as PDMS having the formula $(C_2H_6OSi)_n$ is a mineral-organic polymer of the siloxane family. It is best known for its excellent rheological properties.[46] For this reason PDMS has been mostly used as a structural material in many applications. Its role in soft lithography, food and cosmetics is quite well known. To explore the other functionalities of PDMS and to broaden the range of its application is a critical requirement. It is a damp insulator or dielectric having dielectric constant between 2.3 to 2.8[47] and is often used for encapsulating electronic devices and also as flexible substrate for electronics.[7] Like many other polymers (plastics and rubber) these also repel electrical conductivity. If somehow it is made conducting, apart from the viscoelastic properties it will feature new electrical characteristics as well. The knowledge and improvement of its electrical properties[48] would be beneficial for designing new electromechanical systems.[3] Thus it will become feasible for new types of applications like sensors, gauges etc. The most common way to achieve this is by adding inorganic or organic conductors as fillers to the PDMS matrix. PDMS metallized with Au nanoparticles (Au-PDMS) shows much ameliorated properties than the pristine. Besides this, the biocompatible nature of the Au-PDMS[49] nanocomposite can make it worthy of use in many of the futuristic devices.[50,51]

There are not many reports regarding the electrical characterization of the nanocomposite Au-PDMS. The present work deals with the practical and efficient approach to enhance the electrical properties of PDMS, using gold nanaoparticles to form a nanocomposite. Electrical conductivities of Au-PDMS nanocomposites were checked to find any improvement in the inter-particle charge transport. I-V characteristics of capacitor devices fabricated from Au-PDMS were studied. The mobility of charge carriers in the matrix were determined by the Mott Gurney law. Effects of pressure and high voltages on the devices were analyzed. Also in this study, the role of the surrounding ambience on the devices was checked. The method focused mainly on observing the changes in current while passing vapors of toluene and nitrogen in a chamber containing the circuit.

III.3 Experimental Section

Materials Required

Micro slides of thickness 1.25 mm purchased form Blue Star (deluxe) was used as substrates for thin film deposition. Oddy transparency sheets (PET sheets) were bought from ASM Pvt. Ltd, India. Chemicals used were acetone (99%), nitrogen gas, sulphur free toluene (99%), PDMS kit (Dow Corning, Sylgard 184), $KAuCl_4$ (Aldrich, 98%), ethyl alcohol (99%), APTMS (97%), double distilled water.

Fabrication of device and characterization

The purchased glass slides were cut into 2 x 2 cm^2 and 1 x 1 cm^2 pieces using a glass cutter purchased form ISU industries. PET sheets were also cut into 1 x 1.5 cm^2 size. The Au nanoparticles – PDMS composite was synthesized in the form of a gel. For glass electrodes, gold was sputtered on glass for 150 seconds, using a Polaron Sputter Coater SC502, from Fisons Instruments. For PET electrodes physical vapor deposition of gold was done using the PVD machine by Hindhivac Pvt. Ltd. model number 12A4D. Au-PDMS was coated in the form of a thin film on the top and bottom electrode using a spin coater (6000 TVP from Technoscience Instruments).

Electrical characterizations of the devices were done using Source Measurement Unit (SMU) Keithley 236. Semiconductor Characterization System (SCS) Keithley 4200 was also used for I-V and capacitance measurements respectively. The thickness measurement was carried out in Optical profiler, Veeco Wyko NT9100. Images were taken using an optical microscope by Laben Instruments mounted with Discovery C30 digital imager. Metallization of Au-PDMS film was carried out by dipping the Au-PDMS circuits inside 0.1 M $KAuCl_4$ solution. To understand the type of conduction and the process by which charge carriers are flowing, low temperature measurements were done.

III.4. Results and Discussion

*Synthesis of Au-PDMS nanocomposite**

The Au nanoparticles – PDMS composite,[52] well known in literature,[53,54] was reproduced in the form of a gel. An uncured mixture of PDMS was first prepared by mixing the pre-polymer and the curing agent in 10:1 volume ratio. In a glass vial 20 mM aqueous $KAuCl_4$ solution and uncured PDMS was taken in a 200:1 (m/v) ratio and stirred at 70 °C for 4 hours to from a maroon colored gel. The reaction was arrested by decanting the unreacted $KAuCl_4$ solution. Finally, Au-PDMS mixture was rinsed thoroughly with large amounts of water. Finally to remove any excess water within the Au-PDMS it was washed twice with ethanol. The air bubbles were removed by exposing it to vacuum and heating at 100 °C for 12 hrs. Figure III.1 depicts the process of how the Au-PDMS gel was prepared.

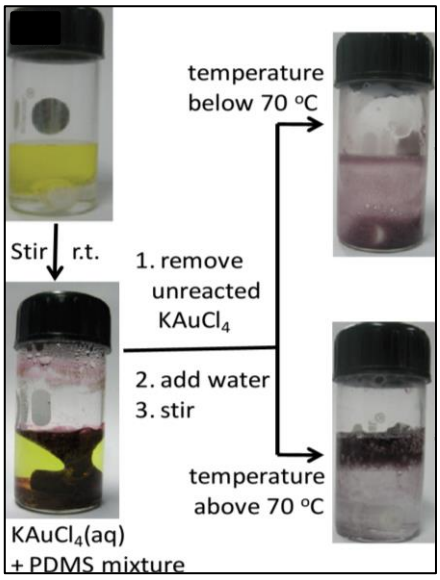

Figure III.1 AuNPs-PDMS nanocomposites: Optical photographs of the vial containing PDMS mixture in $KAuCl_4$ (aq., 20 mM) before (above) and after stirring (below) at room temperature for 30 min. Optical photographs of the vials following gel (above) or foam (below) formation (Reproduced from ref. 55).[55]

The curing of elastomer in the nanocomposite form was very slow even at higher temperatures resulting to a gel rather than a cured composite. The thus formed gel can be casted as a thin film.

Metal ion having a reduction potential (E^0) higher than the polymer when comes in contact with each other spontaneously gets reduced by the polymer to its zero-valent metal form. The polymer matrix transfer the electron to the metal ions and thus itself gets oxidized to a higher oxidation state.[32] The above mentioned synthesis process allows the PDMS to act both as the template and reducing agent. So no involvement of a separate reducing agent was required.

Device Fabrication

In order to make the capacitor geometry,[56] a thin film of the dielectric material was coated on both the electrodes. Capacitor geometry was built using (i) glass as top and bottom electrode and (ii) Glass as bottom electrode and PET as top electrode. The electrodes with 100 µL of Au-PDMS drop were spun at a speed of 1500 rpm for 60 seconds to obtain a thin film. More the rotational speed and time of rotation thinner was the film obtained. Au-PDMS film of approximately 6 to 18 µm was obtained every time.

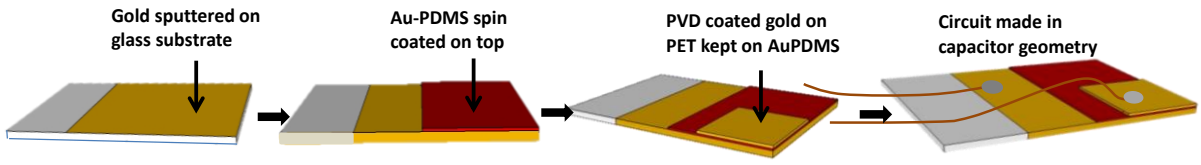

Figure III.2 The schematic shows the steps followed in making the capacitor geometry.

For few experiments involving in-plane geometry measurements, the dielectric material was drop coated instead of spin coating to get sufficiently thick layer. The schematic in Figure III.2 shows the steps of how the device with capacitor geometry was fabricated.

For curing the Au-PDMS film, it was heated at very high temperatures of 140 °C. In order to avoid damaging of film, temperature was gradually increased from 50 °C to 140 °C in steps of 30 °C keeping each temperature for 30 minutes and finally the device was left at 140 °C for 3 hours. The Au-PDMS nanocomposite does not get cured completely as discussed earlier and remains in the gel form. The top electrode was then placed on the bottom electrode firmly without applying much pressure. This was done

to ensure that the electrodes do not come in contact with each other. Copper wires were used to take contact from the top and bottom electrode with the help of silver paste. The enamel at the tip of copper wire was removed using an enamel remover. The photographs of the devices thus fabricated are shown in Figure III.3. Glass sputtered with gold was used as top and bottom electrode and capacitor geometry was made with Au-PDMS as dielectric (Figure III.3a). Due to the weight of top glass electrode Au-PDMS gets squeezed out (Figure III.3b) from the corners of the device. Glass was thus replaced with PVD coated PET as top electrode.

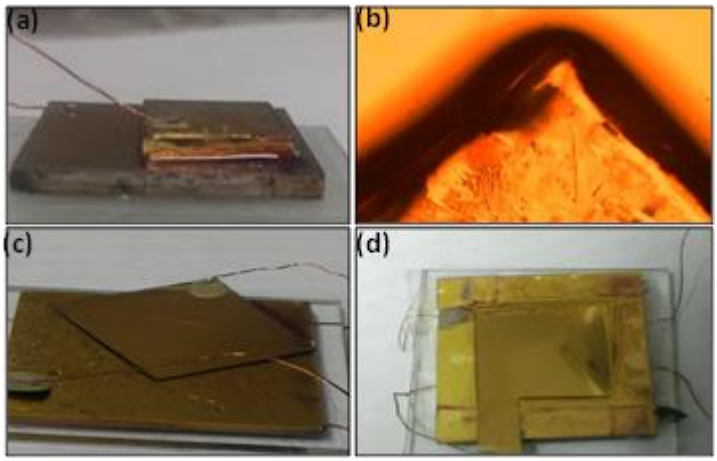

Figure III.3 (a) Capacitor geometry with glass and glass as bottom and top electrode. (b) Optical image showing Au-PDMS squeezing out at the edges causing the two electrodes to touch each other after few hours. (c) and (d) Glass as bottom and PET as top electrode for two different circuits.

Electrical Characterization

The electrical conductivity of polymer composite,[57] doped with metal nanoparticles, depends on the electron tunneling or hopping mechanism and electron migration between nanoparticles linked with polymer groups.[20,31,58] The electrical conductivity σ has a relationship with the charge carrier population (n), the electronic coupling term (β) and the activation energy barrier (E_A in kJ mol^{-1}) for the electron transfer.[19,22]

The relation is given as follows:

$$\sigma = \sigma_0 \exp[-\beta d] \exp[-E_A/RT] \ldots\ldots\ldots\ldots\ldots\ldots\ldots\ldots\ldots\ldots (ii)$$

$$\text{and } \sigma_0 = ne\mu \ldots\ldots\ldots\ldots\ldots\ldots\ldots\ldots\ldots\ldots\ldots\ldots\ldots\ldots\ldots (iii)$$

where d is the average inter-particle distance, R is the universal gas constant, T is temperature in Kelvin, e is the electron charge and μ is the mobility of the charge carriers. It has been observed experimentally that the electrical conductivity decreases when the size of the linker molecule between the nanoparticles increases. This is because higher activation energy is needed for the electron to transport (tunneling/ hopping).

Au-PDMS dielectric thin film was cured at 140 °C for 2 hours in order to avoid shorting of the electrodes. The dielectric still remained in the gel form but the viscosity increased. The performances of the thus formed devices are shown in Figure III.4. The I-V characteristics of the capacitor geometries prepared with glass as top and bottom electrode and glass-PET as bottom and top electrode respectively manifested features of non-linear conduction.[37,59] A distinct blockade region[37] is visible. The current for both glass and PET as top electrode is in the same range 10^{-10}A.

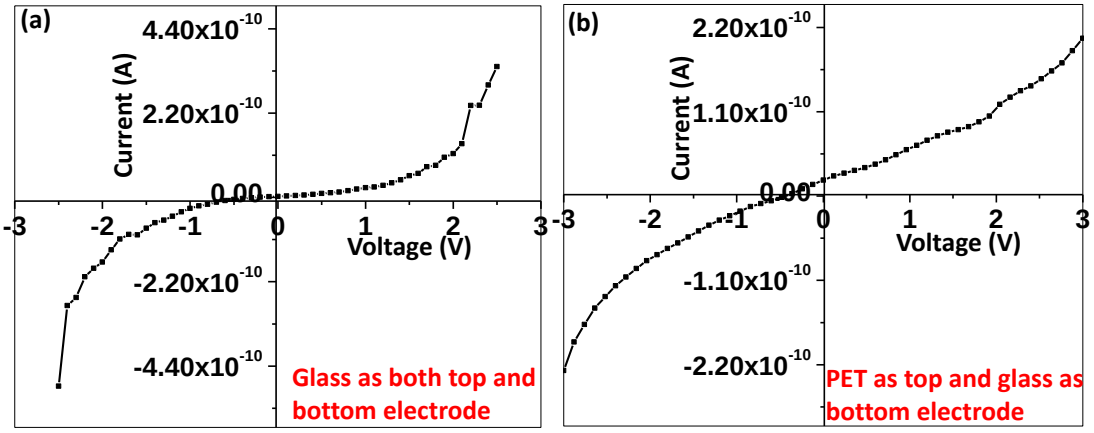

Figure III.4 (a) I-V characteristic for glass sputtered with gold as top electrode. (b) I-V characteristic for PET coated with gold, by PVD method, as top electrode.

Next the mobility of the charge carrier was calculated for the two geometries above using Gurney-Mott equation.[45] Equation (i) is used i.e. $J = 9/8(q\varepsilon_r\varepsilon_0\mu V^2/L^3)$

or, ln J = ln(constant) μ + 2 ln V……(iii)

where ε_r is permittivity of the nanocomposite. It is taken as 2.5. ε_0 = 8.8 x 10^{-12} F/m, the permittivity of vacuum, L is the distance between two electrodes. J is the current density given by I/A (where A = area of the contact pad with polymer). From equation (iii) we calculated lnJ and 2 lnV and plotted (Figure III.5a). The intercept of the graph was equated to the equation and the mobility values were calculated.

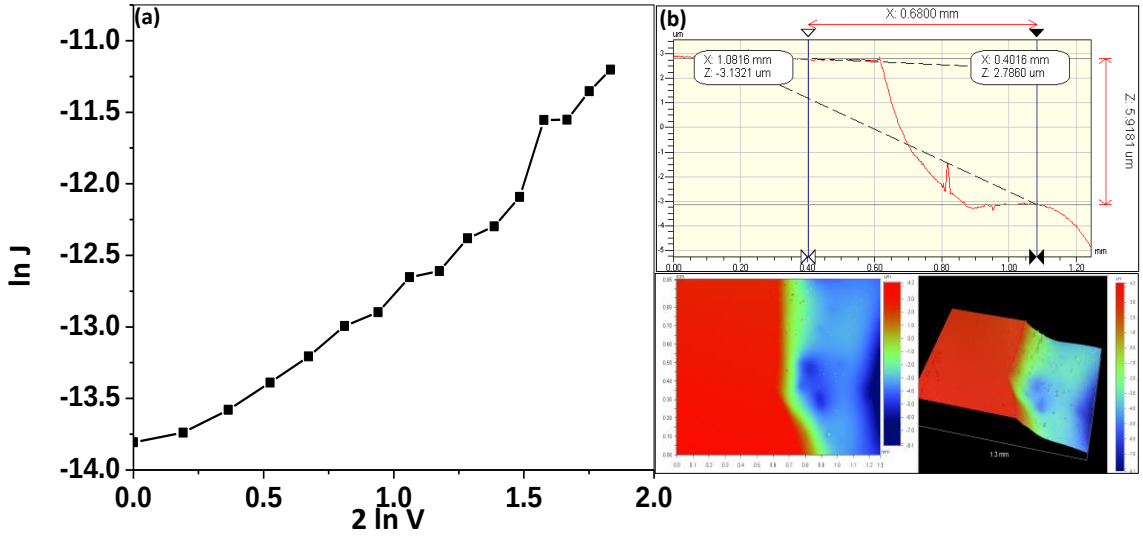

Figure III.5 (a) lnJ vs 2lnV curve for glass as top and bottom electrode. (b) Optical height profilometry along with 2D and 3D images for the Au-PDMS.

For glass as top and bottom electrode, the intercept value obtained from the graph (Figure III.5) is -14.23 which when supplied in the linear equation above gives the value for mobility. The value of the constant is $(9\varepsilon\varepsilon_0)/8L^3$ where L is obtained from the optical profilometry (Figure III.5b). From the height profiler the value of L was obtained to be 5.9 μm. Thus the mobility of the charge carriers was calculated to be 5.5 X 10^{-6} cm^2/V-s. Next the mobility for PET as top electrode and glass as bottom electrode was calculated. The intercept from the graph (Figure III.6) was found to be -13.02. After putting the value of the intercept in the equation (iii) above, the value of mobility for the capacitor geometry having glass as bottom and PET as top electrode was obtained. The length L was found to be 18.8 μm from the height profiler (Figure III.6b). Thus the value of mobility was calculated to be 5.95 x 10^{-6} cm^2/V-s. The change in mobility is influenced by the change in length L between the two electrodes.

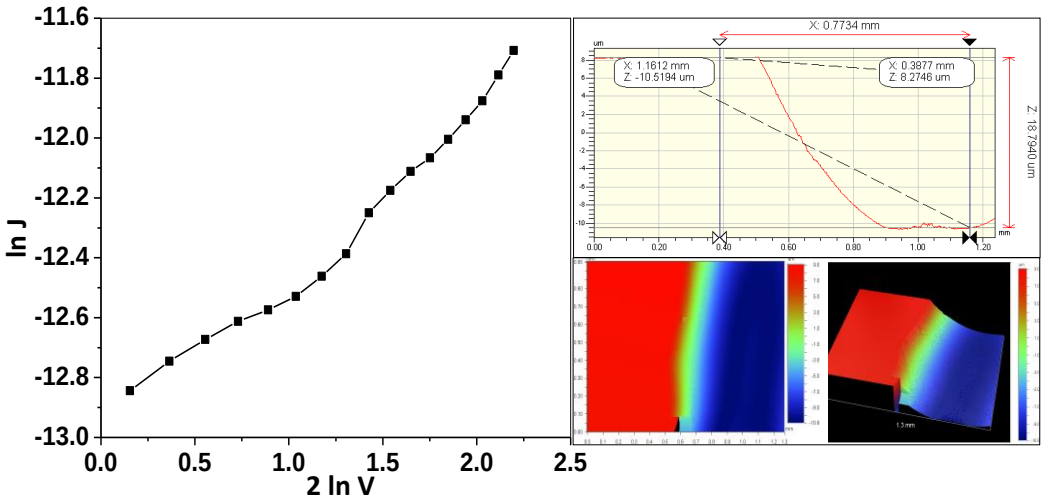

Figure III.6 (a) lnJ vs 2lnV curve for glass as bottom and PET as top electrode. (b) Optical height profilometry along with 2D and 3D images for the Au-PDMS.

The importance and effects of geometry on capacitor function is quite important. From the definition of capacitance one knows that it depends on the geometry completely. For better capacitance the electrode area should be larger with lower thickness of the dielectric. Capacitance has been calculated for the devices built. The Table III.1 gives the details on the values of mobility, resistance and the capacitance.

Table III.1 Values of resistance, capacitance and mobility for the two geometries are listed.

Bottom Electrode	Top Electrode	Dielectric Used	Area (m^2)	Length (µm)	Capacitance (nF)	Resistance (GΩ)	Mobility (cm^2/V-s)	Capacitance (Blockade region) (aF)
Gold coated glass	Gold coated glass	Au-PDMS	1 x10^{-4}	5.92	0.37	2.19	5.5 X 10^{-6}	0.2
Gold coated glass	Gold coated PET	Au-PDMS	1 x10^{-4}	18.82	0.12	14.99	5.95 x 10^{-6}	——

The devices produced have coulomb blockade region where there is no increase in current even though voltage is supplied.[59] This happens because activation energy above a threshold value is required for the charge to move to higher currents. Thus it stores energy before moving to higher current values. The capacitance for the blockade region has also been calculated from the graph using the formula

$$eV = e^2/2C \ldots\ldots\ldots\ldots (iv)$$

where eV is the voltage in electron volts in the blockade region.

A comparison on the context of stability of the devices with time was carried out. On account of stability, the devices made from glass/gold/Au-PDMS/gold/PET geometry showed better results (Figure III.7) than the ones made form glass/gold/Au-PDMS/gold/glass geometry.

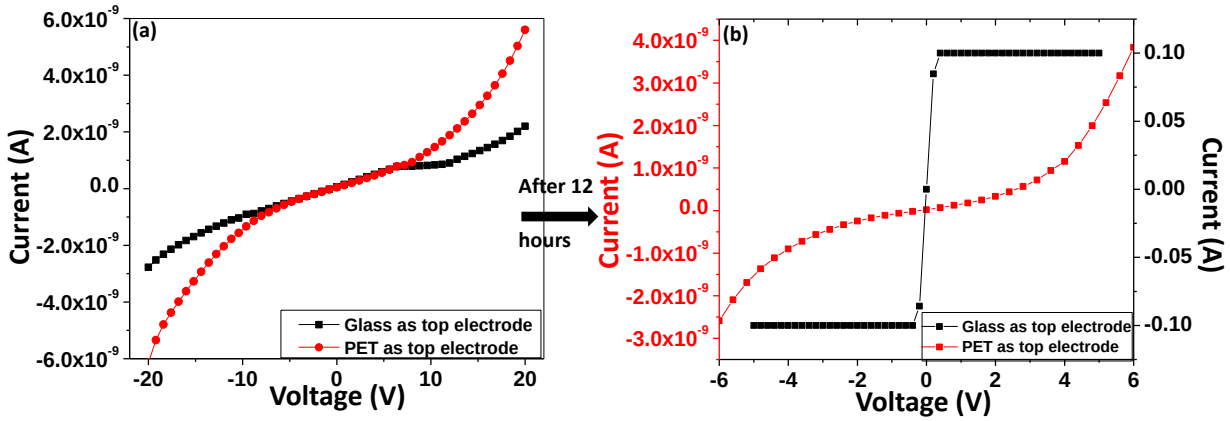

Figure III.7 Comparison between glass and PET as top electrode substrates. (a) Shows characteristics with glass and PET as top electrode when made and (b) shows the circuits after 12 hours. The circuit with glass as top electrode gets shorted and PET as top electrode still retains the same current.

The stability of the circuits was checked after 12 hours and the device with PET as top electrode showed better performance of the two. The device made with glass as top and bottom electrode got shorted thereby questioning the stability of the devices. This happens because, glass being heavy it sinks down into the gel under its own weight. Optical microscope images reveal clearly the spilling of the nanocomposite at the edges leading to the sinking of the top electrode (Figure III.3).

To avoid such electrical shorting, APTMS (3-Aminopropyl)trimethoxysilane, (10 µL) was spin coated on Au-PDMS at 1000 rpm before the top electrode was brought in contact. APTMS when left open in air gets solidified because of the methoxy groups which react with moisture in the air to form the siloxane bonds, helping in crosslinking. The solidification thus encapsulates the Au-PDMS gel. The shorting of the circuits was avoided by confining the Au-PDMS within the APTMS and not allowing it to get compressed and squeezed by the top electrode.

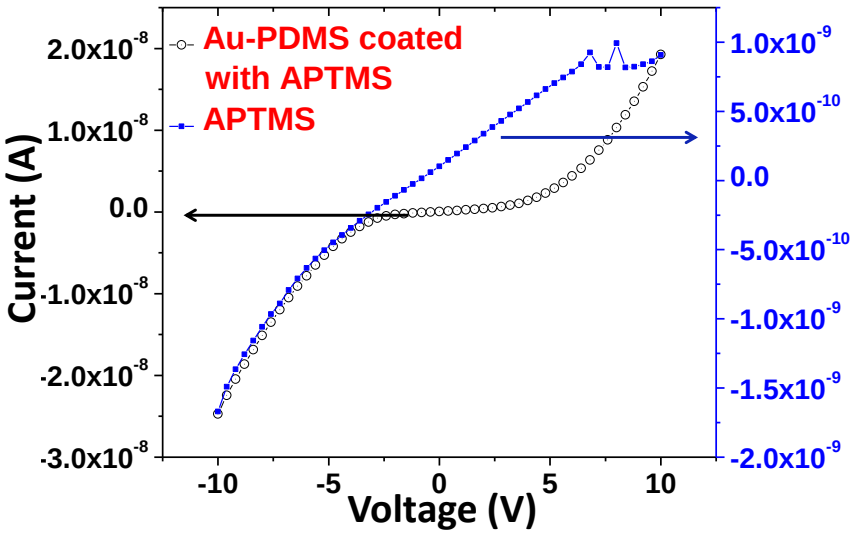

Figure III.8 I-V characteristics of APTMS spin coated on Au-PDMS and only APTMS. Both measurements were done taking glass, coated with gold, as bottom and top electrode.

The I-V characteristics were checked 24 hours later and it was found to be exactly the same. Thus APTMS improved the circuit stability by not allowing it to get shorted. But the I-V characteristics of APTMS alone showed current in nanoamperes for -10 to 10 V. This value is comparable to the values of current for Au-PDMS within the same voltage regime (Figure III.8). Thus the current passing through the APTMS will interfere with that of the Au-PDMS and the result might be a misnomer as both the chemicals will be taking part in conduction. To avoid such confusion, APTMS coating process was discarded and whenever glass coated with gold was used as top and bottom electrode, instead of spin coating the Au-PDMS, it was drop coated. Drop coating increased the thickness of the dielectric thus increasing the space between two electrodes and hence avoiding any kind of shorting.

Improvement of conductivity of the dielectric

To meet the development of smaller flexible and biocompatible electronic properties[56] in modern electronics it is critically important to discover matchable devices with equivalent or improved properties.[6,7] PDMS is known for its rheological properties but it is a damp insulator so no current is

expected to pass through it.[3,60] By embedding Au-nanoparticles in the polymer the conductivity was expected to be improved.[61] The current measured through the composite is in nanoamperes. Attempts to improve the electrical conductivity of the Au-PDMS nanocomposite were tried by using various other methods.

- Electrical stress application

The performance of the device was checked on application of a sudden high voltage. A high voltage of 100 V was applied with the Source Measurement Unit Keithley 236 for 10 seconds.

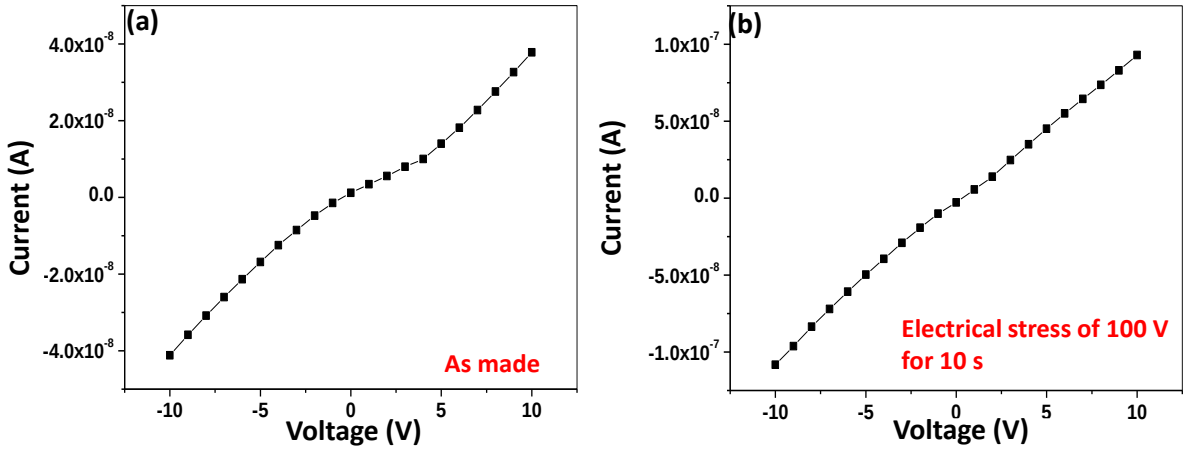

Figure III.9 Breakdown analysis: Applying 100 V to the Au-PDMS circuit for (a) 0 sec (b) 10 sec.

Because of the application of 100 V a sudden electrical stress is generated. The current increased by one order as seen in Figure III.9. The possible reason behind this can be the alignment of gold particles under the application of high voltage. When such elevated electric field is applied, momentum gets transferred from the electrons to the ions causing electromigration. The gold particle thus creates few percolated path for the current to pass through, resulting to an improved current.[47]

- Pressure application

Performance of the device made in capacitor geometry was checked by applying pressure. I-V measurement was checked before application of any pressure. This was followed by I-V measurements of

the device with 5 g weight placed on top of the electrode and then removing it. The schematic (Figure III.10) shows the steps of how experiment was done.

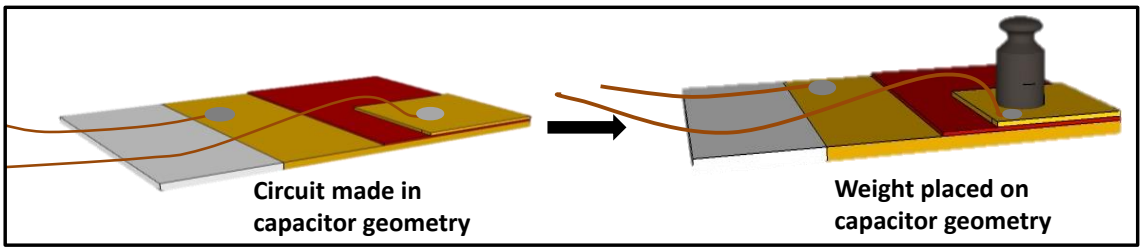

Figure III.10 Schematic showing the steps for the pressure experiment was done by placing known weights on the top electrode.

As seen from Figure III.11, a current of the order 10^{-7}A was observed for the circuit before application of any pressure. On adding 5 g weight (0.1 kPa) one order change was observed, i.e. the current increased to 10^{-6} A. On removing the 5 g weight, the current decreased and settled to its initial value within 10 minutes. The values of the pressure for a particular weight have been calculated (Table III.2).

Table III.1 Weights and their corresponding pressure values.

Weights (g)	Area (m^2)	Pressure (kPa)
5	0.5×10^{-4}	0.995
17	1.13×10^{-4}	1.503
50	2.84×10^{-4}	1.76
100	4.15×10^{-4}	2.41

The reason behind such increment in current can be attributed to the pressure application on the electrode. Au-PDMS gets squeezed between the electrodes causing the gold particles to come close together and form more channels than the initial ones resulting in improvement of current. But when pressure is released the gel returns to its initial configuration because of its viscous nature and so the gold particles embedded in them moves away from each other, decreasing the current.

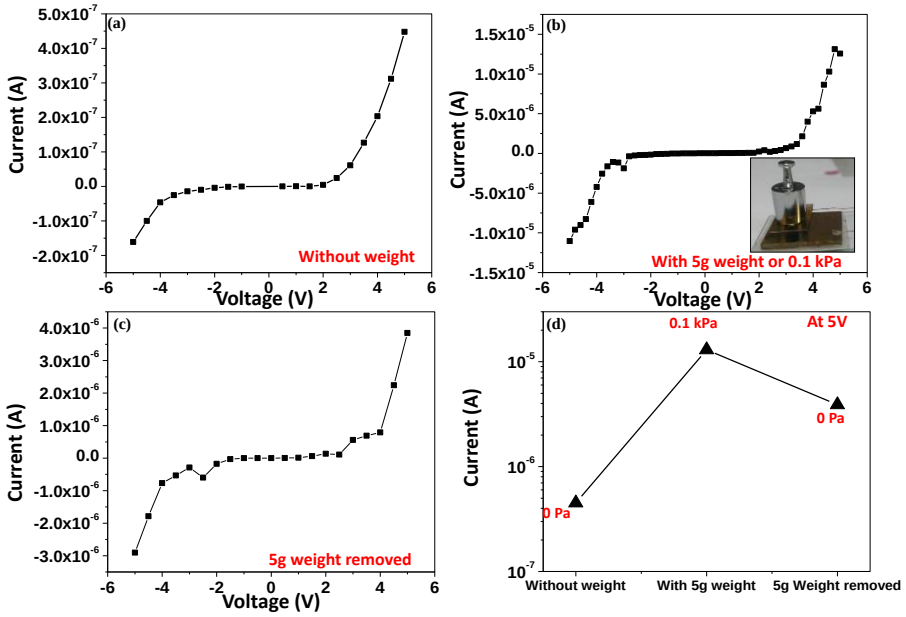

Figure III.11 (a) Performance of the device without any weight. (b) Performance of the device when a weight of 5 g is placed on top of the device. Inset shows image of how pressure was applied on top electrode by putting weights. (c) Performance after weight was removed. (d) Effect of pressure on current at a fixed voltage 5 V.

Next capacitance was measured with time for various pressures. Pressures were applied by varying the weights on top of the circuit as before. As shown in the graph (Figure III.12) when the pressure was increased, capacitance also increased. Initially the increment was less but as the pressure increased to 2.4 kPa the capacitance became as high as 800 pF from the initial value of 5 pF (no pressure). Thus a change of two orders of magnitude in capacitance was clearly observed.

The reason behind this can be explained by the capacitance formula itself. Capacitance is given by:

$$C = (\varepsilon A)/d \quad \text{..... (v)}$$

where ε is the permittivity of the dielectric, A is the area of the electrode and d is the distance between the electrodes. Capacitance for any device depends solely on its geometry and permittivity of the medium. From the equation it can be deduced that lower the thickness of the dielectric higher will be the capacitance. When pressure was applied distance d between the electrodes decreased hence the value of the capacitance increased.

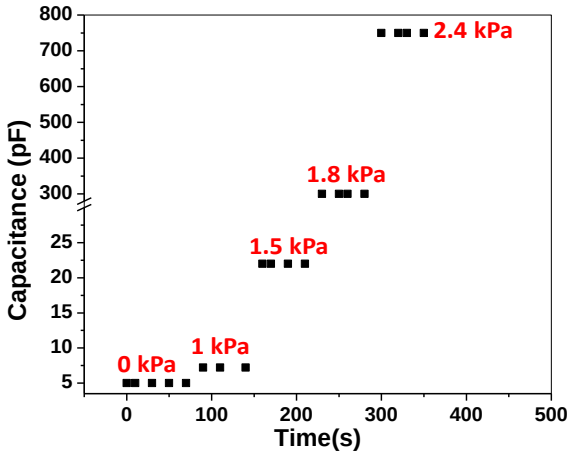

Figure III.12 Capacitance–time measurement: comparison between the capacitance for different applied pressure.

The application of pressure brought significant improvement in both current and capacitance values. To investigate the role of pressure further a screw gauge with least count of 0.01 mm was used to compress the device. Pressure was applied this time by rotating the circular scale reading of the screw gauge.

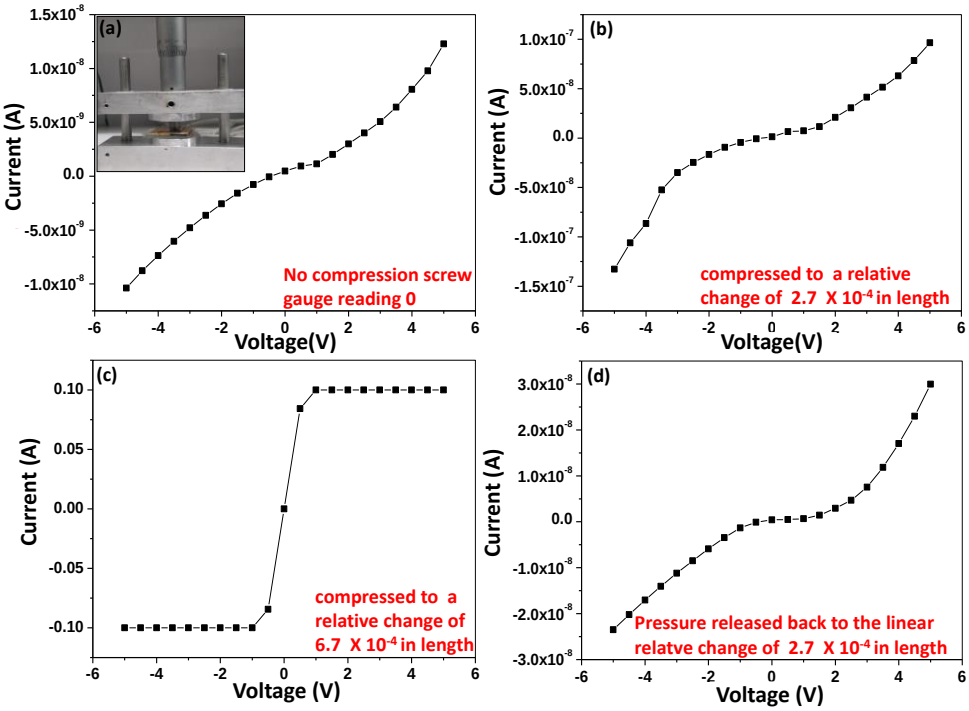

Figure III.13 I-V characteristic at different pressure. Pressure was applied by rotating the screw gauge circular scale. The strains applied on the circuits were (a) 0% (b) 0.027% (c) 0.067% and back to (d) 0.027%.

The device kept in between thus gets compressed. Figure III.13 shows how the current changed drastically by 7 orders of magnitude when the device was strained by rotating the screw gauge to change the linear scale reading by 0.01 cm. The strain applied on the circuit was calculated by the equation

$$\text{Strain} = (\text{Initial length} - \text{final length}) / \text{Initial length} \ldots\ldots\ldots \text{(vi)}$$

It was calculated in percentage.

The relative change in the length of the screw gauge was calculated taking the initial value zero. Initially the current change was gradual from 10^{-9} to 10^{-7} A, when the strain on the circuit was 0.047%. But when the circuit was strained by 0.067% current suddenly increased by, 7 orders of magnitude. On releasing the pressure by rotating the circular scale of the screw gauge back to 15 mm i.e. a strain of 0.027%, the current comes back to its initial values immediately. This happened because of the elastic nature of the Au-PDMS. The gel returns to its initial configuration thus decreasing the current. The improvement of the values of current is due to the same reason as that of the weight application. The linear scale reading of the screw gauge was calculated for every circular scale reading (least count of the screw gauge = 0.001 cm) and the strain was calculated. The current values for every reading have been compared in Figure III.14.

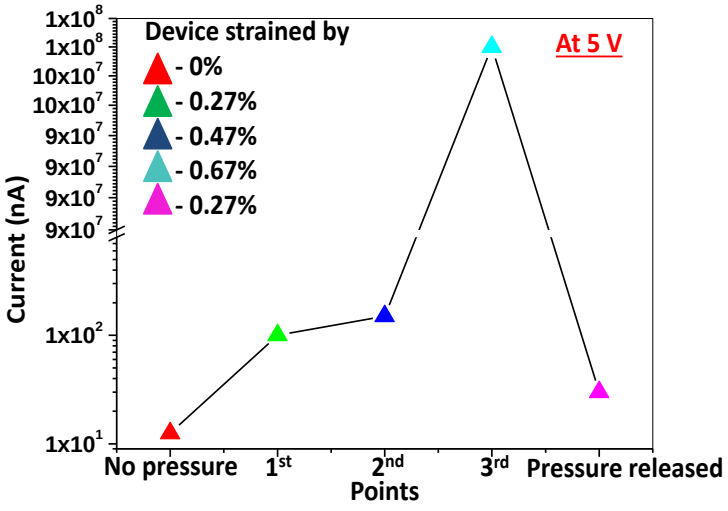

Figure III.14 Comparison between the currents for different compression values applied using the screw gauge.

The graph is plotted in log scale; (Figure III.14) depicts the change in current by 7 orders. The reason being, that gold particles tend to come closer with pressure so more percolated paths were created. This increases the number of levels for hopping of the charge carriers. At the extreme condition when current went to 10 mA the electrodes came to very close proximity because of the squeezing of the nanocomposite gel into very thin film device. Thus the conduction increased drastically. The pressure once released, the elastic polymer nanocomposite regained its previous shape and the electrodes moved away from each other. The current thus returned to its initial values.

- Passing vapor through Au-PDMS

The application of sudden high voltage and pressure helped improving the current in the capacitor geometry with Au-PDMS as dielectric. Further studies were carried out with the capacitor geometry by placing it in various environments. Different environments were created like (i) ambient condition, (ii) Nitrogen vapor and (iii) toluene vapor. Electrical characterization was carried out to check how it behaves at these ambiences. The schematic in Figure III.15 reveals the process of how the vapor was passed through the Au-PDMS devices. The vapor produced was allowed to pass through a closed chamber where the circuit was kept. Nitrogen was released from the nitrogen cylinder with a pressure of 2 kgf/cm^2 and allowed to pass through the chamber. For toluene vapor a setup was prepared shown in Figure III.15b.

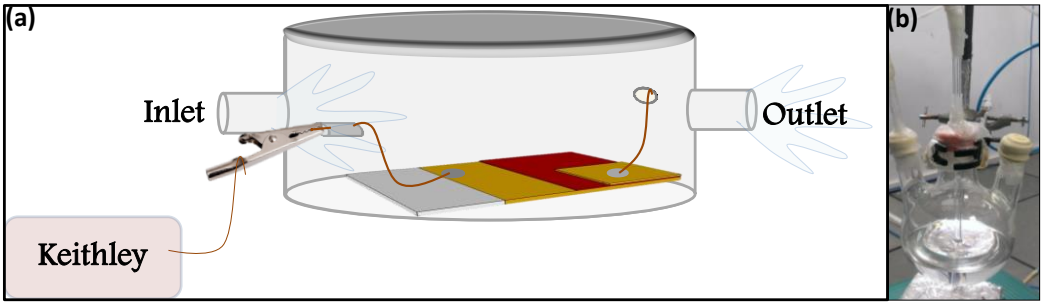

Figure III.15 (a) Schematic showing the chamber in which the circuit was kept and measurements were carried using a keithley while vapors were being passed via the inlet into the air tight chamber. (b) Image showing the setup to create toluene vapor.

Toluene was taken in a round bottom flask and nitrogen, released at a pressure of 3 kgf/cm^2, was bubbled through it to produce the toluene vapor.

It is known in literature that when toluene drop is added to Au-PDMS it swells up[55] due to the solubility of Au-PDMS in toluene. The gap between two gold particles increases due to the swelling therefore the current decreases. But the behavior of Au-PDMS in capacitor geometry with toluene vapor portrays quite a different result. Figure III.16 shows I-V for the device when kept in ambient and in nitrogen vapor. The current did not change much in both the environment (FigureIII.16a, b) and showed a value of the order 10^{-10} A. But when toluene vapor was passed through the chamber there was a visible increase in current (Figure III.16 c). The change in current values was not immediate and was visible only after 10-15 minutes of continuous passage of toluene vapor through the chamber. Several devices were characterized by passing toluene vapor through them and all the analysis repeated same result i.e. the performance improved showing an increase in current values.

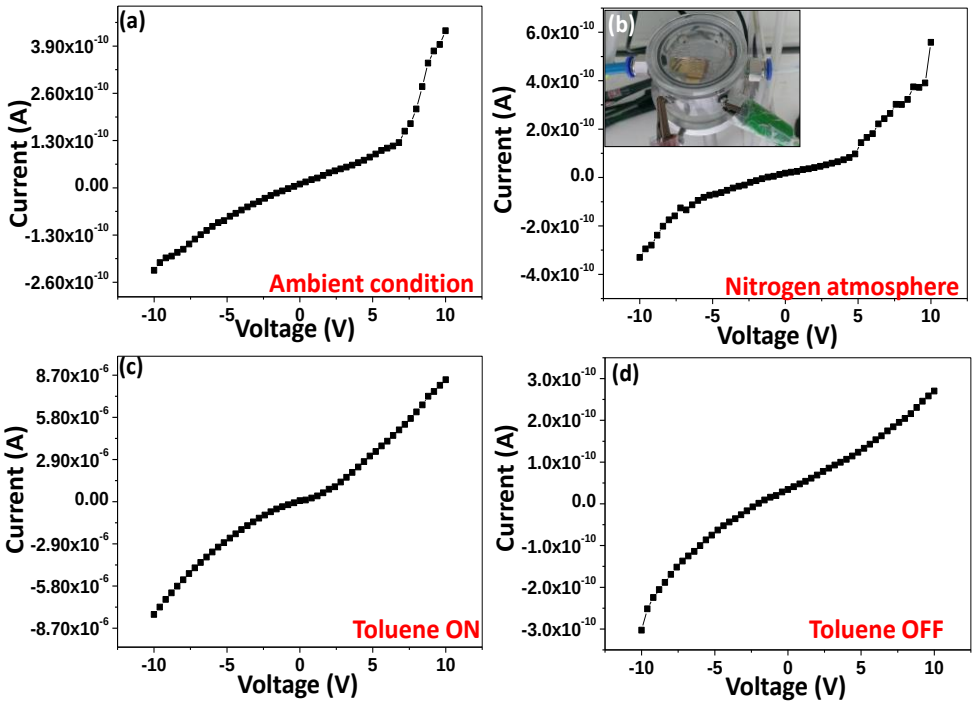

Figure III.16 (a) I-V characteristics in ambient condition and (b) nitrogen atmosphere. (c) and (d) Shows the I-V characteristics after switching on and off the toluene vapor.

The reason behind this increase in current when toluene vapor was passed can be attributed to three possibilities. First, when the vapor was passed through Au-PDMS its viscosity decreased because of its solubility in toluene. Hence the Au-PDMS gel flow rate increased than before causing the top electrode to sink down easily compressing the Au-PDMS. When the polymer gets clutched the Au-nanoparticles come close enough to form new route for the charge carriers to flow. Hopping becomes more efficient and frequent aiding to the increment of current. Second could be attributed to the channels formed by the toluene vapor. Since Au-PDMS is soluble in toluene, it would interact with toluene and hence the toluene vapors itself forms channels inside the polymer composite thus connection between the gold nanoparticles increases resulting to the improvement of current values.

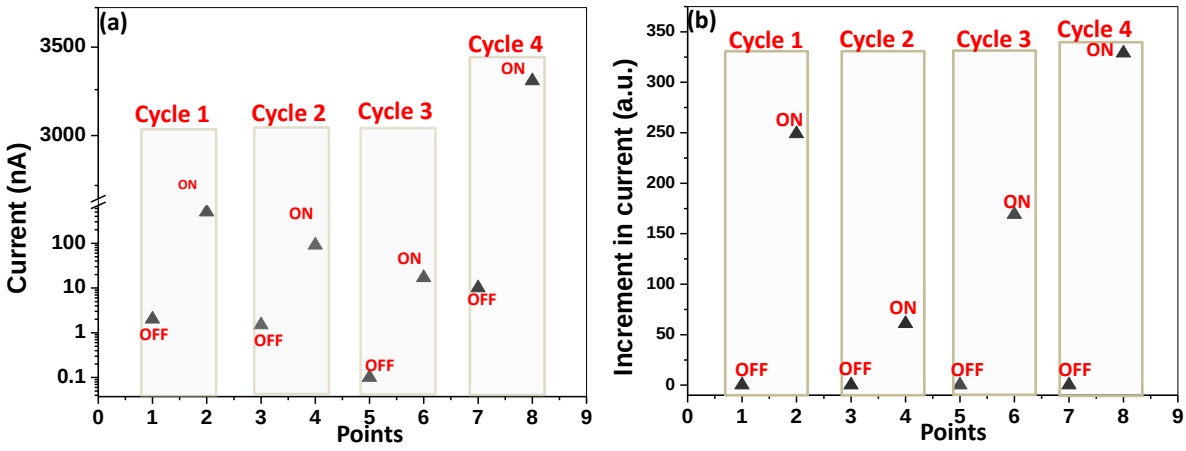

Figure III.17 (a) The graph shows 4 cycles for the same circuit and how the current varied when toluene was switched on and off. (b) Graph depicts the increment in current for graph a keeping the off current same.

The third reason can be accredited to the solubility of Au-PDMS in toluene. The PDMS along with the Au-nanoparticles embedded in the matrix tries to get dissolved in toluene. The barrier energy decreases due to the increased coupling between the particles. Because of this the hopping effect increases through the channels ensuing to the improved current. A comparison of the current values is shown for a given circuit in Figure III.17 to divulge upon how the current changed when toluene vapor was turned on and off during four cycle. However it must be kept in mind that the change seen was not immediate.

In order to understand the above phenomenon in details, I-V measurements in in-plane geometry were carried out, and they are shown in Figure III.18.

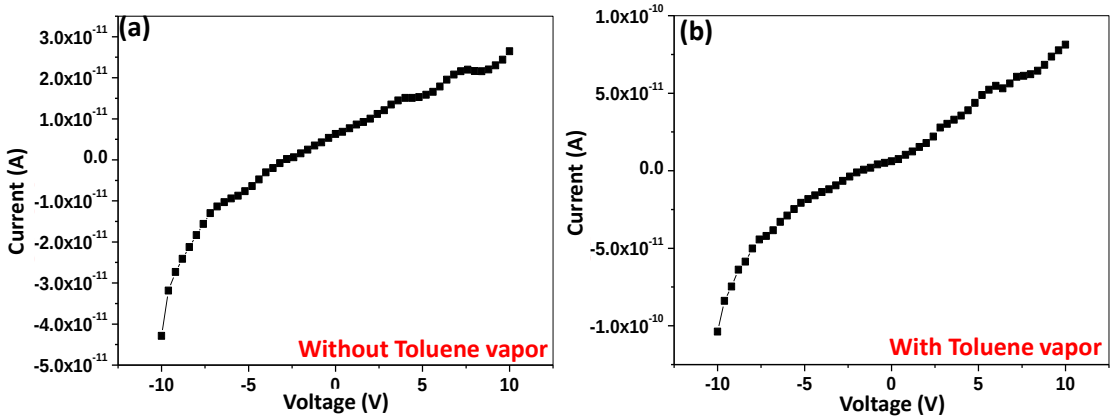

Figure III.18 In-plane geometry (a) and (b) shows the I-V graphs without toluene and with toluene vapor respectively.

For in-plane geometry gap electrodes were prepared by using carbon fiber as shadow mask and Au-PDMS was drop coated on the gap (9µm) between the electrodes. The current through the device in nascent condition is 10^{-11} A. When toluene vapor was passed across the sample the current did not change much like the ones in capacitor geometry implying that the capacitor geometry is playing a vital role here and sinking of top electrode towards the bottom electrode stand out to be an important reason for the improvement of current.

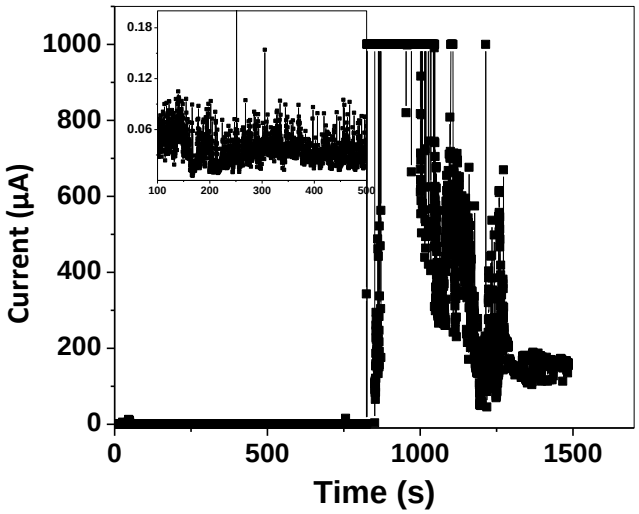

Figure III.19 Current vs time graph. At 800 sec toluene vapor was switched on and at 1030 sec toluene vapor was switched off. The inset shows the current at nascent condition till 600 seconds, when no toluene was passed.

Current versus time measurement with passage of toluene vapor was carried out with a constant input voltage of 45 V and a significant change from 10^{-8} A to 10^{-6} A was found. Initially no toluene vapor was passed. After 800 seconds toluene vapor was allowed to flow and the values of current improved by 2 orders of magnitude as seen in Figure III.19. But the I-t characteristics were noisy (Figure III.19) as the Source Measurement Unit is quite sensitive and also because of the dynamic nature of the Au-PDMS gel.

*Metallization of Au-PDMS**

Many attempts have been made in the past to produce flexible electronics.[62] Literature survey reveals that PDMS can be metallized to make it conducting. Thin layer of gold nanoparticles when forms a film on top of Au-PDMS it shows high conductivity. Au-PDMS being viscous in nature it is quite elastic and can be used for making a stretchable device. On the other hand Au-PDMS being a green material, its use in the living tissue is noteworthy for various applications.

Chemical route has been employed to produce a thin layer of interconnected Au nanoparticle film on Au-PDMS. 500 μL of $KAuCl_4$ of 0.1 M concentration was taken in a beaker and was diluted to 25 ml by adding distilled water to it. Glass slide coated with gold by PVD was used as electrode and a gap of 9 μm was made between the electrodes by masking it using a carbon fiber. On the gap Au-PDMS was drop coated. For the preparation of PDMS higher amount (1 μL extra) of elastomer was used. It was then placed inside the 25 mL diluted $KAuCl_4$. The setup was kept undisturbed on a hot plate at 70 °C for 12 hours. When taken out, the surface of the Au-PDMS was found covered with gold to give a polished shiny look.

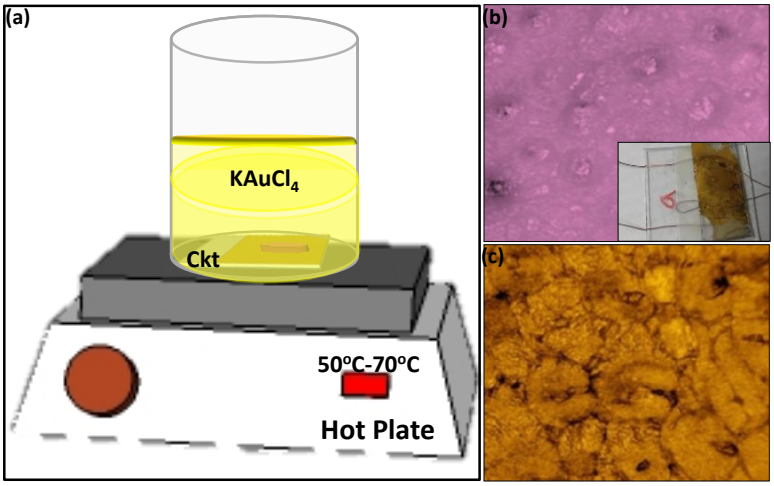

Figure III.20 (a) Schematic showing the process of how the metallization of Au-PDMS was done by dipping it in $KAuCl_4$ solution. (b) and (c) gives the optical image of the Au-PDMS and metallized Au-PDMS respectively. The inset shows the final circuit made out of it.

The schematic showing the setup is given in Figure III.20. Thin layer of gold film was formed on the Au-PDMS as imaged under Optical microscope.

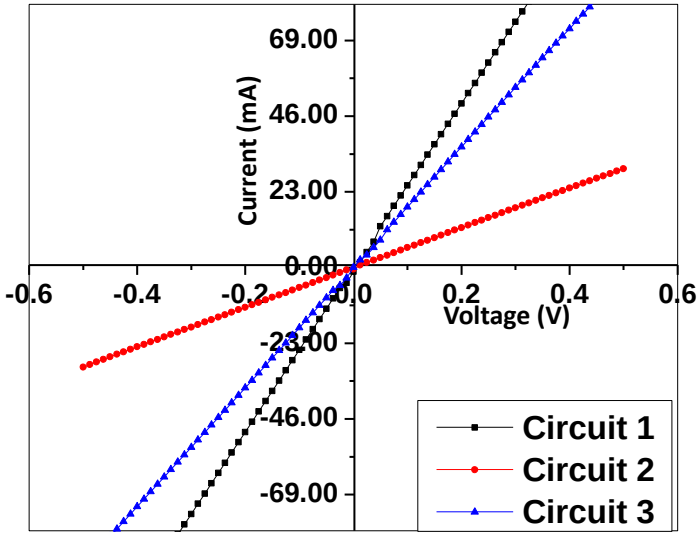

Figure III.16 I-V measurements of the metallized Au-PDMS circuits for three different circuits where the metallized gold film on Au-PDMS took part in conduction.

The I-V measurements showed linear behavior. Current, after metallization, increased to few milliamperes, since the film of gold nanoparticles is now taking part in the conduction. The thin metal layer so formed touched the bottom electrode at the edges so a parallel resistor geometry was formed. The

current passed via the metallized thin film and not the insulating Au-PDMS. Figure III.21 shows the I-V for thin metallized film, it exhibited linear behavior with a resistance of 5 to 10 Ω. The pristine surface having resistance in GΩ range did not show any conduction. One problem with Au film was the formation of cracks very often. It suffered from poor adhesion and generated cracks easily which reduced the current.[63] So the sample must be handled carefully.

Low temperature measurements

The dependence of electrical conductivity on temperature have been studied in various nano systems.[64-67] Two probe measurements were carried out with metallized Au-PDMS in in-plane geometry. It was taken care that the Au film on the Au-PDMS did not touch the bottom electrodes. The conduction thus took place via Au-PDMS and not the gold film. The metallization just helped in improving the electrical responses. By varying the temperature from 303 to 203 K, I-V measurements were recorded. Current was found to decrease with decrease in temperature. Below 203 K, measurement was not possible because of the very low value of the current, which could not be detected by Keithley 236. The linear portion of the curve between -20 to 5 V was taken (shown in Figure III.17) and the slope was calculated to find the resistance. Resistance thus calculated showed values in giga ohms. The high value of resistance is due to the insulating nature of PDMS.

For the electrical activation of Au-PDMS higher voltages (20 to 30 V) was required. At room temperature the current is still higher than the ones at low temperatures (253 to 203K). This is maybe due to the reduction of contact resistance by thermal activation. Two possible effects lead to this behavior and they are joule heating and electron migration i.e. combination of both electrical and thermal activation. Higher temperature also leads to localized joule heating. Thus electron hopping model can be applied for the circuit behavior.

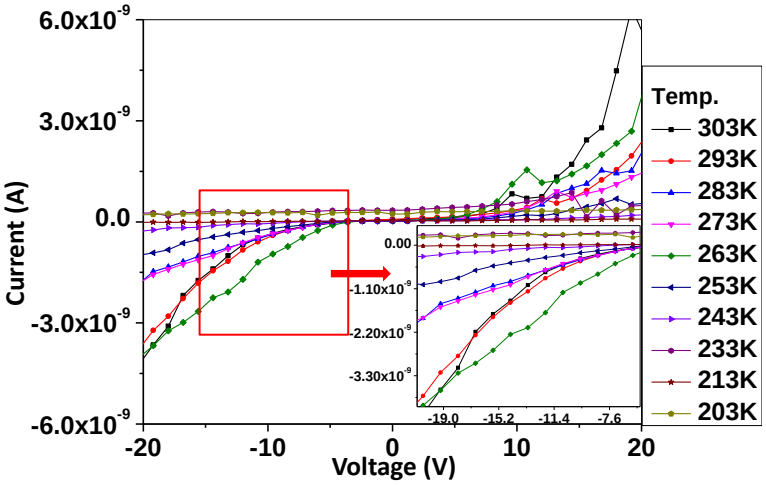

Figure III.17 Two probe current-voltage characteristics of Au-PDMS in in-plane geometry. Inset shows the region from where resistance have been calculated using the value of the slopes.

The resistance values calculated was plotted as a function of temperature (Figure III.18). The resistivity was calculated using the equation

$$\rho = R \times A / L \quad \text{..... (iv)}$$

where R is the resistance of the material in ohms, A is the cross sectional area of the specimen (900 nm x 1 cm) and L is the length of the material (9 μm). Resistivity decreased with increase in temperature, (Figure III.18) characteristics of a semiconductor.

One of the traditional method to analyze the temperature dependence in disordered organic material is based on the Miller–Abrahams expression.[68] It was first considered by Shklovskii to find the field effect on the variable range hopping (VRH) at low temperature. A more systematic derivation of the temperature dependence based on the VRH and percolation theory was studied by Ambegaokar et. al.[69] Joule heating caused at room temperature or even at higher temperatures provoke charge carriers to move and give rise to electrical conduction. The theory successfully described the temperature dependence of conductivity in polymer materials, but it is difficult to account for the experimentally observed electric field dependence. As shown in Figure III.19 $|\ln(\rho)|$ is seen varying almost linearly with $T^{-1/4}$.

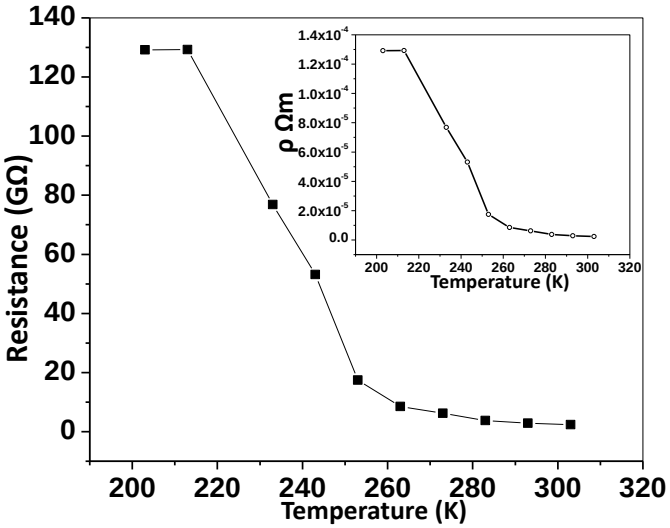

Figure III.18 Resistance of the Au-PDMS measured between 200 and 320 K. Inset plot showing the resistivity vs temperature plot for the polymer composite. The distance between the contacts was 9 μm and area of contact of Au-PDMS with gold is 1 cm x 900 nm.

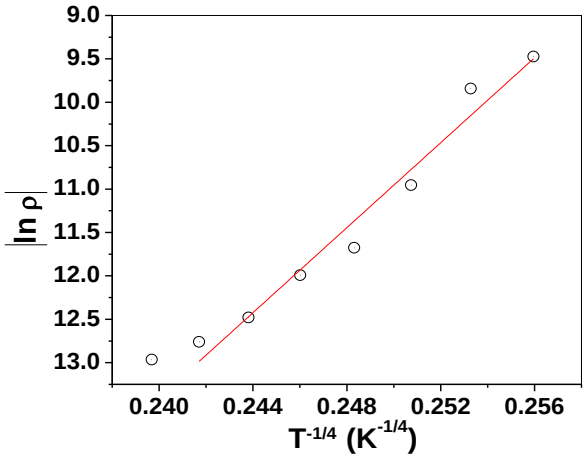

Figure III.19 $|\ln(\rho)|$ vs $T^{-1/4}$ plot, which is linear, characteristic of VRH model of electrical transport at low temperatures (203 to 303 K).

In a disordered polymer system, the localized states are randomly distributed and they form an array of sites, discrete in nature. When a high electric field is applied the voltage drop across a single hopping distance increases. The voltage drop across the Au-PDMS was calculated to be 5 x 10^{-18} J which crossed the order of K_BT, thus site to site hopping takes place rather than normal conductance because the current between the two sites depends on the strength of the electric field which changes its chemical potential. A percolation model is adopted in such cases to explain site-to-site hopping current conductance.[70]

According to percolation theory; a steady-state situation means a constant current throughout the backbone (potential sites for hopping) of the polymer. The charge gets redistributed changing the chemical potentials of sites. This can be approximated by the hopping process. The redistribution of charge is likely to change the hopping current.

III.5 Conclusion

The performances of the Au-PDMS gel capacitor based devices have been examined. Application of pressure on the device brought significant change in conductivity of the nanocomposite. Investigation was carried out by allowing the circuit to stay in different ambience. The environment around the circuit was changed by allowing toluene and nitrogen vapor to pass through it. An improvement in current flow was detected when the circuit was kept immersed in toluene vapor. Investigations were made based on both the capacitor geometry and in-plane geometry with the nanocomposite material to understand the reason behind such changes. In order to prevent the shorting of the electrodes, a surface activator was used and the performance characteristics were measured. Metallization of the Au-PDMS was done to improve the conductivity. The thin film of metallized gold nanoparticles on Au-PDMS showed high conductivity. The devices thus produced can have the potential to be used as touch sensors, stress and strain gauges as well as flexible biocompatible devices.

References

1 D.Y.Godovsky. Applications of Polymer-Nanocomposites. *Advances in Polymer science* 153, 165–205, (2000).

2 Slonimskii, G. L., Musayelyan, I. N. & Kazantseva, V. V. Mechanical properties of polymer mixtures—III. Polyisobutylene with polyethylene. Density of polymeric mixtures. *Polymer Science U.S.S.R.* 6, 906-910, (1964).

3 Lotters, J. C. O., W.; Veltink, P. H.; Bergveld, P. The mechanical properties of the rubber elastic polymer polydimethylsiloxane for sensor applications. J Micromechanics Microengineering 7 (3): 145–147, (1997).

4 Polymers, O. P. o. *Annual Review of Physical Chemistry* 24, 207-234, (1973).

5 U. S. Tewari, S. K. S., H. S. Nalwa*, and P. Vasudevan High permitivitty in polymers: Structure and property correlation *IEEE Transactions on Electrical insulation* 6, (1985).

6 Sotiriou, G. A., Blattmann, C. O. & Pratsinis, S. E. Flexible, Multifunctional, Magnetically Actuated Nanocomposite Films. *Advanced Functional Materials* 23, 34-41, (2013).

7 Sorel, S., Khan, U. & Coleman, J. N. Flexible, transparent dielectric capacitors with nanostructured electrodes. *Applied Physics Letters* 101, (2012).

8 Huang, C. & Zhang, Q. Enhanced Dielectric and Electromechanical Responses in High Dielectric Constant All-Polymer Percolative Composites. *Advanced Functional Materials* 14, 501-506, (2004).

9 Maier, G. Low dielectric constant polymers for microelectronics. *Progress in Polymer Science* 26, 3-65, (2001).

10 Venkataraman, A. L. a. A. Polymer Nanocomposites *Resonance* 10, 49-60, (2005).

11 Yeo, S.-D. & Kiran, E. Formation of polymer particles with supercritical fluids: A review. *The Journal of Supercritical Fluids* 34, 287-308, (2005).

12 Nagasawa, K., Honjoh, M., Takada, T., Miyake, H. & Tanaka, Y. Electric Charge Accumulation in Polar and Non-Polar Polymers under Electron Beam Irradiation. *IEEE Transactions on Fundamentals and Materials* 130, 1105-1112, (2010).

13 Carré, A. Polar interactions at liquid/polymer interfaces. *Journal of Adhesion Science and Technology* 21, (2012).

14 Carrea, J. W. A. Role of Surface Polarity in the Evolution of Polymer Surface Properties in Liquid Medium. *The Journal of Adhesion* 86, (2010).

15 Holliday, S., Donaghey, J. E. & McCulloch, I. Advances in Charge Carrier Mobilities of Semiconducting Polymers Used in Organic Transistors. *Chemistry of Materials* 26, 647-663, (2013).

16 Heeger, A. J., Kivelson, S., Schrieffer, J. & Su, W.-P. Solitons in conducting polymers. *Reviews of Modern Physics* 60, 781, (1988).

17 Shirakawa, H., Louis, E. J., MacDiarmid, A. G., Chiang, C. K. & Heeger, A. J. Synthesis of electrically conducting organic polymers: halogen derivatives of polyacetylene, (CH). *Journal of the Chemical Society, Chemical Communications*, 578-580, (1977).

18 Janata, J. & Josowicz, M. Conducting polymers in electronic chemical sensors. *Nat Mater* 2, 19-24, (2003).

19 Sariciftci, N. S., Smilowitz, L., Heeger, A. J. & Wudl, F. Photoinduced Electron Transfer from a Conducting Polymer to Buckminsterfullerene. *Science* 258, 1474-1476, (1992).

20 George, S. C. & Thomas, S. Transport phenomena through polymeric systems. *Progress in Polymer Science* 26, 985-1017, (2001).

21 Bolto, B., McNeill, R. & Weiss, D. Electronic Conduction in Polymers. III. Electronic Properties of Polypyrrole. *Australian Journal of Chemistry* 16, 1090-1103, (1963).

22 Ferraris, J., Cowan, D. O., Walatka, V. & Perlstein, J. H. Electron transfer in a new highly conducting donor-acceptor complex. *Journal of the American Chemical Society* 95, 948-949, (1973).

23 P.M. Ajayan, L. S. S., P.V. Braun. *Nanocomposite science and technology*. (Wiley, 2003).

24 Y. Mai, Z. Y., Y. Mai, Z. Yu, ed. *Polymer Nanocomposites*. (Woodhead Publ., 2006).

25 M. Roy, J. K. N., R.K. MacCrone, L.S. Schadler Polymer Nanocomposite Dielectrics – The Role of the Interface. *Nanoface*, (2010).

26 Byrne, M. T. & Gun'ko, Y. K. Recent Advances in Research on Carbon Nanotube–Polymer Composites. *Advanced Materials* 22, 1672-1688, (2010).

27 Spitalsky, Z., Tasis, D., Papagelis, K. & Galiotis, C. Carbon nanotube–polymer composites: Chemistry, processing, mechanical and electrical properties. *Progress in Polymer Science* 35, 357-401, (2010).

28 Metal-Polymer Nanocomposites for Functional Applications. *Advanced Engineering Materials*, (2010).

29 Reddy, K. R., Lee, K.-P., Lee, Y. & Gopalan, A. I. Facile synthesis of conducting polymer–metal hybrid nanocomposite by in situ chemical oxidative polymerization with negatively charged metal nanoparticles. *Materials Letters* 62, 1815-1818, (2008).

30 Cho, M. S., Park, S. Y., Hwang, J. Y. & Choi, H. J. Synthesis and electrical properties of polymer composites with polyaniline nanoparticles. *Materials Science and Engineering*, 24, 15-18, (2004).

31 Sih, B. C. & Wolf, M. O. Metal nanoparticle-conjugated polymer nanocomposites. *Chemical Communications*, 3375-3384, (2005).

32 Xu, P., Han, X., Zhang, B., Du, Y. & Wang, H.-L. Multifunctional polymer-metal nanocomposites via direct chemical reduction by conjugated polymers. *Chemical Society Reviews* 43, 1349-1360, (2014).

33 Smirnova, T. N., Kokhtych, L. M., Kutsenko, A. S., Sakhno, O. V. & Stumpe, J. The fabrication of periodic polymer/silver nanoparticle structures: in situ reduction of silver nanoparticles from precursor spatially distributed in polymer using holographic exposure. *Nanotechnology* 20, 405301, (2009).

34 Kelly, K. L., Coronado, E., Zhao, L. L. & Schatz, G. C. The Optical Properties of Metal Nanoparticles: The influence of size, shape, and dielectric environment. *The Journal of Physical Chemistry B* 107, 668-677, (2002).

35 Ozhikandathil, J., Badilescu, S. & Packirisamy, M. Synthesis and characterization of silver-PDMS nanocomposite for the biosensing applications. *Photonics North*, 800707-800707-800706, *(2011).*

36 Glazman, L. I. Single Electron Tunneling. *Journal of Low Temperature Physics* 118, 247-269, (2000).

37 Averin, D. V. & Likharev, K. K. Coulomb blockade of single-electron tunneling, and coherent oscillations in small tunnel junctions. *Journal of Low Temperature Physics* 62, 345-373, (1986).

38 Pooja Devi, A. Y. M., Simona Badilescu, Muthukumaran Packirisamy, Pethaiyan Jeevanandam and Vo-Van Truong in *International Conference on Biosciences* (2010 International Conference on Biosciences).

39 Gangopadhyay, R. & De, A. Conducting Polymer Nanocomposites: A Brief Overview. *Chemistry of Materials* 12, 608-622, (2000).

40 Bredas, J. L. & Street, G. B. Polarons, bipolarons, and solitons in conducting polymers. *Accounts of Chemical Research* 18, 309-315, (1985).

41 Oduor, A. O. & Gould, R. D. Space-charge-limited conductivity in evaporated cadmium selenide thin films. *Thin Solid Films* 270, 387-390, (1995).

42 Grinberg, A. A., Luryi, S., Pinto, M. R. & Schryer, N. L. Space-charge-limited current in a film. *Electron Devices, IEEE Transactions on* 36, 1162-1170, (1989).

43 Takeshita, S., Modelling of space cherge limited current injection incorporating advanced model of the poole-frenkel effect. Clemson University, (2008).

44 Chan, H.-K. *A General Conductivity Expression for Space-Charge-Limited Conduction in Ferroelectrics and Other Solid Dielectrics* School of Physics, Trinity College Dublin, College Green.

45 Chandra, W., Ang, L. K., Pey, K. L. & Ng, C. M. Two-dimensional analytical Mott-Gurney law for a trap-filled solid. *Applied Physics Letters* 90, 153505-153505-153503, (2007).

46 Lee, D.-W. & Choi, Y.-S. A novel pressure sensor with a PDMS diaphragm. *Microelectronic Engineering* 85, 1054-1058, (2008).

47 Bergbreiter, A. P. G. a. S. Dielectric breakdown of PDMS thin films. *Journal of Micromechanics and Microengineering* 23, (2013).

48 Jin, J., Lin, Y., Song, M., Gui, C. & Leesirisan, S. Enhancing the electrical conductivity of polymer composites. *European Polymer Journal* 49, 1066-1072, (2013).

49 Wendy's: Nutrition and ingredient information. Wendy's International, I. S. p.

50 Lalwani, G., Henslee, A. M., Farshid, B., Parmar, P., Lin, L., Qin, Y.-X., Kasper, F. K., Mikos, A. G. & Sitharaman, B. Tungsten disulfide nanotubes reinforced biodegradable polymers for bone tissue engineering. *Acta Biomaterialia* 9, 8365-8373, (2013).

51 Zhang, Q., Xu, J.-J., Liu, Y. & Chen, H.-Y. In-situ synthesis of poly(dimethylsiloxane)-gold nanoparticles composite films and its application in microfluidic systems. *Lab on a Chip* 8, 352-357, (2008).

52 Goyal, A., Kumar, A., Patra, P. K., Mahendra, S., Tabatabaei, S., Alvarez, P. J. J., John, G. & Ajayan, P. M. In situ Synthesis of Metal Nanoparticle Embedded Free Standing Multifunctional PDMS Films. *Macromolecular Rapid Communications* 30, 1116-1122, (2009).

53 Ghisleri, C., Borghi, F., Ravagnan, L., Podest, A., Melis, C., Colombo, L. & Milani, P. Patterning of gold polydimethylsiloxane nanocomposites by supersonic cluster beam implantation. *Journal of Physics D: Applied Physics* 47, 015301, (2014).

54 Kim, J. & Ahn, H. Fabrication and characterization of polystyrene/gold nanoparticle composite nanofibers. *Macromol. Res.* 16, 163-168, (2008).

55 Scott, A., Gupta, R. & Kulkarni, G. U. A simple water-based synthesis of Au nanoparticle/PDMS composites for water purification and targeted drug release. *Macromolecular Chemistry and Physics* 211, 1640-1647, (2010).

56 Khan, M. A., Bhansali, U. S. & Alshareef, H. N. Fabrication and characterization of all-polymer, transparent ferroelectric capacitors on flexible substrates. *Organic Electronics* 12, 2225-2229, (2011).

57 Xia, L., Wei, Z. & Wan, M. Conducting polymer nanostructures and their application in biosensors. *Journal of Colloid and Interface Science* 341, 1-11, (2010).

58 Saito, S., Sasabe, H., Nakajima, T. & Yada, K. Dielectric relaxation and electrical conduction of polymers as a function of pressure and temperature. *Journal of Polymer Science Part A-2: Polymer Physics* 6, 1297-1315, (1968).

59 Hush, N. S. An Overview of the First Half-Century of Molecular Electronics. *Annals of the New York Academy of Sciences* 1006, 1-20, (2003).

60 Ping Du, X. L., and Xin Zhang Dielectric constants of PDMS nanocomposites using conducting polymer nanowires, *IEEE*, (2011).

61 C. Ghisleri, F. B., L. Ravagnan, A. Podestà, C. Melis, L. Colombo, P. Milani Patterning of gold–polydimethylsiloxane (Au–PDMS) nanocomposites by supersonic cluster beam implantation. *Journal of physics. D*, 10, 1-10, (2014).

62 Khang, D.-Y., Jiang, H., Huang, Y. & Rogers, J. A. A Stretchable Form of Single-Crystal Silicon for High-Performance Electronics on Rubber Substrates. *Science* 311, 208-212, (2006).

63 Huck, W. T. S., Bowden, N., Onck, P., Pardoen, T., Hutchinson, J. W. & Whitesides, G. M. Ordering of Spontaneously Formed Buckles on Planar Surfaces. *Langmuir* 16, 3497-3501, (2000).

64 Li, L., Meller, G. & Kosina, H. Temperature and field-dependence of hopping conduction in organic semiconductors. *Microelectronics Journal* 38, 47-51, (2007).

65 Burroughes, J. H., Bradley, D. D. C., Brown, A. R., Marks, R. N., Mackay, K., Friend, R. H., Burns, P. L. & Holmes, A. B. Light-emitting diodes based on conjugated polymers. *Nature* 347, 539-541, (1990).

66 Kulshreshtha, Y. K. & Srivastava, A. P. Electrical Conduction in Polystyrene-Chloranil System. *Polym J* 12, 771-775, (1980).

67 Blom, P. W. M., de Jong, M. J. M. & van Munster, M. G. Electric-field and temperature dependence of the hole mobility in poly(p-phenylene vinylene). *Physical Review B* 55, R656-R659, (1997).

68 Miller, A. & Abrahams, E. Impurity Conduction at Low Concentrations. *Physical Review* 120, 745-755, (1960).

69 Ambegaokar, V., Halperin, B. I. & Langer, J. S. Hopping Conductivity in Disordered Systems. *Physical Review B* 4, 2612-2620, (1971).

70 J.J. van Hapert, P. D. T., University Utrecht, Netherlands, 2002.

OUTLOOK

This thesis work is essentially an exploration on nanocarbon materials and metal-polymer nanocomposites. **Part I** provided the necessary introduction. **Part II** dealt with 2D nanocarbons with special stress on graphene and graphene-like species in pencil traces on paper. Techniques, both physical and chemical, available in literature to obtain large area graphene have been attempted. Among the electrochemical methods, annealing of Ni coated carbonaceous material serves as a potential way to obtain graphene. Electrochemical delamination process was also tried, using Ni/ Graphene as the source, to obtain large area graphene. But all these methods involved wet solvents. On the other hand, physical methods do not involve chemicals and therefore paves a path for obtaining graphene by solvent free approaches. The most popular among them is the famous scotch tape method but graphene thus obtained is hard to be pinpointed. The second physical method attempted was electrostatic exfoliation. This method can be potentially used to transfer large area patterned graphene on a specific site by applying electric field. The electrostatic pressure generated during such attempts by applying 50 V across the electrodes, resulted in amorphous carbon deposition. But if the field is regulated to a threshold value it can manifest a prospective approach in obtaining clean, solvent free, large area graphene. Last section of Part II focuses on pencil traces on paper, its properties and characterization. Its potential in the fabrication of field effect transistors, IR photodectectors and both active and passive devices have been discussed. The cost effective and easy fabrication technique makes the method very attractive. It definitely can be used for many futuristic devices especially for higher order passive devices.

Part III has dealt with Au nanoparticles-polymer nanocomposites with emphasis on its electrical properties. Methods to enhance the conductivity were looked upon. PDMS have been used in mechanical systems because of its rheological properties. But it being a damp insulator, has found very little role in electronics. The electrical properties of PDMS were improved by adding metal nanoparticles to it. Gold nanoparticles with its novel properties, imparted some drastic changes in the characteristics of PDMS matrix. Electrical properties of Au-PDMS were investigated by applying various stimuli like electrical stress, nitrogen and toluene vapor and pressure application. Changes in current values were observed each time. Au-PDMS being biocompatible and viscoelastic, improvement in its electrical properties surely will pave path for it to be used in modern devices like sensors, gauges etc.

List of Publications

1. Kurra, N., **Dutta, D.** & Kulkarni, G. U. Field effect transistors and RC filters from pencil-trace on paper. *Physical Chemistry Chemical Physics* 15, 8367-8372, (2013).